R-02-02

DEMONSTRATION OF IMPROVED OPERATIONAL WATER RESOURCES MANAGEMENT THROUGH USE OF BETTER SNOW WATER EQUIVALENT INFORMATION

September 2002

U.S. DEPARTMENT OF THE INTERIOR
Bureau of Reclamation

Technical Service Center
River Systems and Meteorology Group
Water Resources Services Division
Denver, Colorado

REPORT DOCUMENTATION PAGE

Form Approved
OMB No. 0704-0188

1. AGENCY USE ONLY *(Leave Blank)*	2. REPORT DATE	3. REPORT TYPE AND DATES COVERED
	July 2002	Supplemental

4. TITLE AND SUBTITLE

Demonstration of Improved Operational Water Resources Management Through Use of Better Snow Water Equivalent Information

5. FUNDING NUMBERS

6. AUTHOR(S)

Steven M. Hunter and Edmond W. Holroyd, III

7. PERFORMING ORGANIZATION NAME(S) AND ADDRESS(ES)

Bureau of Reclamation
Technical Service Center
River Systems and Meteorology Group
Water Resources Division
Denver, Colorado

8. PERFORMING ORGANIZATION REPORT NUMBER

R-02-02

9. SPONSORING/MONITORING AGENCY NAME(S) AND ADDRESS(ES)

Same

10. SPONSORING/MONITORING AGENCY REPORT NUMBER

11. SUPPLEMENTARY NOTES

12a. DISTRIBUTION/AVAILABILITY STATEMENT

12b. DISTRIBUTION CODE

13. ABSTRACT (Maximum 200 words)

This research is designed to aid Reclamation's water managers by providing them with decision assistance in the form of enhanced precipitation estimation over watersheds affecting the reservoir system. The overall goal is more efficient use of water. To achieve this goal, the following project objectives were defined: (1) to demonstrate a significant improvement in the technology used to estimate snow water equivalent (SWE) distributions and (2) to demonstrate benefits to Reclamation from improved streamflow forecasting resulting from better SWE information and emerging new NOAA hydrologic prediction schemes.

Reclamation's Snow Accumulation Algorithm (SAA) was deployed in the north-central United States during cool seasons from 1998-2001, providing near-real-time graphical distributions of snow water equivalent (SWE) and snow depth (SD) estimates on the Internet. The SAA has undergone several major modifications in the last year that extend its accuracy and applicability. The SAA now accommodates several more precipitation types, and accordingly, the algorithm is now called the Precipitation Accumulation Algorithm (PAA). The SAA correction for range degradation was replaced by a fixed adjustment for the vertical profile of reflectivity (VPR), and the new PAA uses temperature and relative humidity from numerical (Eta) model soundings and temperature altitude thresholds to classify precipitation type.

14. SUBJECT TERMS

weather radar, NEXRAD, WSR-88D, Snow Accumulation Algorithm, Precipitation Accumulation Algorithm, quantitative precipitation estimation, snow water equivalent, snow depth, snowfall, virga, precipitation type

15. NUMBER OF PAGES

16. PRICE CODE

17. SECURITY CLASSIFICATION OF REPORT	18. SECURITY CLASSIFICATION OF THIS PAGE	19. SECURITY CLASSIFICATION OF ABSTRACT	20. LIMITATION OF ABSTRACT
UL	UL	UL	UL

R-02-02

DEMONSTRATION OF IMPROVED OPERATIONAL WATER RESOURCES MANAGEMENT THROUGH USE OF BETTER SNOW WATER EQUIVALENT INFORMATION

by

Steven M. Hunter and Edmond W. Holroyd, III

Technical Service Center
River Systems and Meteorology Group
Water Resources Services Division
Denver, Colorado

September 2002

EXECUTIVE SUMMARY

The U.S. Bureau of Reclamation (Reclamation) operates over 350 dams and reservoirs throughout the western United States, managing critical water resources for the benefit of the American people. This research is designed to aid Reclamation's water managers by providing them with decision assistance in the form of enhanced precipitation estimation over watersheds affecting the reservoir system. The overall goal is more efficient use of water for agriculture, hydroelectric power generation, Municipal and Industrial (M&I), recreation, and endangered species protection. To achieve this goal, the following project objectives were defined: (1) to demonstrate a significant improvement in the technology used to estimate snow water equivalent (SWE) distributions without requiring instrumentation in addition to that already deployed and (2) to demonstrate benefits to Reclamation from improved streamflow forecasting resulting from better SWE information and emerging new NOAA hydrologic prediction schemes.

During the period 1991-1997, approximately 160 WSR-88D (Weather Surveillance Radar - 1988 Doppler) radars were installed in the United States and abroad. The WSR-88D's operational precipitation algorithms, collectively known as the Precipitation Processing Subsystem (PPS), were designed for rain rather than snow. In 1995, the Bureau of Reclamation was tasked by the WSR-88D Operational Support Facility (OSF) to develop a snow accumulation algorithm (SAA) and did so in the succeeding 3 years. The SAA was targeted for incorporation into the operational WSR-88D software suite. The SAA was designed solely for use with dry (not melting) snow.

Under the auspices of the Global Energy and Water Cycles Experiment (GEWEX) Continental-Scale International Program (GCIP) and Reclamation's Science and Technology Program, a version of the SAA was developed to use real-time Level III radar data. This version was deployed in the north-central United States as a demonstration project during cool seasons from 1998-2001, providing near-real-time graphical distributions of snow water equivalent (SWE) and snow depth (SD) estimates on the Internet.

The SAA underwent several major modifications in the final year of the project. These modifications extend its accuracy and applicability to water management operations. The enhancements were so far reaching that the SAA now accommodates several more precipitation types. Accordingly, the algorithm is now called the Precipitation Accumulation Algorithm (PAA). The modifications are briefly described as follows.

First, the SAA correction for range degradation was replaced by a fixed adjustment for the vertical profile of reflectivity (VPR). This adjustment is widely acknowledged as the most important one in radar precipitation estimation. The adjustment is indispensable for accurate estimates in mountainous terrain, where there is severe radar beam blockage.

Second, the new PAA uses temperature and relative humidity from numerical (Eta) model soundings and temperature altitude thresholds to classify precipitation type. Areas of dry snow, melting snow (bright band precipitation), rain, and virga contamination are distinguished. For all these areas except virga, a liquid-equivalent precipitation at the surface is estimated.

The enhanced PAA may be input to the National Weather Service's Snow Data Assimilation System (SNODAS), a new and sophisticated snow energy and mass balance modeling system. It is anticipated that the SNODAS will provide quantitative snowpack and snowmelt data to the NWS's river models, thereby resulting in more accurate streamflow forecasts for the public and water operations management.

ACKNOWLEDGMENTS

This work was funded by the Weather Surveillance Radar - 1988 Doppler (WSR-88D) Operational Support Facility (now the Radar Operations Center [ROC]), Norman, Oklahoma; Reclamation's Science and Technology Program; and the National Oceanic and Atmospheric Administration's (NOAA's) Office of Global Programs (OGP), through the Global Energy and Water Cycle Experiment (GEWEX) Continental-Scale International Program (GCIP). We thank the following people for their support: Mark Fresch of the ROC, Dr. Rick Lawford of NOAA OGP, Reclamation research directors Dr. Stanley Ponce and Shannon Cunniff. Curt Hartzell and Dr. David Matthews provided consultation and peer reviews. Ra Aman supplied extensive programming support.

U.S. Department of the Interior
Mission Statement

The Mission of the Department of the Interior is to protect and provide access to our Nation's natural and cultural heritage and honor our trust responsibilities to tribes.

Bureau of Reclamation
Mission Statement

The mission of the Bureau of Reclamation is to manage, develop, and protect water and related resources in an environmentally and economically sound manner in the interest of the American public.

CONTENTS

CONTENTS – Continued

APPENDIX

TABLES

FIGURES

FIGURES – Continued

FIGURES – Continued

1. INTRODUCTION

1.1 Background, Purpose, and Goals – Water Resources Management Applications

The Bureau of Reclamation's (Reclamation) water management engineers continue to learn more about emerging technologies that the Global Energy and Water Cycles Experiment (GEWEX) Continental-Scale International Program (GCIP) has sponsored since 1995. Reclamation's partnership with National Oceanic and Atmospheric Administration's (NOAA) Office of Global Programs (OGP) began with a jointly sponsored Water Resources Management Applications Workshop, held March 13-14, 1997. This was the first opportunity for Reclamation engineers to meet with GCIP scientists to discuss needs and potential applications of GCIP tools. Over 30 scientists and engineers met to discuss needs of water managers and water-related GCIP research. Most of Reclamation's regional water operations teams were represented at the meeting. This meeting set the stage for a dialogue among these water operations managers, GCIP, and National Weather Service (NWS) forecast teams.

The goals of this study were to: (1) to demonstrate a significant improvement in the technology used to estimate snow water equivalent (SWE) distributions without requiring instrumentation in addition to that already deployed and (2) to demonstrate benefits to Reclamation from improved streamflow forecasting resulting from better SWE information and emerging new NOAA hydrologic prediction schemes. Knowledge and trust are the foundations for increased awareness and confidence in new research tools that are emerging for water managers from the GCIP program. Reclamation's engineers recognize that verification is essential to building trust. We attended workshops and meetings where Reclamation shared its needs and GCIP experts provided technical reviews of their research studies and products that may have value to water managers. This final report details progress since 1997 toward developing Snow Accumulation Algorithm (SAA) and Precipitation Accumulation Algorithm (PAA) tests and helping our managers better understand and eventually use streamflow forecasts enhanced by near-real-time precipitation data estimated by radar. Such streamflow forecasts are critical elements in the decision processes of water management, and precipitation is the most elusive, yet important, variable within these forecasts.

The partnership between the GCIP project and Reclamation's Science and Technology (S&T) Program has fostered the development, testing, and improvement of the Weather Surveillance Radar - 1988 Doppler (WSR-88D) SAA and PAA for precipitation estimation. In 2000, Reclamation's S&T Program leveraged the GCIP efforts to improve communications and clarify specific forecasting needs to improve streamflow forecasts in the upper Missouri Basin. Meetings with Reclamation's upper Missouri water managers and the Missouri Basin River Forecast Center (MBRFC) resulted in the MBRFC Advanced Hydrologic Prediction Services (AHPS) Demonstration Project. These AHPS streamflow forecasts are experimental and under evaluation. These forecasts use ensemble streamflow forecasts that have benefited from GCIP and AHPS research; however, they lack operational reservoir and diversion interfaces that would make them true operational forecasts.

Basins currently targeted for prototype testing of the SAA/PAA are:

- Several basins in the north-central U.S. from Minnesota to Montana
- Truckee - AHPS tests beginning fiscal year 2001
- Jefferson, Madison, Missouri in the Upper Missouri
- Yakima, Columbia, Umatilla
- Tualatin
- Rogue
- Lower Colorado - Yuma water operations and Lower Colorado River Accounting System
- South Platte

Reclamation water operations partners include: Upper Missouri Basin Water Operations/ Montana Area Office, Tim Felchle; Yakima Project Water Operations/Upper Columbia Area Office, Warren Sharp; Lower Colorado Water Operations/Yuma Area Office, Robert Adams; Lower Colorado Water Operations/Boulder Canyon Operations Office, Bruce Williams and Paul Matuska; Truckee River Operations/Lahonton Basin Area Office, Tom Scott; Truckee River Federal Water Master, Reno, Nevada, Jeff Boyer; Tualatin and Rogue Projects/Bend Field Office, Kathy Kihara, and Leo Busch.

GCIP funded the following projects:

- Use of NEXRAD Radar Snow Accumulation Algorithm in the GCIP-Large Scale Area-North Central (LSA-NC)
- Demonstration of Improved Operational Water Resources Management through Utilization of Better SWE Information
- Practical Implementation of GCIP Research Tools for Water Managers in USBR GP Region

This report summarizes results from these studies that were also leveraged by additional Reclamation S&T Program funding.

1.2 The WSR-88D Radar, Precipitation Processing Subsystem System, and SAA

During the period 1991-97, approximately 160 WSR-88D radars were installed in the United States and abroad (Crum et al., 1993). This radar network was a major part of the modernization of the NWS and was a significant upgrade of the aging conventional radar network that it replaced. The network was installed and maintained by three Federal agencies—U.S. Department of Commerce (NWS), U.S. Department of Defense (U.S. Air Force), and U.S. Department of Transportation (Federal Aviation Administration).

The operational precipitation algorithms within the WSR-88D are collectively known as the Precipitation Processing Subsystem (PPS). The PPS was described by Fulton et al. (1998). The system was designed for rain rather than snow. To meet the need for snowfall estimation by the NWS and other users, Reclamation responded to a 1994 request for proposals by the WSR-88D Operational Support Facility (OSF) for a SAA. Reclamation was selected in 1995 to carry out

the applied research and development of such an SAA and did so in the succeeding 3 years. The results were published in Super and Holroyd (1998).

1.3 GCIP Applications of the SAA

In 1997, Reclamation submitted a proposal to the GCIP. The proposal, No. GC97-0045, was selected for funding by NOAA's OGP, and work began in 1998. The principal goal of the proposal, entitled "Demonstration of Improved Operational Water Resources Management Through Utilization of Better Snow Water Equivalent Information," was to significantly improve estimation of SWE distributions and snow cover. This was to be accomplished by the SAA's provision of SWE estimates to the NWS's National Operational Hydrologic Remote Sensing Center (NOHRSC), which would use them in their snowpack models and direct the results to the operational river models at the MBRFC. These river models, which provide crucial streamflow forecasts to Reclamation, would thus be improved by more accurate snowpack inputs.

1.4 Snowpack Estimation and Hydrologic Modeling

NOHRSC is the NWS center of expertise in satellite and airborne remote sensing and geographic information systems (GIS) used to support the NWS operational hydrology program for the United States. The most widely used NOHRSC products estimate snow cover properties with data collected by airborne, satellite, and ground-based sensors. The center operates two terrestrial gamma radiation detection systems on low-flying aircraft to infer snow water equivalent over a network of more than 1,900 flight lines covering portions of 27 States and 7 Canadian provinces. NOHRSC developed the Snow Estimation and Updating System (SEUS), which uses a geographic information system to store, analyze, and display the spatial data necessary to perform the estimation. Reclamation originally intended for SAA SWE estimates to be ingested in SEUS, but NOHRSC later decided to replace it with a more sophisticated system called the Snow Data Assimilation System (SNODAS). This system is currently being implemented on a test basis. SEUS never had the ability to assimilate SWE observations from radar, as does SNODAS.

The NWS River Forecast System (NWSRFS) (Burnash, 1995) consists of various components, including the Operational Forecast System (OFS). Within the OFS is the SNOW-17 model, which calculates snow accumulation and ablation (sublimation and melting). This model passes rain plus snowmelt to a bulk hydrologic runoff model called the Sacramento Soil Moisture Accounting (SAC-SMA) model. Neither model now has input from SNODAS, but this will change once the latter becomes operational. Reclamation has recently completed work to input SAA SWE estimates to SNODAS.

1.5 Annual Progress

This final report addresses Reclamation's activities and findings during the past 3 years of effort under the contract. Work done in the first and second years is described in two previous annual reports. The following summarizes work in the third and final year.

The principal investigator (PI) for this research was Dr. Arlin Super, who retired in August 1999. Dr. Super was replaced by Steven Hunter in May 2000. During the intervening time, work was carried on by Dr. Edmond Holroyd, the co-PI. The observational network in the north-central U.S. was extended westward to Great Falls, Montana, for a total of 10 WSR-88D stations. The radar at Sioux Falls, South Dakota, was added for the most recent winter season. SAA observations were monitored to assess accuracy and to identify features for improvement. A new algorithm, named the Precipitation Accumulation Algorithm, was developed to address the additional tasks of rain accumulation, bright band identification and its precipitation equivalent, and virga.

2. TASK SUMMARIES

Tasks as given in the Statement of Work (in italics), along with resulting accomplishments, are as follows:

1. *Access near real-time NEXRAD radar Level III reflectivity products from the Chanhassen, Minnesota, (KMPX) WSR-88D radar through a NEXRAD Information Dissemination Service (NIDS) vendor:* This was accomplished in the first year of effort. Data were obtained from the NIDS vendor Weather Services International (WSI) Corporation.

2. *Modify Reclamation's SAA to use Level III reflectivities from KMPX as input to the SAA:* Programming and testing of archived KMPX Level III data occurred in the first year, showing that it was feasible to use such data. Further testing in the second year indicated good results, and the methodology was recommended for operational implementation.

3. *Use the modified SAA to provide near real-time SWE estimates with a stand-alone computer that ingests the Level III data, runs the SAA, displays visual outputs, and provides numerical outputs:* This was accomplished on a Sun UNIX workstation in the second year.

4. *Develop software to display the SWE estimates for the past 1 and 3 hours and since the beginning of each snowstorm, on the same computer used to run the SAA:* FORTRAN77, C, net Common Data Format (netCDF), and NCAR graphics routines were developed and used to perform this task; storm-total amounts were converted to 24-hour increments instead of 1- and 3-hour increments.

5. *Develop the means to convert radar SWE estimates from polar coordinates into a gridded field coordinate system specified by NOHRSC (in Chanhassen, Minnesota):* This method was developed with output to an approximately 4- by 4-kilometer (km) Hydrologic Rainfall Analysis Project (HRAP) grid. This grid is standard for operational hydrologic purposes.

6. *Develop the means to provide gridded fields of radar-estimated SWE to NOHRSC in a timely fashion.* This task has been delayed because NOHRSC did not implement a system (SNODAS) to ingest such SWEs until recently and is still testing the system. PAA output resolution for NOHRSC was increased to a nominal 2- by 2-km subset of the HRAP grid. Operational data flow is expected in late 2002, using Reclamation S&T Program funds.

7. *Begin to use special snow gauge and airborne SWE observations to better "calibrate" the SAA for the GCIP LSA-NC and Large Scale Area-Northwest (LSA-NW) regions.* This was done for the GCIP LSA-NC and LSA-NW region, beginning in the 1998-99 winter season (Super and Holroyd, 1998).

8. *Provide an annual report describing accomplishments and findings.* This was completed in 1998 and is addressed in section 3.1.

9. Access near-real-time NEXRAD radar Level III reflectivity products at:

- KMPX, Chanhassen, Minnesota
- KBIS, Bismarck, North Dakota
- KABR, Aberdeen, South Dakota
- KMVX, Grand Forks, North Dakota
- KMPX, Minneapolis, Minnesota
- KDLH, Duluth, Minnesota
- KMBX, Minot, North Dakota
- KUDX, Rapid City, South Dakota
- KBLX, Billings, Montana
- KGGW, Glasgow, Montana
- KTFX, Great Falls, Montana

This was done before the 1999-2000 cool season. A year later, a radar was added at KFSD, Sioux Falls, South Dakota.

10. *Update hourly accumulations for all 10 radars according to the approximate 4-km HRAP grid specified by the NOHRSC.* This was done before the 1999-2000 cool season.

11. *Provide a real-time, 10 radar composite that extended from Duluth, Minnesota, to Great Falls, Montana.* This was also done before the 1999-2000 cool season. An 11th radar (Sioux Falls, South Dakota) was added before the following cool season.

12. *Update the SAA to account for range correction and virga errors.* A climatological range correction based on data from nine KMPX-area snowstorms was implemented before the 1999-2000 cool season. A virga rejection scheme was finished in early 2000.

13. *Provide radar SWE estimates to NOHRSC in near-real-time for them to merge with other data sets in development of gridded fields of SWE and snow cover. The first winter (1998-99) of near-real-time use of WSR-88D SWE estimates will use the Chanhassen radar.* PAA output has

been prepared for this task; but because NOHRSC's SNODAS system was not implemented until recently and is still in the testing phase, data are not being sent to SNODAS yet.

14. *Develop a scheme to merge (mosaic) SAA radar-estimated SWE fields from several adjoining radars.* This was achieved using a lookup-table method, based on the nearest radar's data. In 2001, beam elevations were taken into account, allowing the lowest beam from any radar to be used.

15. *Provide an annual report describing accomplishments and findings.* This was completed in spring 2000 and is addressed in section 3.2.

16. *Conduct initial operational testing of the new scheme of merging data sets from radar, aircraft, satellite, SNOTEL, and snow courses within the upper Missouri River Basin. Reclamation has considerable facilities within this basin and, therefore, is quite interested in improved spring and early summer streamflow forecasting in the basin.* Pending additional support, this may begin in late 2002 at NOHRSC, during the second season of operational testing for SNODAS.

17. *Develop and implement procedures to test and evaluate the degree of improvement that better NWS snowmelt and streamflow forecasts provide to Reclamation's water resources management. The focus of this work will be to demonstrate how Reclamation benefits by using improved streamflow forecasts, based on better model initialization and more accurate SWE and snow cover distributions, partially based on NEXRAD estimates.* This was not accomplished during the period of effort because of delays in SNODAS implementation. Resources for this task, however, were used to convert the SAA into the more generic PAA.

18. *Provide a final report describing accomplishments and findings.* This report completes this task.

3. TOPICS IN PREVIOUS REPORTS

Important research results have been summarized in two SAA annual reports. In addition, a supplemental SAA report (Holroyd, 1999) presented research that was partly supported by GCIP. The following subsections are from the summary sections of the annual reports and from the supplemental report abstract.

3.1 Annual Report 1998 (Super, 1998)

This applied research addressed two tasks related to estimating snowfall with NEXRAD radar measurements and Reclamation's SAA. The first task was to begin development of a range correction scheme based on the measured vertical profile of reflectivity (VPR), converted into vertical profiles of radar-estimated SWE (VPS). It has been shown that the VPS of Minnesota

winter snowfall, based on a sample of 9 storms, increases downward in the lowest 3 km above the radar. That is, maximum SWE estimates were usually at the lowest sampled level, about 380 meters (m) above the radar.

Linear least squares regression equations were fit to averaged SWE values for the five lowest radar beam tilts at about 35-km range. These equations, with one exception, explained 93 to 100 percent of the variance, indicating that the VPS is linear. While the slope of the equations varied among storms, it was demonstrated that use of the median case worked reasonably well in correcting range underestimation. Estimates at 150-km range would have been within a factor of two of the assumed "true" value in all nine storms and within about 20 percent of "true" for six of the nine storms. These results are believed to justify continued pursuit of a range correction scheme for the SAA that is based on the radar observed vertical profile of reflectivity.

The second task was to determine the feasibility of using "degraded" Level III reflectivity data instead of high resolution (0.5 decibel [dB]) Level II data with the SAA. Although it has less resolution (4.0 to 5.0 dB), the Level III product is readily available in near real-time from NIDS vendors. Moreover, Level III reflectivities have been and are being archived for several radars in the GCIP LSA-NC. The ability to use Level III reflectivities with the SAA would allow for radar-estimation of SWE over most of the LSA-NC for a two-winter period. This would greatly enhance SWE estimation in view of the limited number of suitable precipitation gauges in protected locations in the LSA-NC.

Considerable programming and testing were needed to produce a version of the SAA that could use Level III data. The Level III product is in the form of binary files intended for visual display, not for use as discrete digital dB values. Moreover, each of the four lowest radar beam tilts was in a separate file, and these had to be combined into pseudo volume scans. However, the SAA can now run successfully with archived Level III reflectivity files.

Parallel runs of the SAA, using Level II and Level III reflectivities as input, were made for five major Minnesota snowstorms, one with mixed rain and snow. The degree of agreement was shown to be quite good, especially at ranges of less than 150 km, where radar estimates are most reliable. Most Level III runs had area average SWE accumulations within 10 percent or less of the standard Level II runs for the same volume scans, at least within the 150-km range. These results indicate that use of archived Level III data from Minnesota snowstorms provide quite reasonable SWE estimates, using Level II estimates as the standard.

The next step in this applied research will be to continue work on the VPR range correction scheme so that the SAA can apply appropriate corrections for all ranges between about 50 and 150 km and perhaps farther. It would, of course, be very desirable to test this scheme against "ground truth" SWE observations. It is difficult to find accurate surface measurements of snowfall, either of depth or SWE. However, attempts will be made to find the means to test the SAA range correction scheme against some surface observations.

3.2 Annual Report 1999 (Matthews et al., 2000)

This GCIP research application effort and the work for the OSF produced a different style of field testing of the SAA under the GCIP program. The algorithm was modified to accept Level III data from NIDS providers in near-real time for a series of five radars across the Dakotas and Minnesota. Products were provided via the Internet in the 4-km HRAP grid so as to be useful for forecast groups. Accumulations of snowfall rate (S) and snow depth (SD) were produced for a variety of time intervals up to 24-hours, ending at 1200 Universal Time Coordinated (UTC) each day. The products of the five radars were combined in a mosaic to show regional accumulations.

Working with the NIDS data was generally successful. The mosaic process indicated that one or two radars appeared to be calibrated differently from the others, as shown by S and SD discontinuities across lines equidistant between the radars.

Virga was a persistent problem. An experimental procedure eliminated most virga without sacrificing the reliability of the algorithm in widespread, intense storms. That algorithm still needs further testing and adjustment before becoming part of the operational version of the SAA.

The SAA failed to match surface observations during a snowstorm in arctic air. An analysis indicated that the storm was shallow and had temperatures in the dendritic growth band for snow crystals. The radar beam generally was above the clouds, missing the rapid crystal growth close to the ground. Furthermore, dendritic crystals have the least density as snow on the ground. A change in a few adaptable parameters could have remedied the problem, but such was not possible in the routine production of products from the NIDS data stream.

Though desired in the specifications for tasks, it was not possible to derive local parameters of alpha and beta for radars in Alaska, Washington, and Illinois. There was insufficient quality data for those sites. Analyses of the California (Sierra Nevada) data indicated that the radar beam was far above the snow growth zones, which resulted in small alpha values.

A separate program was written to combine many days of SAA files to produce composite accumulations for three partitions of area coverage: scattered, moderate, and widespread. The output gave guidance for adjusting the hybrid scan file for inadequate or excessive suppression of clutter. The same products using widespread storm data could be useful in determining adjustments in the occultation correction file.

As part of the virga investigations, experimental coding was produced to generate images of the vertical profile of reflectivities. The images gave insights into the changing vertical structure of the storms. Parts of the code could be used for producing a better algorithm that is sensitive to vertical gradients. There is potential for better performance with virga and bright band events and for a better range correction scheme.

In general, this extension of effort has shown that the original SAA tends to be robust in an operational mode. Therefore, no major modifications to the operational versions of the SAA

were made. There are lingering localized errors to work on, such as virga and bright band effects; but for now, forecasters can be alerted to their effects by the natures of the patterns (rings and intense gradients) in the SAA output.

Interaction with water resources managers at a series of meetings with water operations managers, people from river forecast centers, and NOHRSC researchers and active communications with water managers is leading to better understanding of the NEXRAD SWE products and how they may be integrated into the operational NOHRSC SNODAS system that will replace the SEUS.

3.3 SAA Supplemental Report (Holroyd, 1999)

This report documents an extension of work done on the SAA development for NEXRAD WSR-88D radars. An expansion of operational testing using Level III data shows that the algorithm continues to be robust. For the 1998-99 season (November-April), a variety of accumulation products were made available on the Internet for five radars across the Dakotas and Minnesota, including a regional mosaic. The Z_e-S relationship used was 150 $R^{2.0}$. That network was expanded to 10 radars for the 1999-2000 winter season.

Issues involving the vertical gradient of reflectivity and snowfall continued to be prominent. The vertical gradient of falling snow was used to generate a range correction which boosts integrations by a factor of three at 230 km. The use of this correction scheme appears to be appropriate when compared to surface observations. Experimental work was performed that reduces the effects of virga at far range. A visualization routine was created to display the vertical gradient in the lowest 5 km of altitude above the radar. Parts of that routine may be useful in future efforts to reduce virga and bright band effects.

Work should continue to examine the vertical gradient issue to identify the best style of algorithm. One that can simultaneously adjust for virga, bright band, and range correction would be preferred. In addition, individual radar hybrid scan and occultation files can be adjusted by hand editing to reduce localized errors in the SAA product, caused mainly by anomalous echo enhancements or reductions.

4. SAA DEVELOPMENT

4.1 Background and Approach

The SAA was developed from 1995-98, with support from the WSR-88D Operational Support Facility (now Radar Operations Center) in Norman, Oklahoma. The development was thoroughly described in Super and Holroyd (1998), and the detail of that report will not be repeated here. Nevertheless, some background is needed because the SAA lies at the heart of the

GCIP taskings. Much of the following was taken from Super and Holroyd (1997b). Enhancements to the SAA since its development and initial implementation will be elaborated in section 6.

As stated in the Introduction, the SAA endeavored to provide quantitative precipitation estimation (QPE) for snow rather than rain. The role of the PPS is to estimate rain only. Radar remote sensing of frozen precipitation presents challenges different from sensing rain. Snow has more complicated shapes than rain as well as a different dielectric constant, resulting in lesser reflectivities. Furthermore, if the snow is melting, a spuriously strong reflectivity layer known as the "bright band" will result. Estimates are therefore valid for *dry snow* only and not for equivalent radar reflectivity (Z_e) measurements contaminated by such bright band effects. The SAA provides estimates of both SWE and SD over 1-hour (hr), 2-hr, 3-hr, 6-hr, and 24-hr periods.

Despite the limitations, the relationship between equivalent radar reflectivity Z_e and snowfall rate S may be approximated by the same power law used for rainfall (with S substituted for rainfall rate R),

$$Z_e = \alpha S^{\beta} \tag{1}$$

where α and β are empirically determined coefficients. We calibrate to Z_e rather than Z as in the rainfall equation, because of the non-Rayleigh scattering of incident radar energy by snow.

The SAA related Z_e to hourly S accumulations sampled by Universal gauges and snow boards within ~60 km of each radar. All matching of Z_e and S used the single "nearest neighbor" range bin directly over the surface observing site. The algorithm uses equation (1) to convert Z_e values (in decibels) to S for each range bin location and volume scan, to avoid a bias caused by averaging Z_e over time. We determine the power (β) and coefficient (α) by minimizing a criterion function (absolute difference between gauge measurements and radar estimates) as β is incremented from 1.0 to 3.0.

It is difficult to obtain accurate hourly S accumulations for reasons discussed by Super and Holroyd (1996). These reasons are related primarily to serious wind-caused undercatch by most existing recording gauges. Accordingly, special observations were made during the 1995-96 and 1996-97 winters in sheltered locations. These locations were geographically diverse, including Albany, New York; Cleveland, Ohio; Minneapolis, Minnesota; and Denver and Grand Junction, Colorado.

An optimization scheme, based on the work of Smith et al. (1975) and described in Super and Holroyd (1996), was used to determine appropriate Z_e-S relationships. The optimization scheme yielded β values near 2.0 for all three sites, essentially the same as the theoretical value derived by Matrosov (1992) for S-band radar, and similar to the 2.21 value from re-analysis of snow particle-size distribution data by Sekhon and Srivastava (1970). If the scheme failed to optimize, an alternative iterative process was used instead. Final results were reported (Super and Holroyd, 1998) as follows: With Z_e in millimeters^6 (mm) m^{-3} and S in mm hr^{-1}, values of α were 120 for Albany, 130 for Denver, 260 for Cleveland, and 180 for Minneapolis. An α value of 150 was

found to be adequate for most radars in the GCIP LSA-NC (north-central U.S.) area. In mountainous terrain where it is necessary to use higher tilt data or where gauges are well below the sampling beam, relatively weak Z_e values are measured. Therefore, a small α value is required to match actual surface snowfalls. Data from Grand Junction (KGJX), for example, pointed to $\alpha = 40$. Further inspection, however, showed that the 0.5-degree (°) beam was largely blocked in the sector where the gauges were located. Therefore, results at KGJX are questionable.

Hourly data generally produced more scatter when comparing radar and gauge measurements of snow accumulation than when comparing longer-period data. Storm-total estimates exhibited much better agreement with actual measurements, generally within 0.20 inches and with much better correlation coefficients. We found that surface observations of S and SD were closely associated, with correlation coefficients $r = 0.71$-0.75 for the Denver and Albany hourly data sets and 0.85 for approximately daily values from Cleveland. The best SAA estimations of SD resulted from dividing the accumulated S by the median fresh snow density for each locale. Median hourly or daily snowfall densities observed at Albany, Denver, and Cleveland for the entire 1995-96 winter were near 0.08, 0.07, and 0.06 gram (g) centimeter^{-3} (cm), respectively. This represents snow-to-liquid ratios of about 12:1 to 17:1, considerably drier snow than the commonly used 10:1 ratio.

The WSR-88D PPS has an occultation file for every radar site. This file is based on terrain data and specifies how much to add to Z_e values as compensation for any partial (< 60%) beam blockage by terrain. Based on the occultation file, the PPS uses a "hybrid scan" construction for Z_e in precipitation estimation. The original hybrid scan used decreasing elevation ("tilt") scans with increasing radar range, from 3.4° at 20-km range to 0.5° beyond 50 km. Steps upward or downward in the nominal construction, unfortunately, resulted in spurious discontinuities in shallow snowfall, in which the vertical profile of Z_e is normally maximized near the surface. Later, the WSR-88D and SAA initially used a terrain-based hybrid scan (O'Bannon, 1997), which attempts to use the lowest tilt *at all ranges* beyond 2 km, unless the bottom of that tilt fails to clear the terrain by 500 feet. Even this hybrid scan caused frequent data collection from the 1.5° beam to about 45- through 60-km range, with a discontinuity at these ranges where the 0.5° beam usage commenced. Moreover, S underestimates sometimes still occurred along particular azimuths, apparently caused by beam blockage by objects (buildings, towers, trees) not described in the terrain elevation files. To remedy these problems, an empirical scheme was developed that involves hand editing and specifies the lowest practical radar scan that can be used for each range bin while still avoiding serious ground clutter. This scheme was successfully tested with actual snowstorm data. For terrain with limited relief, such as near Minneapolis, it was usually possible to employ the 0.5° tilt beam within 20 km of the radar. Such low scanning would often be impractical with rain because of anomalous propagation (AP) echoes, but it is apparently not a serious problem with snowfall.

4.2 Early Modifications

A wind advection scheme was developed using the radar's velocity-azimuth display (VAD) vertical wind profile, which compared radar estimates from upwind range bins to those from range bins directly over the gauges. This scheme revealed no improvement. In fact, the advection scheme increased variability beyond 100 km of the Cleveland radar. Moreover, the use of a range of assumed snowflake fall speeds did not improve analysis results. This logic was removed from the SAA after the first year of effort.

The SAA was modified to convert occultation and hybrid scan files from binary representation to ASCII. This allows text editor adjustments of the values to account for surface features not detected by the digital terrain data-based algorithms that generated the initial files. It also allows use of the closest beam to the ground that does not generate ground clutter.

A simple range correction scheme was devised before testing at Albany (see section 5). Such a range correction was specified by the memorandum of understanding with the OSF and was described in Super (1998). This scheme applies a second-order polynomial multiplier beyond a stated range (like 35 km). The snow precipitation rate was:

$$S = (Z_e/\alpha)^{**}(1/\beta), \qquad (2)$$

where $\alpha = 150$ and $\beta = 2.0$ for the north-central U.S. The range correction factor F_R was, for range $R > 35$ km,

$$F_R = 1.04607 - 0.0029590*R + 0.0000506*R^2 \qquad (3)$$

Determining the appropriate coefficients for use with this correction scheme is a challenge that must be met for each climate zone. Widespread synoptic storms need less correction than shallow storms. An optional routine to remove speckle from the SAA accumulations was added using a median filter on arrays of 3 km by 3 degrees of reflectivity data.

4.3 Real-Time Data Ingest

The early version of the SAA operated on archived Z_e data, obtained on tapes from the National Climatic Data Center (NCDC). These data had the following resolutions out to a 230-km maximum range: 1 km in range, 1° in azimuth, and 0.5 dB in reflectivity. Later, the algorithm was converted to use real-time data from the National Severe Storms Laboratory's (NSSL) Warning Decision Support System (WDSS), which was hosted at several of the testing Weather Forecast Offices.

A later conversion allowed the use of real-time data from a NIDS vendor. These NIDS data were available for all radars in the north-central U.S. Despite the reduced reflectivity resolution (see section 3.1) and limited elevation scans (lowest four tilts) of these data, SAA accuracy did not suffer appreciably.

5. SAA IMPLEMENTATION, TESTING, AND RESULTS

The SAA was run locally at Cleveland and Minneapolis on WDSS systems (1996-97). SAA users indicated satisfaction after these field tests, with some need for improvement (Super and Holroyd, 1997a). The simple range correction scheme was implemented before 1997-98 testing at Albany. Bright-band contamination of SAA output was frequent at this site. Unexpectedly, however, the algorithm outperformed the PPS for cold stratiform rain in that region (Quinlan and Sinsabaugh, 1999).

Data from Super and Holroyd (1998) showed that the power β in the Z-S relationship varied little from 2.0 and that S was insensitive to these variations. The coefficient α, however, showed significant spatial variation and a corresponding strong influence on S. Figure 1 illustrates this variation with radar range for several radar sites. Invariance of β and substantial variation of α was also evident in a climatological study of rain in Mississippi (Steiner and Smith, 2000). Note that while all sites show a decrease in α with range, this decrease (slope) is highly variable between them.

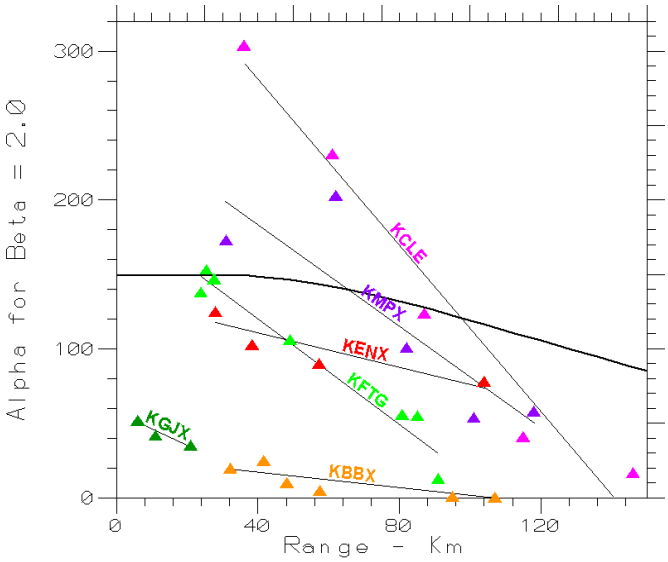

Figure 1.—Plots of individual relations for variation of alpha with range. Thick curved line is VPR range correction used for the 1998-99 season for the north-central States.

Since the radar beam becomes increasingly elevated above the earth's surface with increasing range from the radar, the depicted decrease in α also represents a decrease with elevation. Because α controls S, which is calculated from Z_e, then Z_e is also diminishing with beam elevation. This change of Z_e with height is referred to as the vertical profile of reflectivity, or VPR. The usual decrease in S with radar range is caused by the radar's inability to sample precipitation near the surface at long ranges. This situation is exacerbated with stratiform rain and snowfall, which are shallow and tend to have maximum Z_e values near the terrain (Joss and Lee, 1995). The range correction was initially formulated by constructing a VPR, then the vertical position was converted to an equivalent range using standard beam refraction. This modification was related by Holroyd (1999). The VPR profile assumed a linear decrease of about 20 percent in Z_e per kilometer height above ground. It was realized that, in certain situations, a VPR rather than range correction should be applied. Reclamation submitted a January 1997 proposal to the OSF, at their request, to pursue this change. This proposed work was not funded. Reclamation eventually developed a VPR correction for the SAA with GCIP and Reclamation's S&T Program support, and this modification will be discussed in section 6.2.

During a 1998-99 winter test, real-time SAA accumulations (S and SD products, based on NIDS input) were provided for five radars: KBIS, Bismarck; KABR, Aberdeen; KMVX, Grand Forks; KMPX, Minneapolis (the required site); and KDLH, Duluth. Accumulation updates were provided hourly for all five radars on the approximate 4-km HRAP grid. A five-radar composite was also offered. Data from five additional radars (KTFX, Great Falls; KMBX, Minot Air Force Base; KGGW, Glasgow; KUDX, Rapid City; and KBLX, Billings) were added for the cool season of 1999-2000. An 11th radar, KFSD, Sioux Falls, was added for the 2000-2001 cool season. All these data were made available in real time on the Internet at our web site http://yampa.earthsci.do.usbr.gov:8080/awards/Mn/index.html (figure 2).

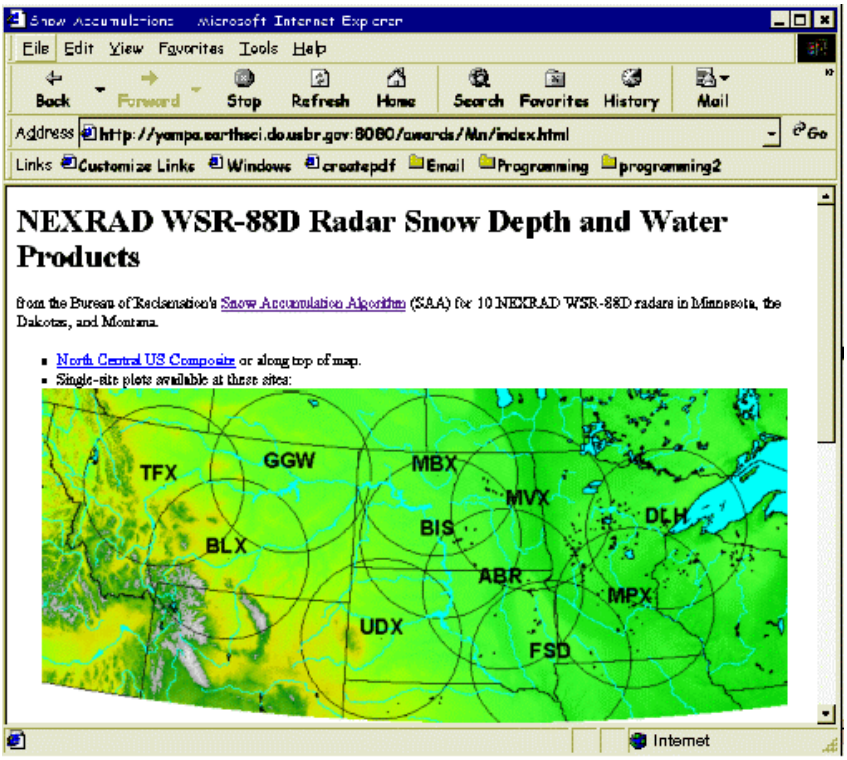

Figure 2.—North-central United States composite WSR-88D set of 11 radars from KDLH to KTFX, as displayed on Reclamation web site.

The SAA has been independently tested near Reno, Nevada; Missoula, Montana; and Salt Lake City, Utah. As is typical in the Western U.S., WSR-88D radars at these locations are on mountaintops, at elevations of 2530 m, 2395 m, and 1970 m, respectively. These radars will, thus, have more severe precipitation overshooting problems than radars in flat terrain, especially when sampling over valleys. Despite this problem, there were some encouraging results. In the Reno area, 3-hour SWEs estimated by the SAA and eight mid-range (77- to 150-km) gauges showed a high correlation coefficient r = 0.83 (Cairns et al., 1999). In Missoula, spotter-reported SD measurements within 150 km and SAA SDs showed a moderate r = 0.64, despite the assumption of a fixed snow-water ratio of 13:1 (Barker et al., 2000). The Salt Lake City area study (Vasiloff, 2002) did not use the range correction but rather multiplicative regression coefficients ("correction factors") to adjust SAA SWEs toward gauge SWEs. This was done because of the expected influence of the nearby Wasatch Mountains on precipitation growth and beam blockage, both of which are unaccounted for by the range correction. After such corrections, there was good agreement ($0.87 < r < 0.90$) between these SWEs. The principal correction was for radar underestimation in the mountains.

6. SAA REFINEMENT

6.1 Adjustments to the Hybrid Scan and Occultation Files

The radar's hybrid scan strategy (O'Bannon, 1997) is primarily based on a minimum 500-foot clearance of the terrain by the beam bottom. This scheme, which uses a terrain elevation file, was used initially. Since it was discovered that there were still echo anomalies evident after applying this scheme, a new approach was taken. Numerous cases of either widespread precipitation or clear air echoes were composited for the separate tilts for all radar sites to reveal these echo anomalies, which were caused by the beam striking surface targets and producing persistent echo enhancement (ground clutter echoes) or persistent echo reduction (preprocessing suppression from zero Doppler shift). The hybrid scan files were then constructed to specify the lowest tilt that avoided such anomalies. Case studies were run with the new hybrid scan files, and the files were hand-edited to remove further localized errors caused by echo anomalies. These procedures, though laborious, allowed for "manual" adjustments of reflectivity in the anomalous areas and the best QPE available. We call the result our empirical hybrid scan.

The widespread precipitation cases revealed radial streaking, signifying inadequacies in the occultation file. By using azimuthal profiles of SWE, estimates were made for the dB additions to particular radials beyond some appropriate range at which blockages began. The occultation file was manually adjusted, and the cases were rerun until anomalies were minimized. Unlike the original occultation files that attempted no correction if more than 4 dB additions were needed, the new changes maintained a 4-dB correction to 230 km if a vertical blockage greater than 60 percent was apparent. We preferred an insufficient correction of first tilt reflectivities to having the hybrid scan file stepping up to the second tilt, which overshot the tops of far range echoes. In a few mountainous areas where the first tilt was totally blocked, the hybrid scan files were adjusted to rise above the obstruction for the rest of the farther ranges. These changes were implemented before the 2000-2001 winter season.

6.2 Vertical Profile of Reflectivity Correction

This correction and others in the remainder of section 6 were first described in Hunter et al., 2001. The importance of some type of VPR correction is reinforced by the literature. Joss and Waldvogel (1990) assert that VPR measurement is ". . .the main problem in using radar for precipitation measurements and hydrology in operational applications." This is affirmed by several researchers, including Koistinen (1991), Galli and Joss (1991), Andrieu and Creutin (1991), and Smith (1990). Joss and Waldvogel (1990) reinforce the importance of VPR correction by asserting that it should be done before any other adjustment, such as gauge data. Hunter (1996) recapitulated these findings regarding the operational WSR-88D. The NWS embarked on a VPR correction for precipitation in general in the late 1990s, as described by Seo et al. (2000).

As described in section 4.2, Reclamation had developed a simple second-order polynomial range correction. This correction was actually formulated from a mean of several VPRs (more precisely vertical profiles of snowfall rate S, since that is calculated from Z_e at each vertical

location) from nine Minnesota snowstorms, from 1996-97 data collected at 35-km range. This relationship was transformed to be a function of range rather than elevation. It was realized, however, that a VPR correction would be superior to a range correction in certain circumstances, i.e., whenever the hybrid scan specifies that Z_e (therefore S) estimates be gathered from tilts that are stepped upward to avoid terrain blockage. This upward step worsens the partial beam filling problem described in section 5, diminishing Z_e and S compared to the desired values at the ground (depicted by figure 3). Such steps may occur close to the radar, where the minimal or zero range correction will not compensate for this diminishment.

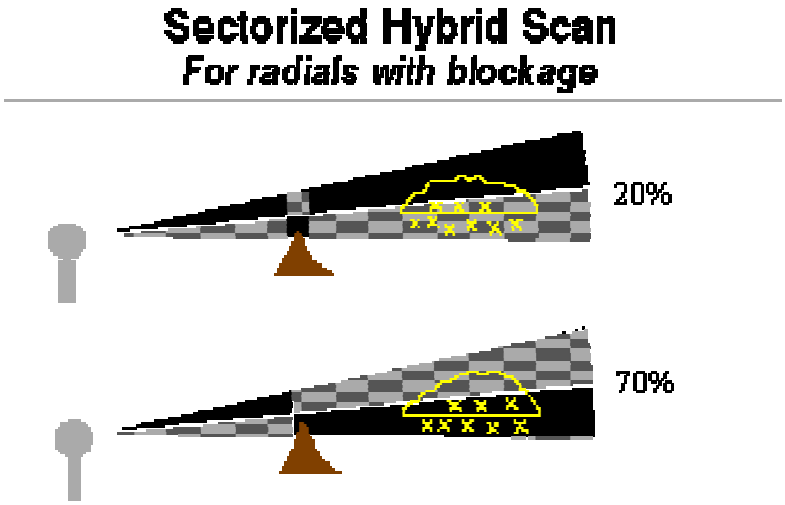

Figure 3.—Examples of hybrid scan and its possible effect on S. Top shows small amount (20%) of blockage of lowest beam so that data is still gathered beyond the blockage (checkerboard beam). Bottom shows large amount (70%) of blockage of the lowest beam so that data are no longer collected from that beam (black beam) but rather the next beam above. Yellow outline and Xs connote shallow cloud and snow particles, respectively.

Such circumstances are not present for most radars in the north-central U.S. (figure 2), because these areas are relatively flat with little significant blockage of the lowest (0.5°) beam. Three radars, however, KTFX, KBLX, and KUDX, have more than 60% blockage of this tilt in some sectors, according to the radar height (RDRHGT) program (Barker, 1994). Therefore, the artificial reduction in S by blockage and the hybrid scan step is a serious problem at these sites.

The mean range correction of α that has been applied for the north-central States in the past is shown by the curved line in figure 1. As evident from that figure, α profiles are site-specific with range and, therefore, height. Therefore, VPRs are also site-specific. Nevertheless, even a crude seasonal estimate can significantly improve precipitation estimates at midrange to far range (Joss and Waldvogel, 1989; Vignal et al., 2000). Our new VPR correction is a single profile based on many additional measurements from several different geographic regions.

The new VPR correction uses the *clearance* C (meters) between the beam center and the ground. In effect, the coefficient α becomes dependent on this C and is now termed α_C. The new snow precipitation rate, S, then becomes:

$$S = (Z_e/\alpha_C)^{**}(1/\beta) \quad (4)$$

If a correction factor F_C is defined as the ratio corrected/uncorrected, or

$$F_C = (\alpha/\alpha_C)^{**}(1/\beta), \quad (5)$$

then (4) may be expressed as:

$$S = F_C * (Z_e/\alpha)^{**}(1/\beta) \quad (6)$$

The α versus C profile is a linear least squares fit to 21 data points from four sites: Minneapolis, Albany, Denver, and Cleveland. This fit is expressed by equation (7) and portrayed in figure 4.

$$\alpha_C = \exp(-0.0004092687 * C + 5.225943), \text{ or} \quad (7)$$
$$\ln(\alpha_C) = -0.0004092687 * C + 5.225943.$$

From equation (7), it is evident that α_C decreases with increasing clearance C. This means that in equation (7) and the VPR, a larger F_C will be applied (yielding a greater S) not only if data are

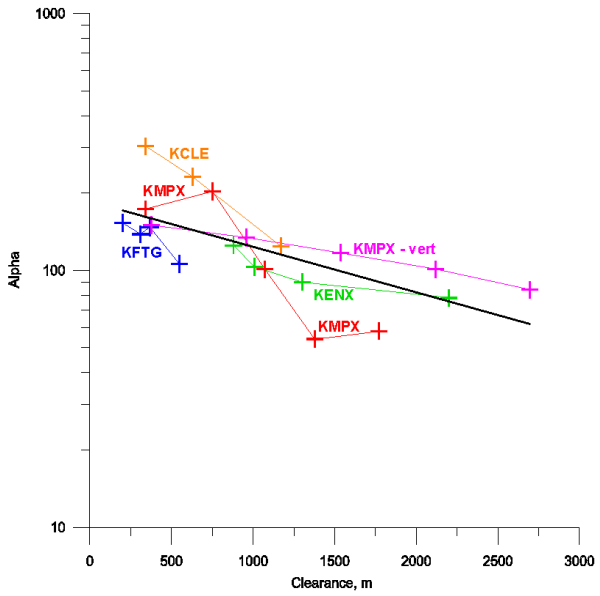

Figure 4.—Relation between α and beam clearance for several radars (colored curves). Data sources include sheltered gauges and snow boards. Black line is linear least squares fit to the exponential relationship (α_c, equation 7). VPR used for the previous range correction (F_R) included for reference (KMPX-vert).

taken from increasing range with the first tilt (0.5°), but also if taken from the second (1.5°) or higher tilts. Either application will compensate for VPR sampling limitations, but F_R does not account for the latter occurrence.

For our previously-used SAA parameters, F_C would become = $(150/\alpha_C)^{**}(1/2.0)$. Compare this to equation (3), which is for F_R. We can use these relationships to compare F_R and F_C as a function of range, as presented in table 1.

Table 1.—Range, F_R, and clearance, F_C, correction factors as a function of range in km for the 0.5° tilt (assuming flat terrain), α = 150, and β = 2.0

Range	0	10	20	30	40	50	60	70	80	90	100	110
F_R	1.000	1.000	1.000	1.000	1.009	1.025	1.051	1.087	1.133	1.190	1.256	1.333
F_C	0.898	0.915	0.934	0.957	0.982	1.010	1.041	1.076	1.115	1.158	1.205	1.258

Range	120	130	140	150	160	170	180	190	200	210	220	230
F_R	1.420	1.517	1.624	1.741	1.868	2.005	2.153	2.311	2.478	2.656	2.844	3.042
F_C	1.315	1.379	1.449	1.526	1.612	1.706	1.810	1.924	2.051	2.192	2.347	2.520

F_R and F_C are graphed as a function of range in figure 5. For ranges up to 35 km, F_R was fixed at 1.00 (no correction). It is evident that the VPR clearance correction factor results in less calculated precipitation than does the earlier range correction factor. Previously, at 230-km maximum range, values were boosted by about a factor of three; whereas with the clearance correction factor, they are increased by a factor of about 2.5. The new factor is based on more data from differing geographic regions (as opposed to just Minnesota, and 21 versus 9 data points), so it may have wider geographic applicability. In practice, the difference between the two systems over flat regions may not be noticed during real time operations. Again, however, the clearance correction factor should reduce discontinuities associated with changing tilts over complex terrain. Such a reduction would be a major benefit.

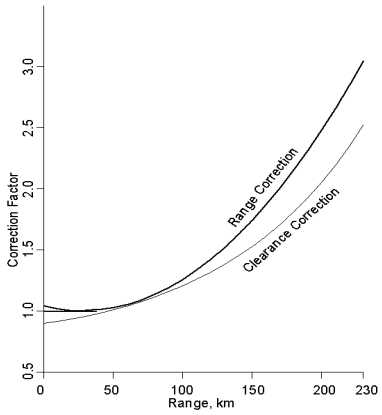

Figure 5.—Range and clearance correction factors as a function of range for the 0.5-degree beam for old range correction and new clearance correction (both with α = 150 and β = 2.0).

In the longer term, we would like to collect data and develop site-specific VPR corrections (Huggins, personal communication). Such corrections hold promise for more accurate QPEs in mountainous terrain (see section 5). For further improvement, it would be desirable to sample actual VPRs near the radar (if precipitation exists there) and use them to extrapolate from the lowest beam to the surface at long ranges in real time. Such a correction would demand considerably more computer resources.

6.3 Precipitation Type Classification

Mixed-phase precipitation has been another major hindrance to SAA accuracy. As related in section 4.1, the SAA was designed for "dry" snow only. If the melting level is aloft, the algorithm will convert data from rain areas to snowfall S because there were no criteria to ascertain if snow is melting, causing errors in SD estimates. Furthermore, in such instances, the radar bright band will exist, compounding the problem by producing significant radar QPE overestimation (figure 6). The unusually warm 1999-2000 season had an abundance of such cases. Therefore, some method was needed to identify such situations and segregate these different precipitation regimes.

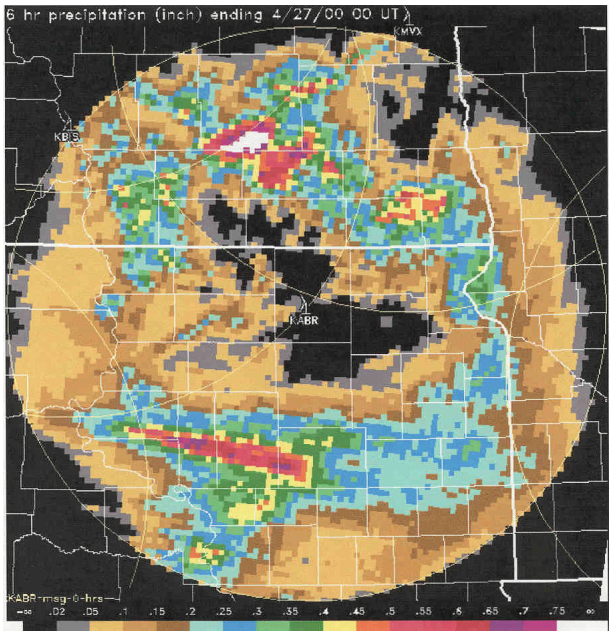

Figure 6.—S accumulation over 6 hours for the KABR radar, Aberdeen, South Dakota (at center). Ring of S > 0.25 inch is largely overestimation caused by bright band effect just below the melting (0 °C) level, which was about 2.2 km Above Ground Level (AGL) (reached by 0.5° beam center at approximately midrange, or 120 km).

Just distinguishing rain from snow, operationally, can be a daunting task, because the meteorological processes controlling the phase at the surface are often subtle. Even after an event, researchers may differ as to which processes were most influential (e.g., Steigerwaldt, 1998; Kain et al., 2000). We adopted a simple scheme that classifies radar-sensed precipitation into three types: rain, melting ice or slush (bright band), and snow. This modification is the most ambitious one undertaken in the effort to convert the SAA into a new, more generic PAA. The scheme is based on vertical profiles of temperature and moisture and is described below.

6.3.1 Bright Band Characteristics

An illustration of beam geometry in the presence of a bright band is given by figure 7. Figure 7a shows the altitudes of the lowest beam's bottom, center, and top over flat terrain. The 0 ° Centigrade (C) altitude is indicated at 2.36 km above the radar, while the +4 °C altitude is at 1.68 km above the radar. Figure 7a also indicates beam width with sample circles and the portion of the beam affected by bright band. Figure 7b graphs the portion of the beam contaminated by the bright band versus range. The curve is asymmetric because of the expanding beam diameter and loss of resolution with distance. Most rain studies show a Z_e enhancement of 5-10 dB in the bright band, leading to precipitation rates up to five times too large there (Austin 1987; Joss and Waldvogel, 1990).

The case study for figure 7 (section 6.6.3) suitably illustrates the bright band effect. The study employed data from KMPX (Minneapolis, Minnesota) between 1200 UTC on 5 November 2000 and 1200 UTC on 7 November 2000, especially during the middle 24 hours of that period. Precipitation was widespread. Local rawinsonde balloons gave temperature profiles at 12-hour intervals. The melting level (0 °C) was at about 2.4 km AGL for most of the period, associated with a strong bright band. At 0000 UTC 7 November, there was an inversion that resulted in three different melting levels. This became one level at about 1.9-km AGL 12 hours later. Unfortunately, rawinsonde temperature soundings at intermediate hours are unavailable.

For a quantitative representation of the bright band effect versus range, we use the SAA. Figure 7c depicts the ratio of SAA-calculated precipitation and actual observed rainfall for two 24-hour periods (5-6 and 6-7 November 2000) versus range. All precipitation observations at the surface were of rain. At near ranges, rain was also observed by the radar, and the SAA underestimated it. Only snow was observed by the radar at far ranges, and the precipitation was also underestimated there, probably because the large beam was only partly filled by the shallow precipitation. At intermediate ranges, melting snow ("slush" in the figure) created a bright band, enhancing the SAA calculation of precipitation and erroneously increasing the plotted ratio up to 2.5 times, in accord with previously cited bright band research. The large ratios are offset in range from the curve of figure 7b, probably because of changing bright band elevations during the 48-hour period.

Hourly VPRs (section 6.2 and figure 8) were produced for this case at 50-km range intervals for altitudes of 0-5 km above the radar. At 50-km range, these VPRs resembled a classic bright band profile with good resolution. As the range increased, bright band effects broadened vertically and weakened as the radar beam increased in diameter and resolution was lost. At still longer ranges, beyond 150 km, only the first tilt contributed to the profiles, and resulting data were from the mid-troposphere (we restricted data gathering to the first 5 km above the radar). The beam was above the bright band beyond 200 km.

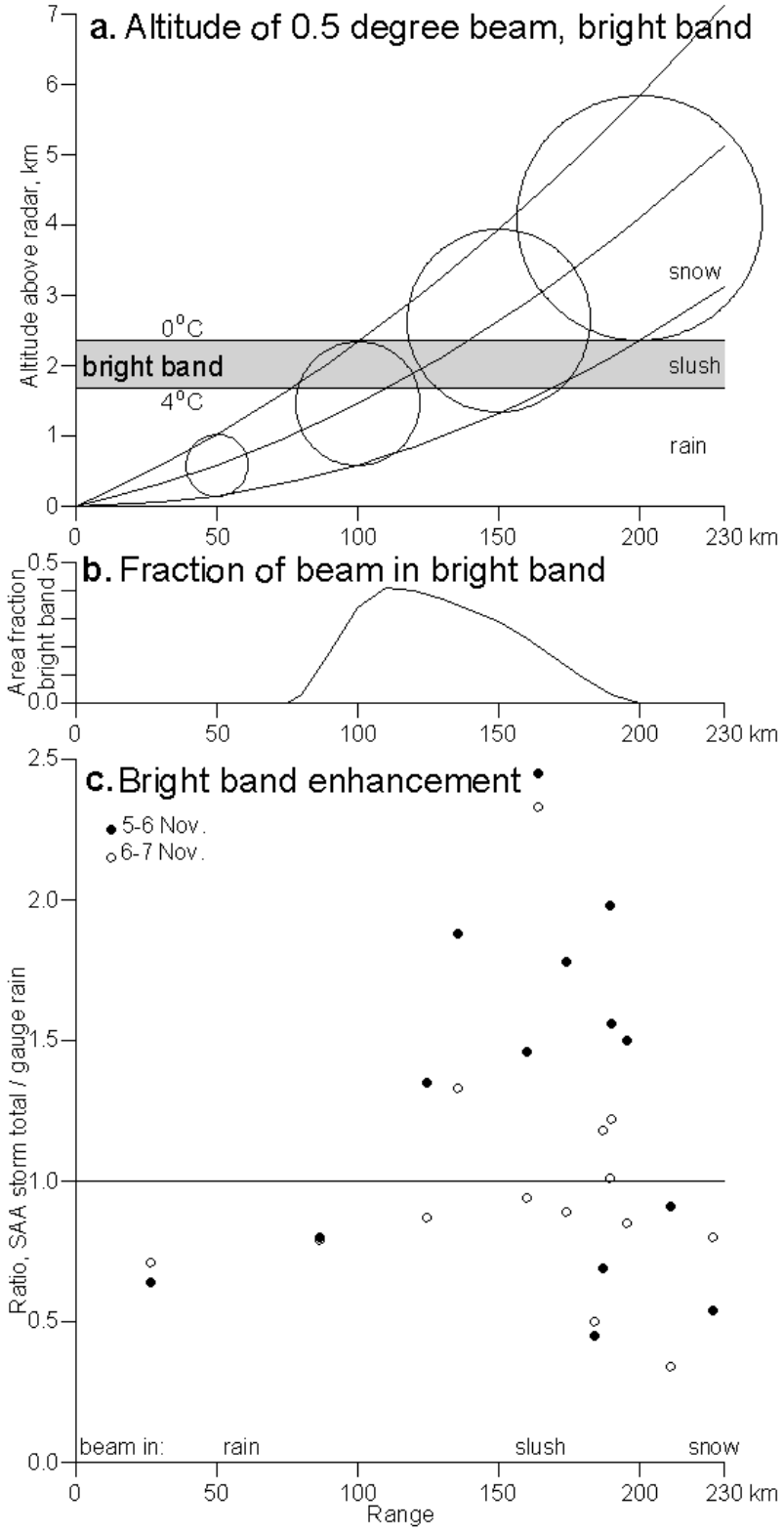

Figure 7.—Bright band effects partly fill the radar beam and create spurious enhancements of precipitation in the SAA that vary with range. See text for further explanation of the associated case study (section 6.6.3).

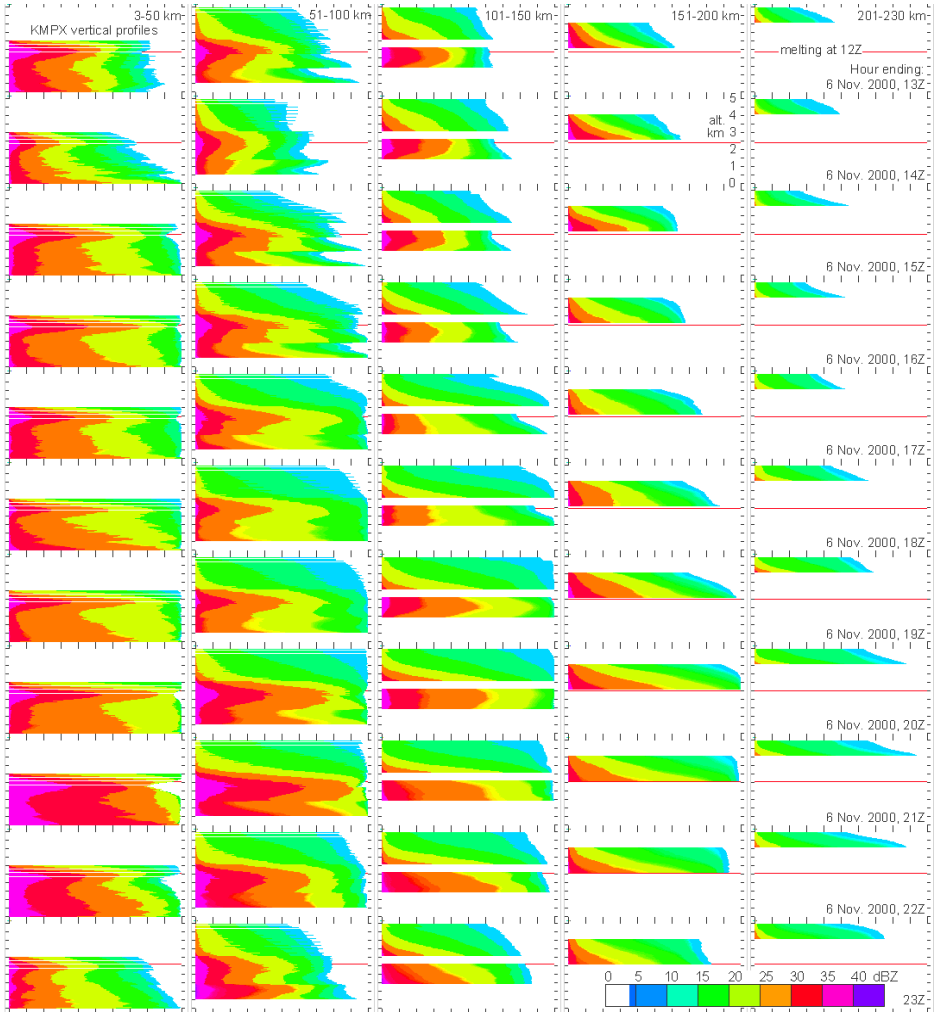

Figure 8.—Hourly VPRs with bright band at 50-km range intervals (range increasing to right), for altitudes 0-5 km above the Minneapolis radar level. Thin red line is melting level as measured at first (top) hour. Horizontal axis of each panel is cumulative percentage of range bins. Date is 6 November 2000 (same case study as figure 7).

6.3.2 Snow, Melting Snow, Rain Classification

Several cases with obvious bright band contamination were analyzed to develop a precipitation-typing scheme. The altitude of the top of the bright band was determined at near-to-intermediate ranges using all four lower tilts. It appeared that there was no contamination as long as the *entire* beam was higher than the 0 °C altitude and in only dry snow. This observation also matches what one would expect from bright band theory. Therefore, it is important to know the altitude above radar level of the *highest* 0 °C altitude. From the reference frame of a snow particle, this is the (first) melting level. Data from beam elevations entirely above this level are therefore used to generate S and SD, as with the old SAA.

At altitudes just below the 0 °C level, melting ice (the bright band) exists, and nearly any temperature profile is possible, including more than a 1-km thickness of near-isothermal air and multiple inversions. The altitude of the *bottom* of the bright band was noted and compared with temperatures from rawinsondes. This altitude was temporally unstable, as were the altitudes of other temperatures. It appeared, however, that the temperature of the bottom of the bright band was usually about +4 °C. This is in agreement with typical experiences at the surface, where wet snow is seldom seen at temperatures warmer than +4 °C. Though this threshold is more variable than the melting level, a conservative transition from melting ice to rain is declared to be at the *lowest* altitude of +4 °C, i.e., exclusively rain is assumed if the *top* of the radar beam is entirely below the lowest altitude of +4 °C. In this instance, a Z-R instead of Z-S relationship is used to produce rainfall rates. Super and Holroyd (1998) showed results near Albany, however, indicating that these two relationships may not be substantially different. Our preliminary case study results (section 6.6) confirm this similarity.

Any beam even partially sampling the layer *between* 0 °C and +4 °C is assumed by the new algorithm to be contaminated by bright band effects. These data require a different relationship between Z_e and precipitation rate. Coding has recently been added to estimate the proportion of the beam contaminated by the bright band, thereby decreasing the bright band correction with range. This coding was being tested in early 2002. We adopted the earlier, more conservative approach because of the large temporal and spatial variability of bright band structure observed in the Northern Plains. Fabry and Zawadzki (1995) also reported great variability in bright band intensities. A preliminary Z-R relationship viewing a mixture of snow, rain, and melting snow ("slush") was calculated from three case studies, as mentioned in section 6.6.

Once the precipitation type (snow, melting snow, or rain) is determined, the most appropriate Z-R (or Z-S) equation (section 6.6) is applied to calculate a precipitation amount for that radar bin. This amount is then extrapolated to the surface using the new climatological VPR and the bin clearance C (section 6.2). Then, from the terrain file, the surface elevation under the bin is determined, and its temperature is obtained from a sounding (see next paragraph). This temperature is also compared to the 0 °C and +4 °C thresholds and, using the same logic as the radar bin sample, a "final" precipitation type at the surface is prescribed. No SD is accumulated in areas of rain; for areas of melting snow, a larger snow density ρ is used for SD than is used for areas of dry snow. The entire precipitation typing is diagramed in figure 9.

We chose to extract the 0 °C altitude from vertical profiles of temperature and dew point from numerical weather prediction (NWP) models ("model soundings") instead of rawinsonde soundings. The latter may be unrepresentative if they are distant or if several hours have passed since the rawinsonde was released (recall the 12-hour rawinsonde frequency). While model soundings are subject to the same errors as NWP in general, they have additional advantages over rawinsonde soundings. First, models have recently offered soundings at hourly forecast intervals. Second, these soundings are available for many more locations than those with rawinsonde soundings. This is useful for obtaining soundings at WSR-88D sites that are not also upper-air sites.

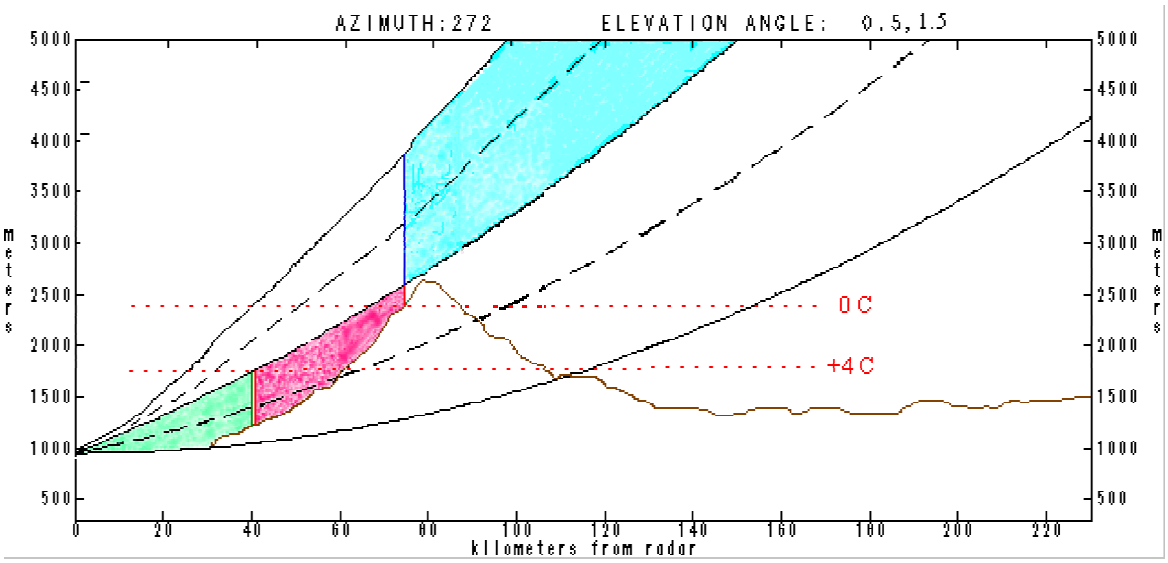

Figure 9.—Hypothetical diagram of precipitation-typing logic of PAA. Altitudes of threshold temperatures are given by dotted red lines and terrain by solid brown line. Extent of 0.5° and 1.5° beams are solid black lines, and the centers of the beams are dashed black lines. Green, red, and blue areas of the beam represent beam samples producing rain, melting snow (bright band), and snow, respectively. Snow samples, in this case, are taken from 1.5° beam, as prescribed by the hybrid scan. Other samples are from 0.5° beam.

We continuously download soundings from the National Centers for Environmental Prediction (NCEP) Eta model (12-km horizontal resolution) for the 0000, 0600, 1200, and 1800 UTC runs. Since these data become available 2-3 hours after the run cycles, soundings from the 3- to 9-hour forecast times are nominally used (at 9 hours, the next run becomes available). From each hourly sounding, the highest 0 °C levels and lowest +4 °C levels are calculated for the precipitation type determination within the algorithm. If such levels are below the ground at the sounding site, they are approximately determined by extrapolating the temperature downward at the dry adiabatic lapse rate.

Since the Rapid Update Cycle (RUC2, Benjamin et al., 1998) model is updated hourly, 1-hour forecast soundings from this model were compared to the Eta 3-hour forecast soundings for a few snowstorms in the 2000-2001 cool season. The Eta produced slightly better forecasts of low-level temperatures in these storms, so we continued to use soundings from the Eta model.

The precipitation-typing procedure is subject to numerical model errors (e.g., Evans and Grumm, 2000) that can adversely affect the altitude of relevant bright band elevations. For purposes of PAA output into the NWS river models, however, the new output will be fed into a more rigorous precipitation typing system that lessens the need to further refine our procedure at this time (SNODAS, see section 7).

There are other efforts to deal with the bright band problem. NSSL's Worldwide Integrated Sensor Hydrometeorology (WISH) group is developing a bright band identification scheme (Calvert and Gourley, 2000) that uses only radar data, updated every volume scan. The VPR adjustments of Seo et al. (2000) correct Z_e values for precipitation estimation within the bright

band, but this scheme is probably several years from implementation in the WSR-88D PPS. Nevertheless, such efforts will be monitored for possible use in the PAA.

6.4 Virga Identification

Virga, or precipitation that is not reaching the ground, has presented a continuing problem in estimating surface precipitation for the SAA and PPS. This problem is greatest at far ranges, where the lowest radar beam senses precipitation in the middle troposphere or when a dry sub-cloud atmosphere causes evaporation or sublimation. On a conventional plan-position indicator (PPI) plan-position indicator display, virga causes a "donut" pattern that indicates echoes almost exclusively at far range and high elevations (figure 10). The earlier range correction sometimes aggravated the virga problem. A vertical cross-section display of virga will appear similar to figure 11. The situation is related to the aforementioned VPR correction, except that the Z_e slope with height is inverted.

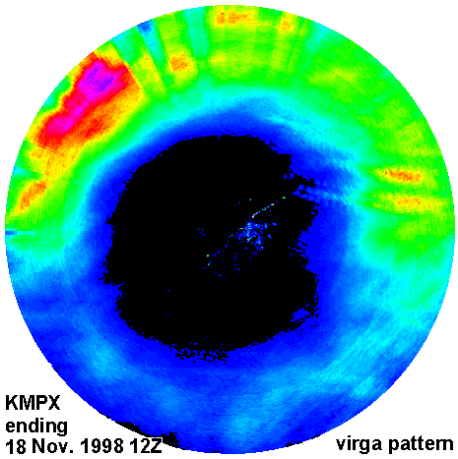

Figure 10.—PPI-like presentation of virga echo from KMPX,Minneapolis, radar.

The new algorithm applies two tests for possible virga. First, from each hourly model sounding a mean relative humidity (RH) is extracted for each 1.5-km layer above the terrain at every radar bin location. If that RH is less than a threshold, indicating dry air in low layers, a virga class flag is set, and the VPR correction is not made at that bin, avoiding an increase in the surface precipitation estimate. The current value of 70% is considered a conservatively low threshold so as to prevent elimination of valid surface precipitation. If the layer-mean RH is less than this threshold, a second, radar-based technique is executed every volume scan to refine testing for the presence of virga. If the mean RH is greater than the threshold, results of the second technique are not used, and virga is assumed to be absent.

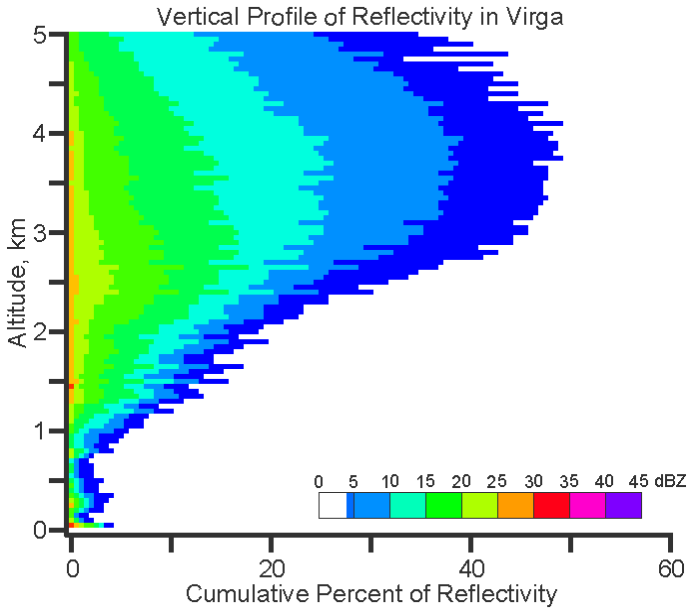

Figure 11.—Diagram of cumulative percentage of range bins exceeding a dBz value specified by color bar versus altitude above radar, for a typical virga situation.

For the radar-based technique, a cylindrical volume was defined (figure 12) whose dimensions are specified with adaptable parameters (variable names in capitals, defaults in parentheses) as follows: TOPIN, the top height (1.5 km above the radar); BOTIN, the bottom height (0.2 km

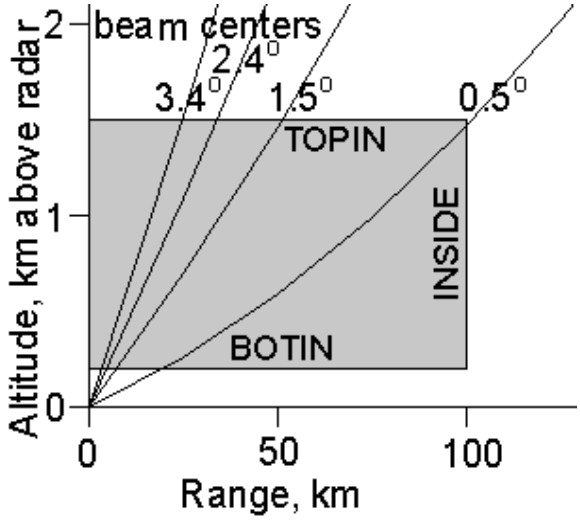

Figure 12.—Schematic illustrating virga-testing cylindrical volume with default 100-km range and 1.5-km depth dimensions and variable names, including radar beam geometries.

above the radar); INSIDE, range (100 km); and FRACTION (0.05). The 0.2-km bottom level was chosen to reduce the potential contribution of AP echoes. The fraction of the hybrid scan's radar bins within the cylinder that have a reflectivity greater than a specified minimum (DBZMIN, currently 0 dBZ_e) is then computed. If this fraction is at least FRACTION, the PAA accumulates a VPR-corrected S at all ranges. If the fraction is less than FRACTION *and* the dry air class flag for a range bin is set from the RH test, virga is probable. In this instance, precipitation is zeroed for ranges *beyond* the cylinder; echoes *within* the cylinder contribute to precipitation, but their contribution is not augmented by the VPR correction. This procedure may result in a sharp discontinuity in the S and SD products at the range INSIDE. Such a discontinuity should alert an analyst that virga is involved and that results at farther ranges may be unreliable. Such occurrences should be minimized by application of the RH test, which was developed after the cylinder test.

We are considering a future modification that will allow storms moving away from the radar to continue to contribute to snow accumulations at ranges beyond INSIDE. This might work as follows. After precipitation (echo) coverage within the cylinder has decreased to less than FRACTION, accumulations (with VPR correction) would be allowed at ranges greater than INSIDE for a time DURATION. There is no value yet for DURATION, although a value of 1 to 3 hours seems reasonable from qualitative data perusal.

Before development of the RH technique, the virga-testing cylinder was applied to both intense precipitation and obvious virga for some November 1998 storms around KABR, Aberdeen, North Dakota; KMVX, Fargo, North Dakota; and KMPX, Minneapolis, Minnesota. The default values produced no obvious change to (real) major accumulations of snow over 24-hour periods, while virga was essentially eliminated. The improvement from using the RH profile has been examined only qualitatively.

The new PAA program has been named RADAR14.F (or RADAR14.FOR). Unit descriptions of this program are detailed in appendix A.

6.5 Time-Height Diagram

As explained in the last section, parts of the PAA algorithm evaluate the volume close to the ground for virga conditions and precipitation phase changes. To help visualize the factors affecting those evaluations, a time-height diagram has been added as an output product. There

are three panels in the diagram, each showing conditions in the lowest 3 km above the radar for a 24-hour period ending at time 1200 UTC. Refer to figure 15 for the first example of this diagram.

The bottom panel shows temperature profiles from the Eta sounding forecasts, with color coding creating contours at 10 °C intervals. The 0 °C level, critical to bright band evaluations, is colored magenta. The middle panel shows hourly RH profiles from the Eta sounding, with color coding creating contours at 10% intervals. The 50% contour is colored magenta to aid interpretation.

The altitude in the two sounding (bottom and middle) panels is pressure altitude above the radar elevation. Pressure altitude usually varies from true altitude. The Eta soundings give a surface pressure, but that surface elevation may not correspond to the radar elevation, so no correction is attempted. During passage of a low pressure system, there is an elevated discontinuity at the bottom of the sounding graphs that indicates the vertical offset throughout the graph. That offset is an artifact from using the pressure altitude relation. This error does not significantly affect interpretation of the sounding patterns, however.

The top panel shows the maximum reflectivities observed at each altitude and time anywhere around the radar and at any tilt allowed by the hybrid scan file. This is akin to picking the maximum reflectivity from a constant-altitude PPI (CAPPI) constructed from a volume scan. The altitude is that above the radar, as derived for a beam under standard refractive conditions. With the top of the volume restricted to 3 km above the radar, all data illustrated are necessarily at near-to-intermediate ranges from the radar. The panels show virga, bright band, vertical gradient, and showery patterns if they are present in the data.

The PAA program imports a standard annotated diagram and then writes coded numbers within each panel. At present, the output diagram needs to be imported into the GIS software, *TNTmips*, to add a color lookup table, a size scale for printing, and final annotation with radar identification letters and start/stop dates. Sample diagrams are shown with the case studies in the next section.

6.6 Case Studies

Precipitation estimates from the radar were compared to gauge precipitation measurements for several case studies. In the old SAA, $\alpha = 150$ for dry snow was applied uniformly to all precipitation. The case studies to follow suggest that the new PAA should retain $\alpha = 150$ for snow and set $\alpha = 100$ for rain, $\alpha = 300$ for slush (melting snow/bright band). A preliminary value of $\alpha = 130$ was used for rain in some of the following case studies, however. β was kept constant at 2.0. Liquid equivalent gauge accumulations for 24 hours ending about 1200 UTC came from METAR data and from an Ohio State University web site (http://twister.sbs.ohio-state.edu). Sometimes, these two sources of surface data did not agree; in which case, the larger precipitation value was chosen. In comparing radar PAA and gauge measurements, gauge records with less than about 0.08 inch (2.0 mm) of precipitation were ignored, except in the virga case study (section 6.6.4). Such values make the ratio of the measurements too noisy.

A map of gauge locations is included as figure 13. Unlike the gauges used for SAA development, these gauges are variable in type, surroundings, and exposure to the wind. Most are Automated Surface Observing System (ASOS) platforms with heated tipping bucket gauges and a single modified Alter wind shield. Rasmussen et al. (2001) showed that for gauges with such a shield, an undercatch of about 40% of SWE may be expected with surface winds of 5-6 meters per second $^{-1}$ (s). In the Northern Plains, such winds frequently accompany snowstorms. Furthermore, the heating mechanism of the tipping bucket causes a substantial thermal plume above the gauge (Super and Holroyd, 1998), further increasing undercatch. Johnson et al. (1994) found a frozen precipitation catch efficiency for a tipping bucket gauge of only 35%. These case studies and resulting Z-R parameterizations should, therefore, be treated as tentative.

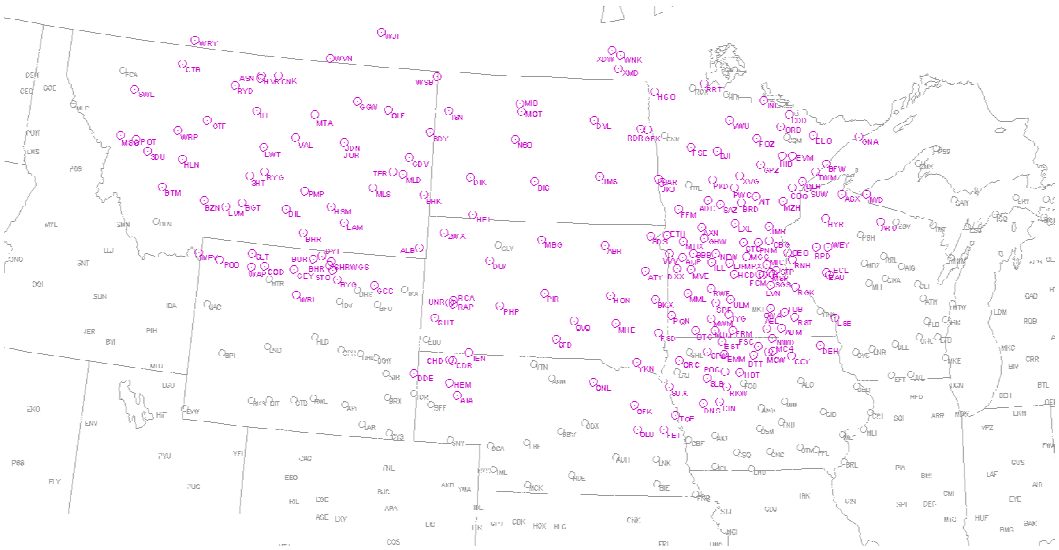

Figure 13.—Operational gauge sites (in magenta) used for surface precipitation measurements in PAA development. Gray sites are beyond radar range or do not report.

Keeping these limitations in mind, gauge precipitation is compared to radar QPEs in several figures in the following subsections. The first figure of this type is figure 16. Panels a. and c. of this figure plot the ratio of QPE from each radar algorithm (SAA and PAA) to gauge precipitation (R/G) versus range; panels b. and d. plot R/G versus gauge precipitation G. The latter panels exemplify the general tendency for radar QPEs to overestimate light precipitation and underestimate intense precipitation. In all panels, the red lines bound ratios that are a factor of two from the ratio of 1.0 (perfect agreement), denoted by the green line.

6.6.1 14 October 2000 - Predominately Rain

The first day of the cool season for which we gathered data was 14 October 2000. The standard SAA (RADAR11.F) mosaic from the web site is shown in figure 14. Some intense showers were present in North Dakota and northern Minnesota. The saturation of the colors (white, SWE > 1.5 inches) indicates that the bright band was involved. This is confirmed by the time-height diagram of figure 15. Reddish colors in the upper part of the reflectivity panel (top) exhibit

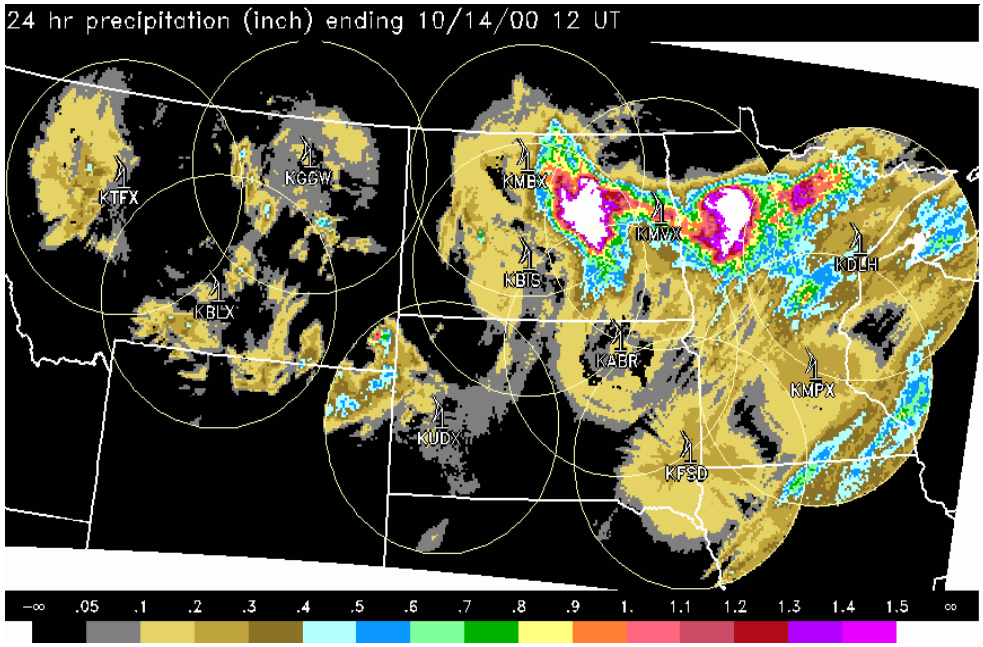

Figure 14.—SAA mosaic of 24-hour radar-estimated snow water equivalent precipitation, ending 1200 UTC 14 October 2000.

bright band signatures, contemporaneous with a descent of the melting level (magenta band in temperature panel, bottom). Earlier, weaker echoes (left side, top panel) seemed to be from AP associated with a low-level inversion (the PAA does not detect and exclude AP echoes). After a dry air intrusion aloft ended around 0000 UTC of 001014 (upper left of the RH panel, middle), showers began. Reflectivities intensified near the surface (top panel), manifesting a typical vertical gradient configuration.

The ratios of SAA and PAA estimates to gauge precipitation (R/G) versus range are shown in panels a. and c. of figure 16, for two radars sensing intense precipitation. The PAA was run in this case with a preliminary $\alpha = 130$ for rain, rather than our final value of 100. Despite this discrepancy, the new algorithm did very well in estimating surface rain, within a factor of two for all but the farthest surface station. There is no degradation with range, probably because of tall precipitating clouds, the VPR correction, or both. The PAA's bright band adjustment ($\alpha = 300$) was applied at intermediate ranges, where the sampling radar beam encountered the 0 to 4 °C layer. This adjustment appears to be effective, yielding no R/G increase at those ranges.

Panels b. and d. of figure 16 plot R/G versus gauge precipitation G. They also illustrate good agreement and that the PAA substantially reduced SAA overestimation for $G < 10$ mm.

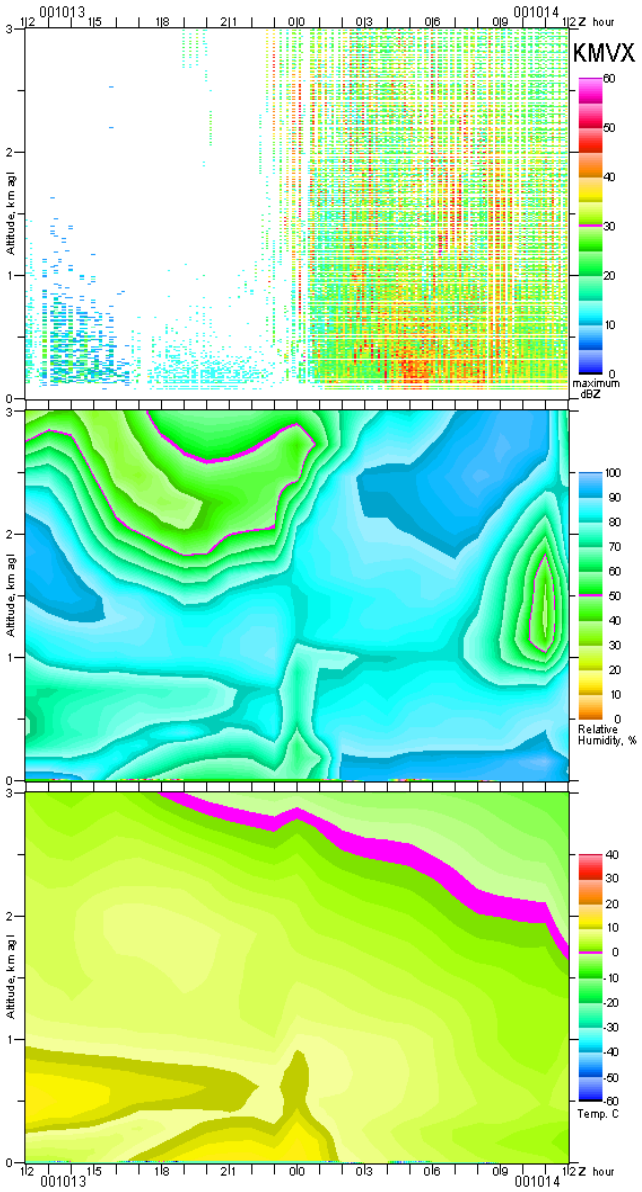

Figure 15.—Time-height diagrams of reflectivity, RH, and temperature from top to bottom. Values and units given by color bars to right of each panel. Data for lower two panels are from initialized Eta model soundings, updated every hour. Further explanation in section 6.5. All data are for radar site KMVX (Grand Forks, North Dakota), 13-14 October 2000.

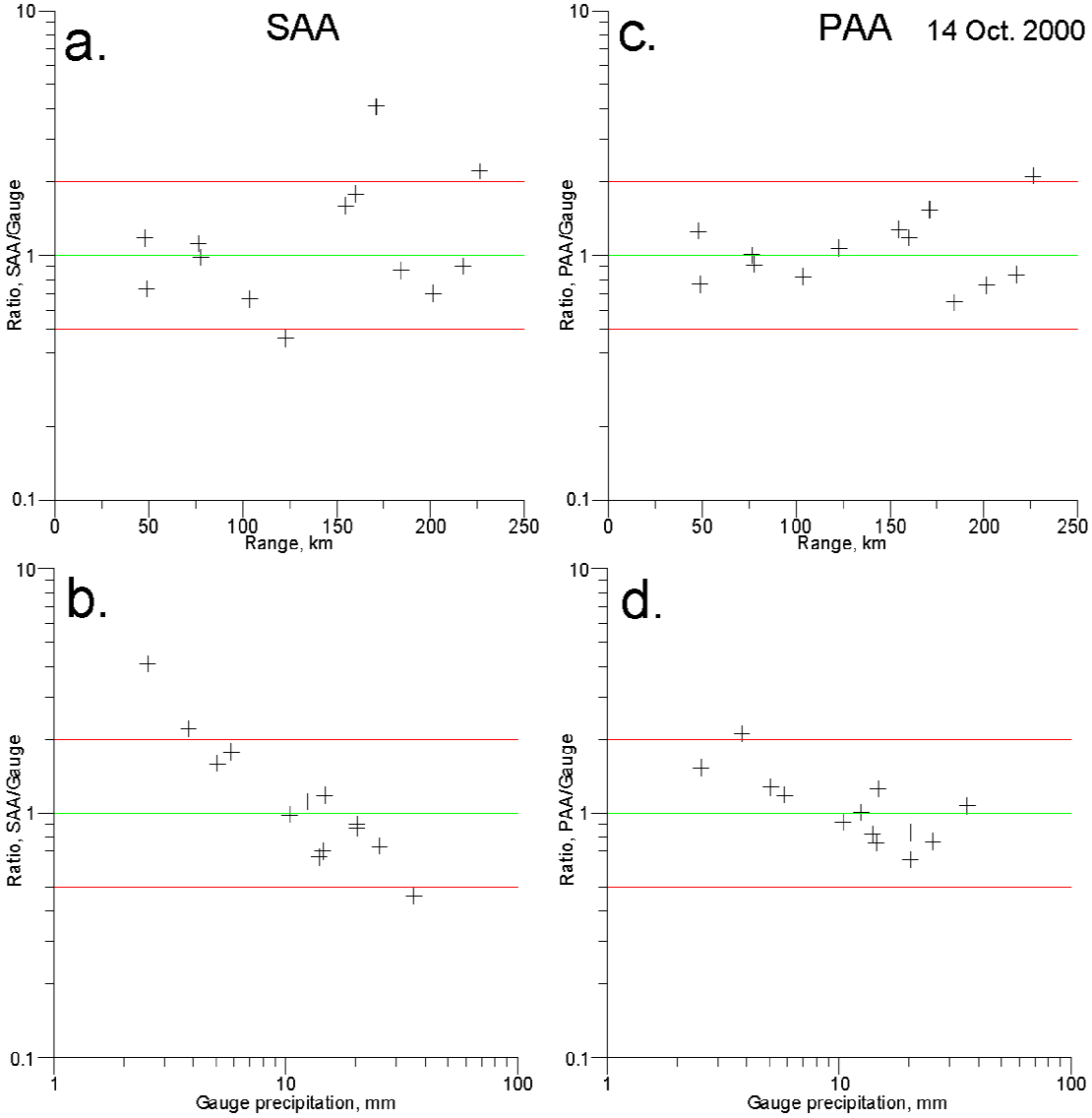

Figure 16.—Relationships of SAA (left panels) and PAA (right panels) radar estimates divided by gauge readings (R/G) to range (a. and c.) and gauge readings G (b. and d.) for 24 hours ending 1200 UTC 14 October 2000, KMVX, Grand Forks and KDLH, Duluth radars only. Red and green lines explained in text in section 6.6.

6.6.2 2 November 2000 - Predominately Rain Showers

Weather on this date was characterized by a major thrust of warm, moist air into the Northern Plains, ahead of a deep cyclone migrating north-northeast across the Dakotas. The SAA mosaic reflects this cyclonic circulation, with a precipitation-free dry slot in the eastern Dakotas. The bright band is clearly evidenced by widespread areas of saturated (white) precipitation values in figure 17.

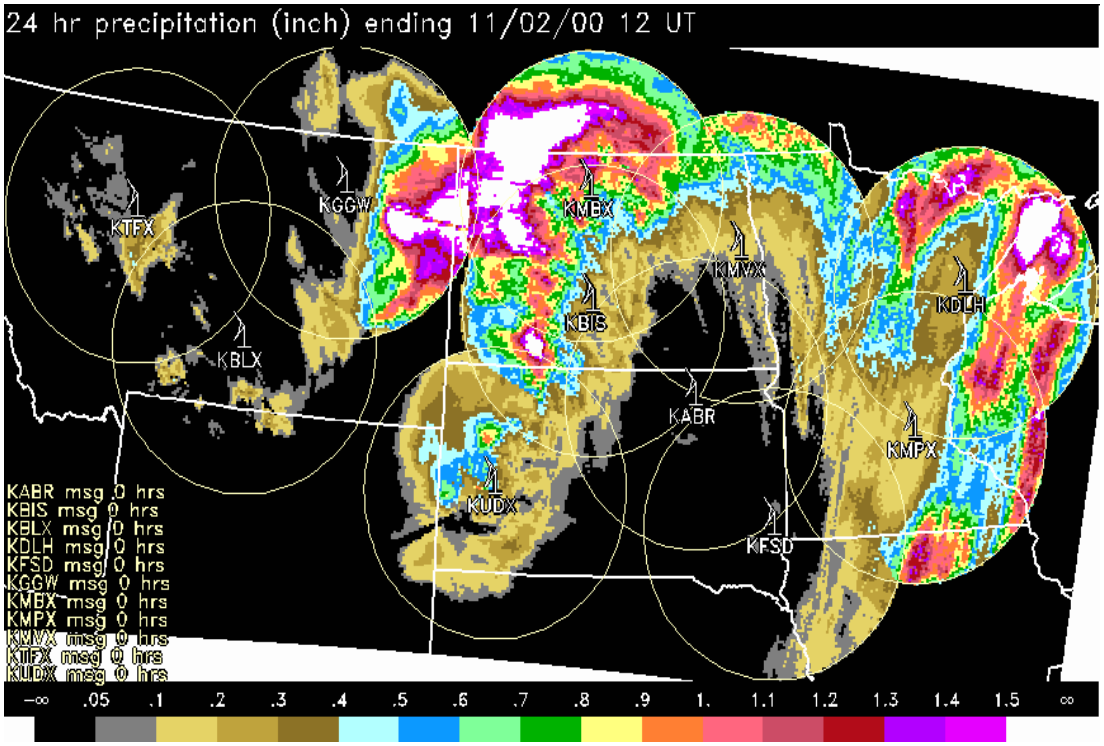

Figure 17.—SAA mosaic for ending time 1200 UTC 2 November 2000.

The KDLH (Duluth, Minnesota) time-height graph is displayed in figure 18. It shows showery patterns in the reflectivity panel (top) and a high melting level (magenta band, bottom panel). The most humid air is near the surface.

The R/G precipitation ratio versus range is shown in figure 19, panels a. and c. Much of the scatter exceeds a factor of two. (These are the points outside the red lines.) This is probably the result of showery precipitation, which was poorly sampled by the region's relatively sparse operational gauge network. There is relatively minimal degradation of the R/G ratio with range because of tall precipitating systems in this case and the effectiveness of the VPR correction with increasing range. Panels b. and d. show R/G versus G. Again, the PAA reduced overestimation at lighter gauge amounts (G < 10 mm) relative to the SAA.

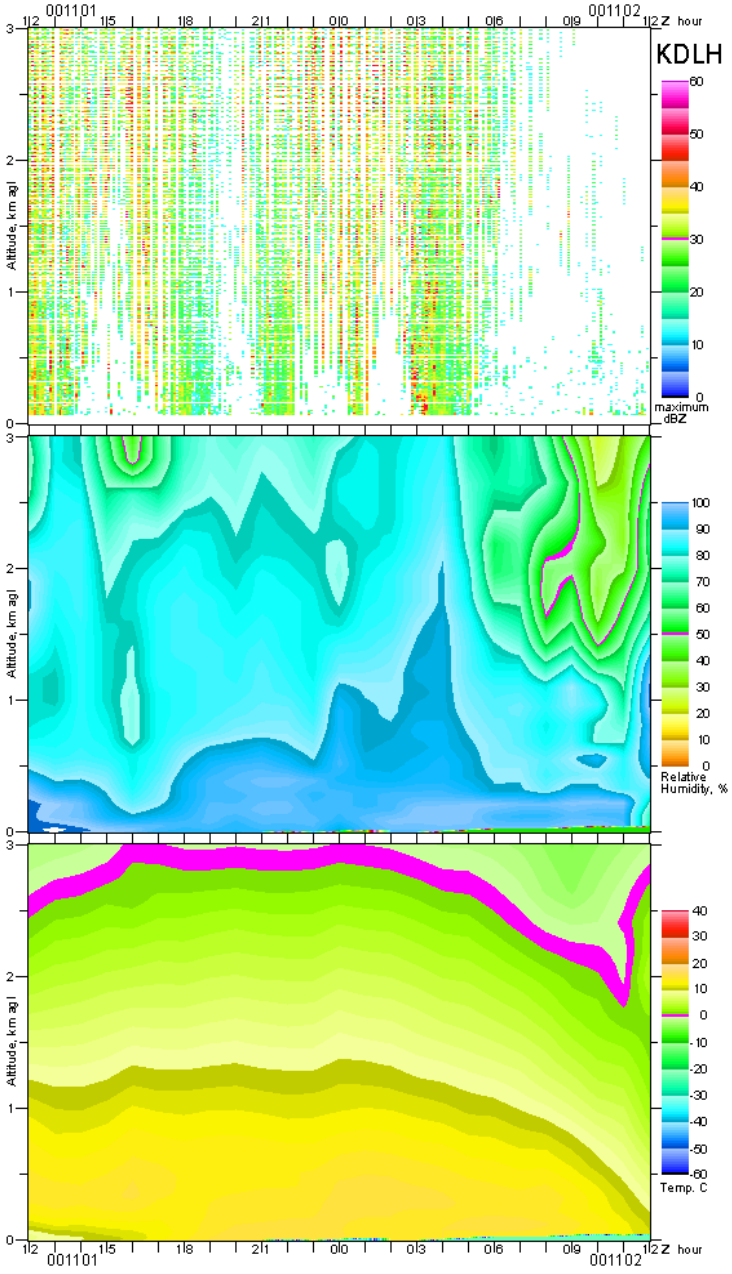

Figure 18.—Time-height diagrams of reflectivity, RH, and temperature from top to bottom. Values and units given by color bars to right of each panel. Data for the lower two panels are from initialized Eta model soundings, updated every hour. Further explanation is provided in section 6.5. All data are for radar site KDLH (Duluth, Minnesota), 1-2 November 2000.

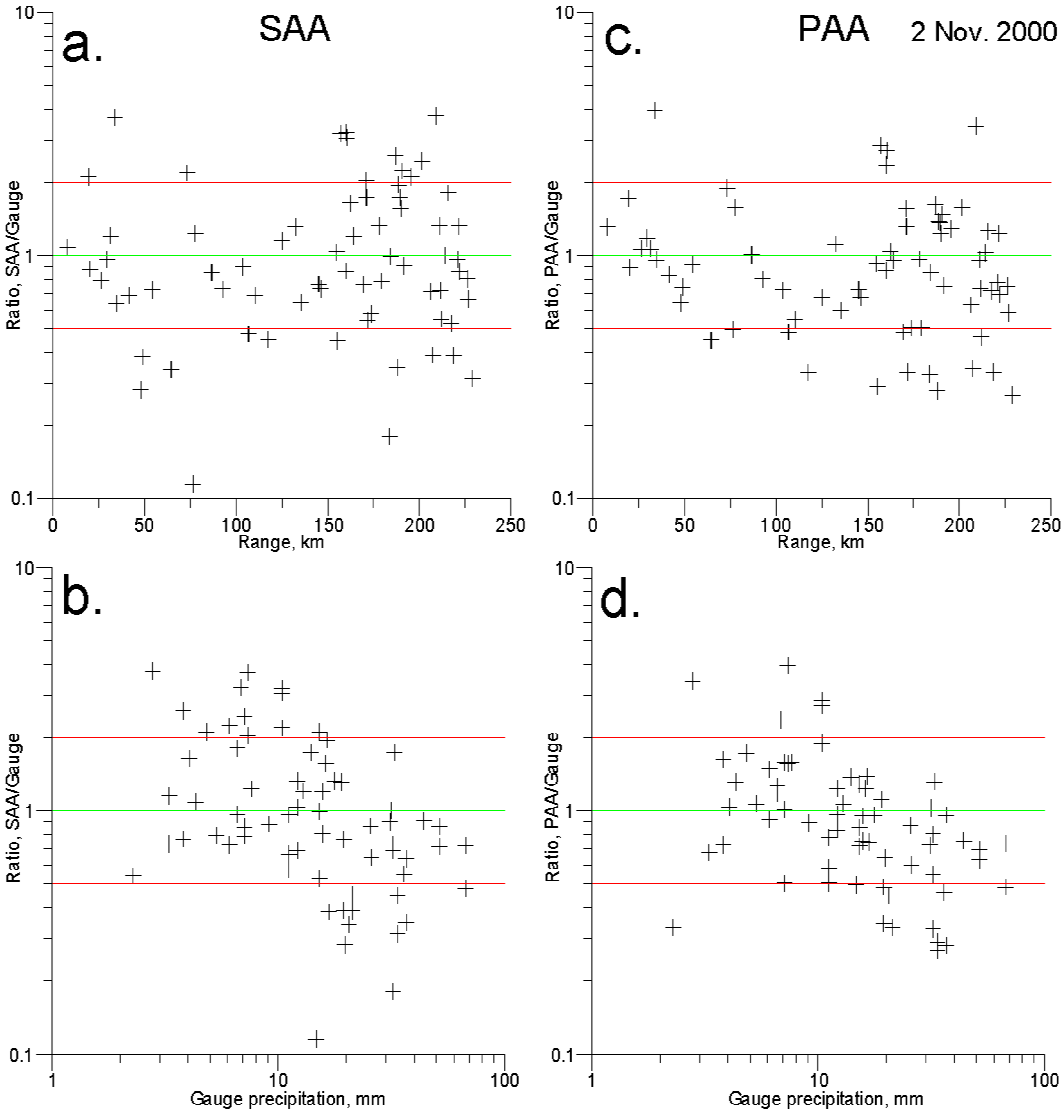

Figure 19.—Relationships of SAA (left panels) and PAA (right panels) radar estimates divided by gauge readings (R/G) to range (a. and c.) and gauge readings G (b. and d.) for 24 hours ending 1200 UTC 2 November 2000, for seven radars (KGGW, KMBX, KMVX, KUDX, KBIS, KDLH, KMPX). Green and red lines denote the 1:1 ratio and a factor of two spread from that ratio, respectively.

6.6.3 6-7 November 2000 - Strong Stable Bright Band

Figure 20 shows banded precipitation in the warm sector ahead of a surface low/trough along the Dakotas/Minnesota border. In the cyclone's cold sector over eastern Montana, there was snow. Data for several hours at KDLH (Duluth, Minnesota) were missing, so lighter accumulations are displayed there. Figure 21 for KMPX (Minneapolis) shows that the first shower in the reflectivity panel (top) is contemporaneous with a rapid erosion of a dry air intrusion in the lower 3 km of the troposphere, as shown in the middle RH panel. More continuous precipitation commences about 9 hours later. The high melting level (bottom panel) coincides with bright band echoes in the upper part of the top reflectivity panel, while vertical gradient processes intensify echoes near the surface.

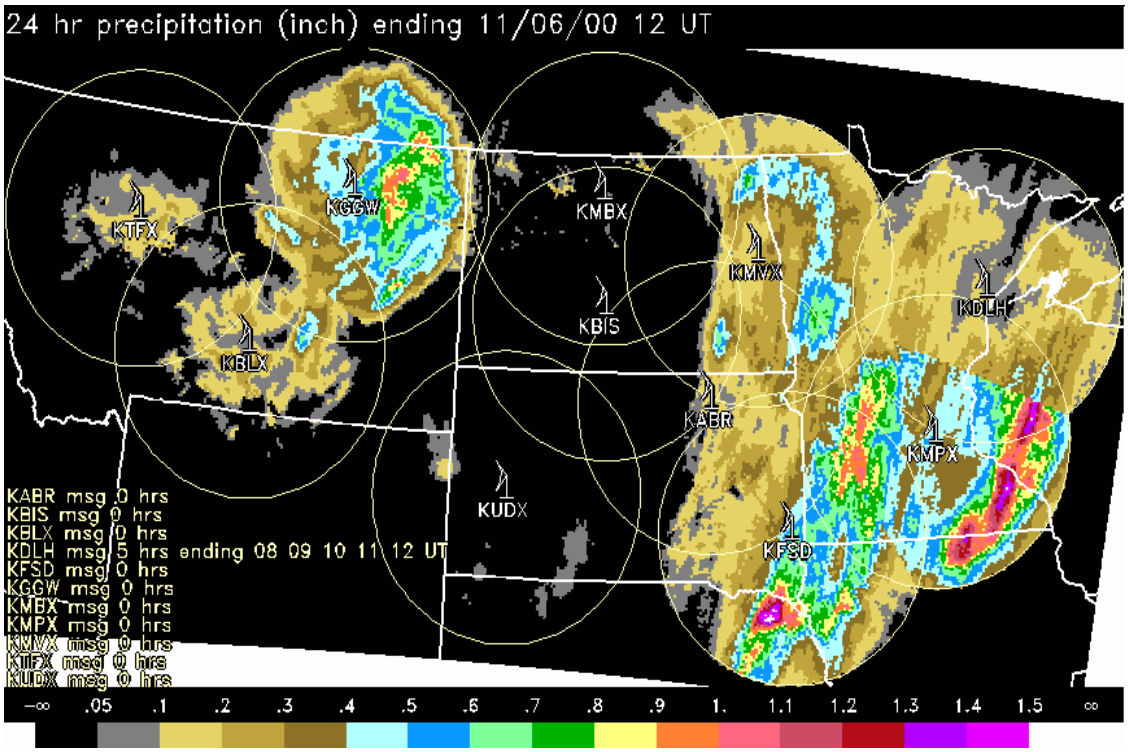

Figure 20.—SAA mosaic for period ending 1200 UTC 6 November 2000.

The next day's precipitation (7 November) is shown in figure 22. KDLH (Duluth) continued to have missing data. A strong bright band continued in Minnesota and North Dakota. The time-height graph for KMVX, Grand Forks, North Dakota, (figure 23) shows a wave-like melting band (magenta, in lower panel). The air is thoroughly moist, with white patches in the middle RH panel indicating RH values of 101%. Reflectivities in the top panel depict an intense bright band (in red) below the lowered melting level.

The R/G precipitation ratios versus range are compared for the old SAA estimates and the new PAA estimates in panels a. and c. of figure 24. The SAA underestimated the rain (near ranges) and overestimated bright band precipitation (middle ranges). The radar's lowest sampling beam

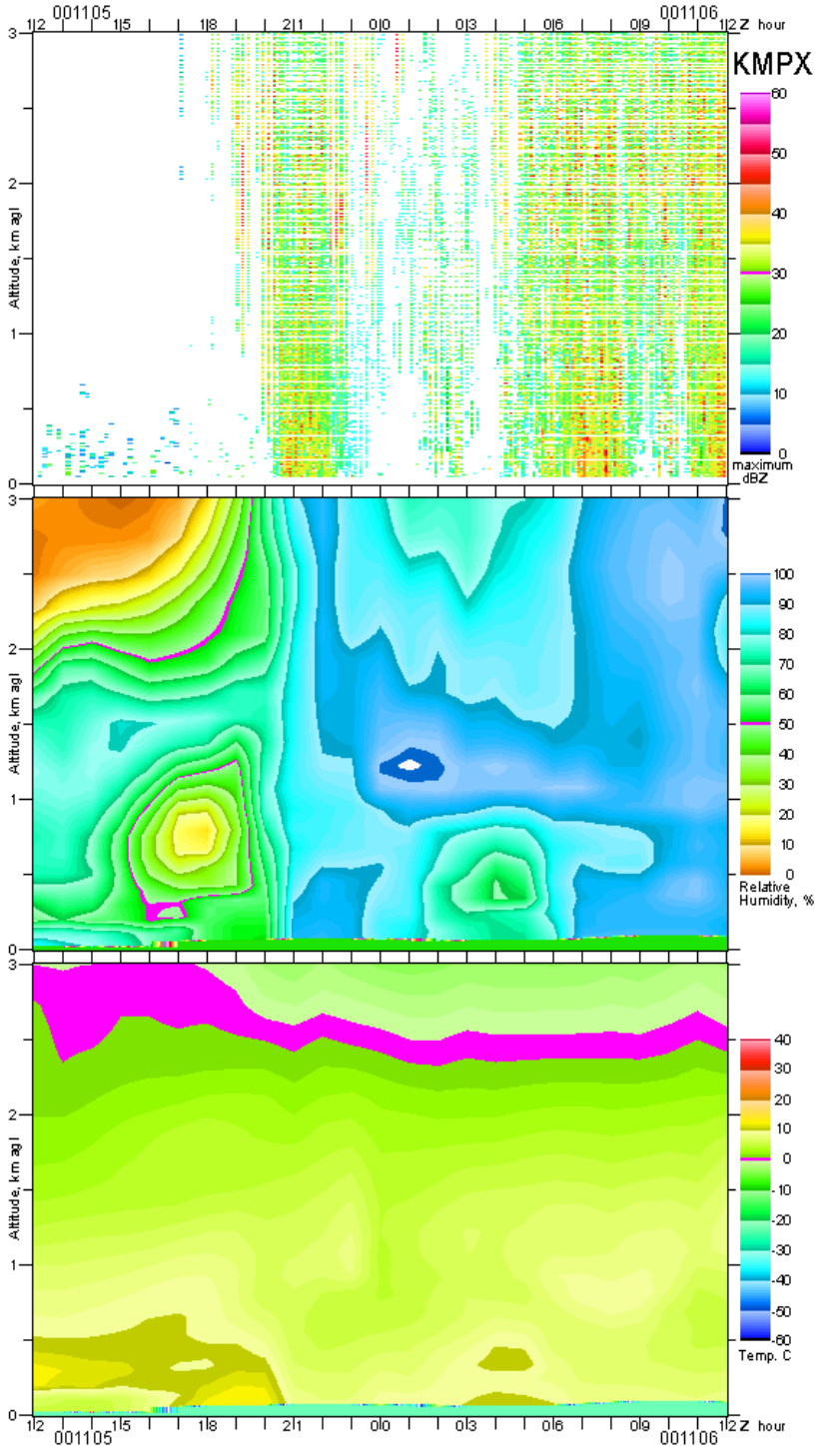

Figure 21.—Time-height diagrams of reflectivity, RH, and temperature from top to bottom. Values and units given by color bars to right of each panel. Data for lower two panels are from initialized Eta model soundings, updated every hour. Further explanation is provided in section 6.5. All data are for radar site KMPX (Minneapolis), 5-6 November 2000.

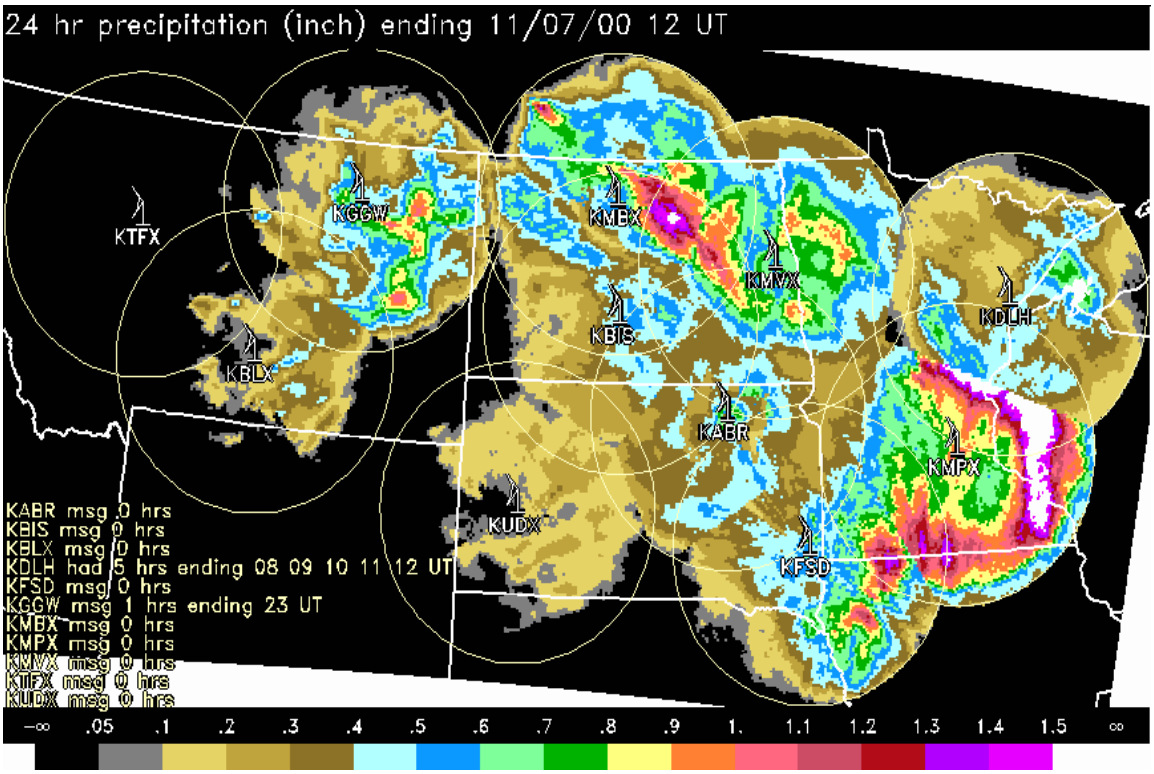

Figure 22.—SAA mosaic for period ending 1200 UTC 7 November 2000.

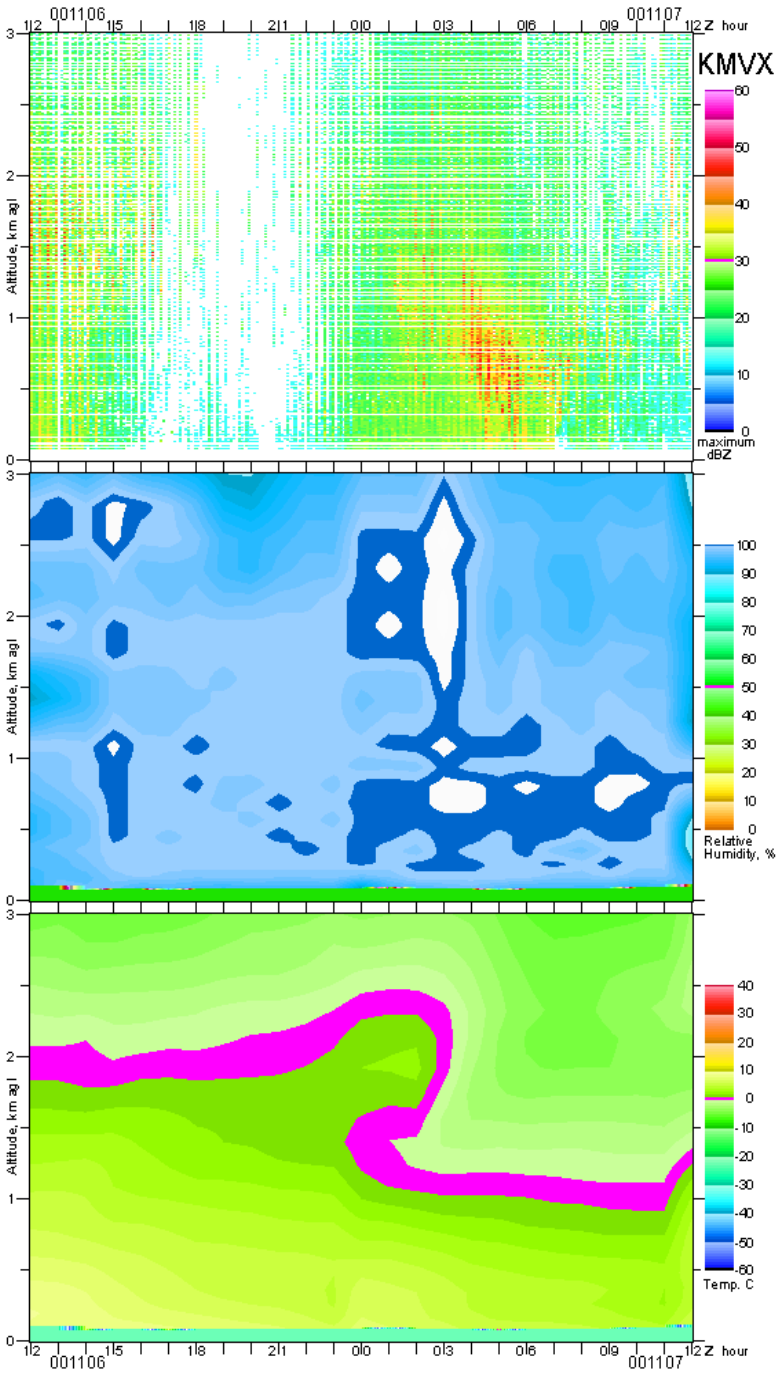

Figure 23.—Time-height diagrams of reflectivity, RH, and temperature from top to bottom. Values and units given by color bars to right of each panel. Data for lower two panels are from initialized Eta model soundings, updated every hour. Further explanation is provided in section 6.5. All data are for radar site KMVX (Grand Forks, North Dakota), 6-7 November 2000.

overshot most precipitation at far ranges; so the R/G ratios from both algorithms decrease rapidly there. The PAA yields better estimates than the SAA in the rain (< 50 km range) and less bright band overestimation bias from about 50-150 km. The SAA seems to have less underestimation than the PAA at far (> 150 km) ranges, however, perhaps because the F_R correction is greater than the F_C correction. This situation needs examination through further case study to ascertain if there is a systematic far-range degradation with the PAA.

Panels b. and d. of figure 24 depict R/G versus G and the typical overestimation of small G amounts and underestimation of large G amounts. There was again some improvement for small G amounts by the PAA versus the SAA, but otherwise there was little difference in the performance of the two algorithms.

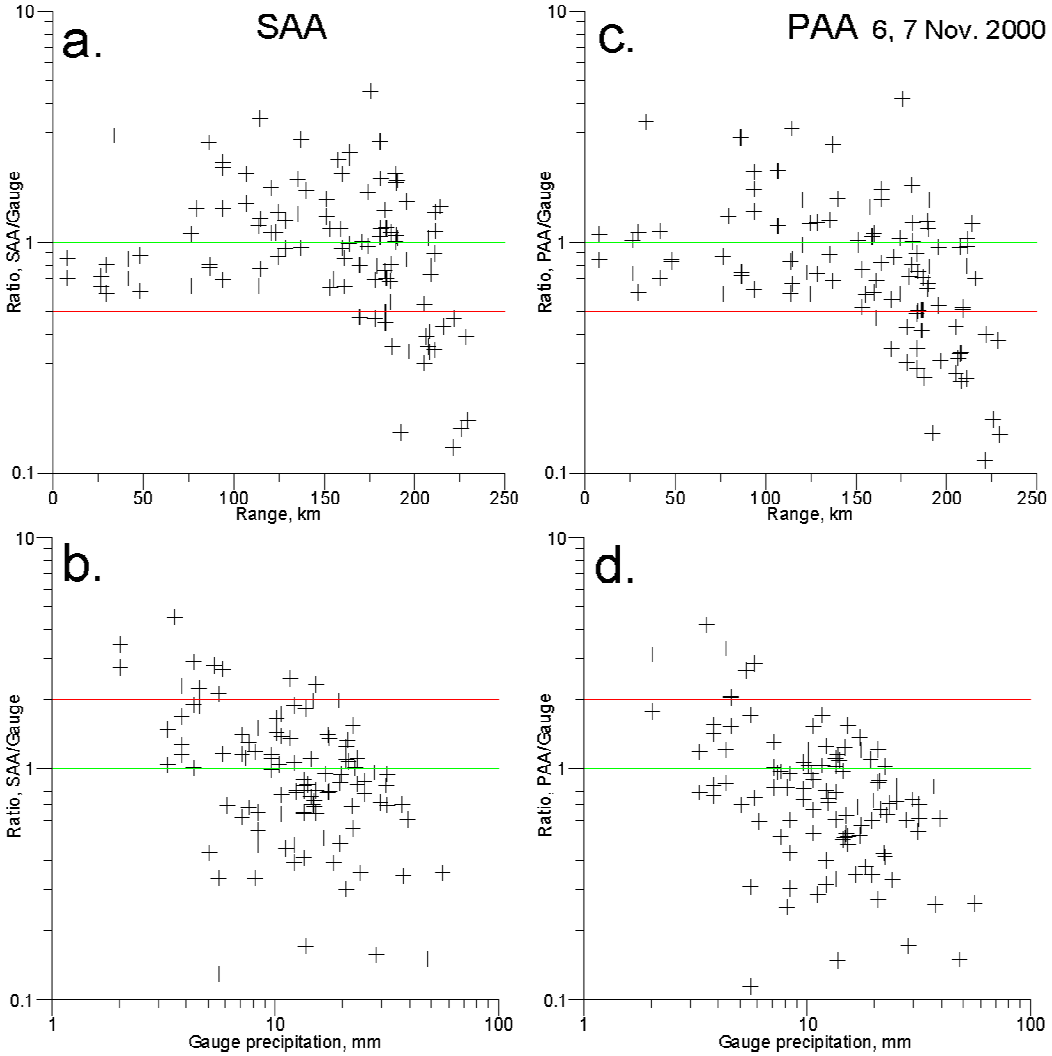

Figure 24.—Relationships of SAA (left panels) and PAA (right panels) radar estimates divided by gauge readings (R/G) to range (a. and c.) and gauge readings G (b. and d.) for 48 hours ending 1200 UTC 7 November 2000, eight radars.

6.6.4 6 January 2001 - Virga Predominant

A fast-moving minor storm system was chosen to study virga. Precipitation did reach the ground in a few places. The SAA product showed the characteristic donut-shaped virga signatures (figure 25). Though warm air existed ahead of the storm, all air containing echoes was subfreezing (figure 26, bottom panel). The middle RH panel for KDLH, Duluth (figure 26), evidences a deep tongue of very dry air just before the slow descent of radar echoes (top panel). The initial edge of this echo column is sloping and does not extend to the surface for several hours, confirming its virga nature.

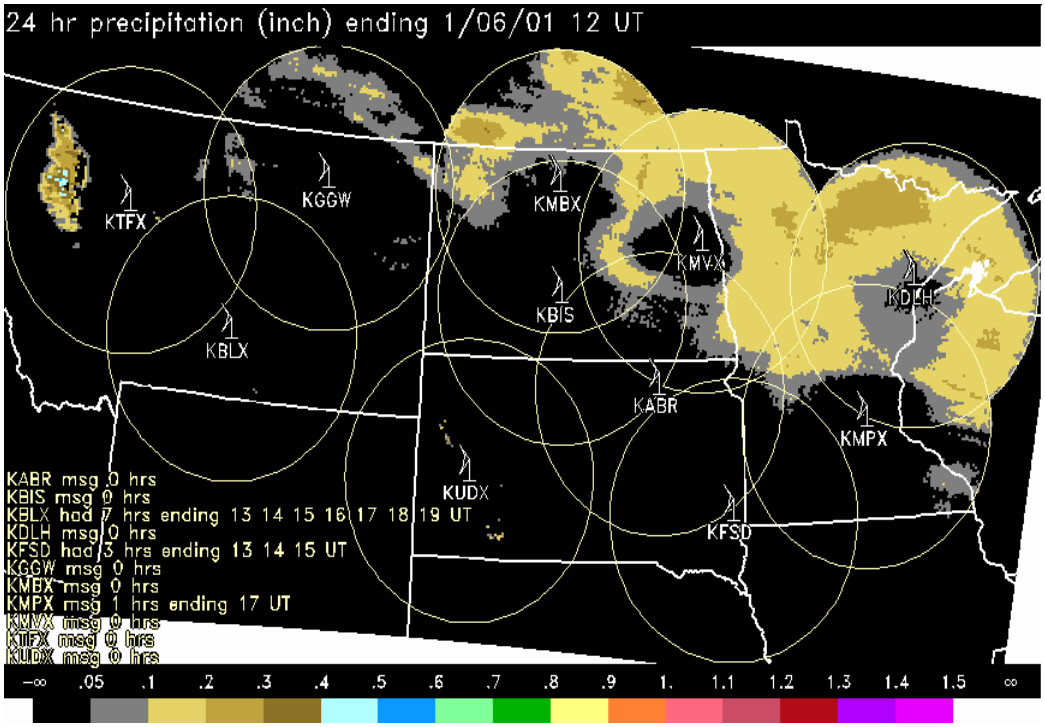

Figure 25.—SAA mosaic for ending time of 1200 UTC 6 January 2001.

Figure 27 compares gauge amounts G with R from the SAA and PAA, respectively (trace amounts are plotted as 0.08 mm). Both algorithms show poor agreement with G, with pronounced overestimation at smaller G values. Such poor agreement may be attributed, in part, to the zero G values. A more optimistic picture is given by figure 28, which plots R estimates from the SAA versus those from the PAA. The PAA's virga reduction algorithm significantly reduced the precipitation estimated by the SAA. Graphs of R/G ratios versus range that omit points with trace G amounts (not shown) also depict overestimation by both algorithms at all ranges, but a pronounced reduction of the overestimation by the PAA versus the SAA at ranges > 175 km. Nevertheless, it is evident that the virga reduction routine still needs refinement because most points are more than a factor of two different from actual amounts reaching the surface.

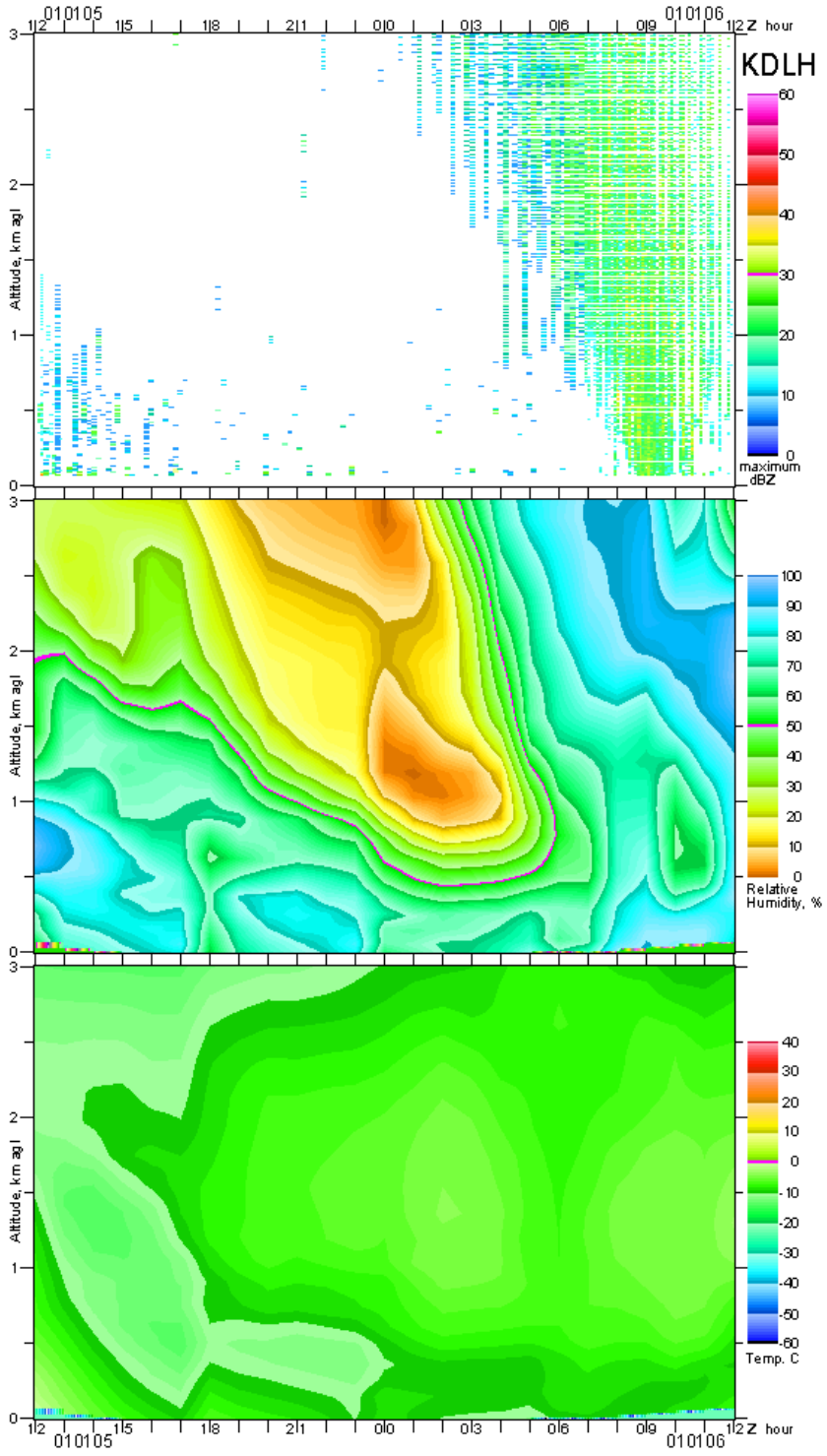

Figure 26.—Time-height diagrams of reflectivity, RH, and temperature from top to bottom. Values and units given by color bars to right of each panel. Data for lower two panels are from initialized Eta model soundings, updated every hour. Further explanation in section 6.5. All data are for radar site KDLH (Duluth, Minnesota), 5-6 January 2001.

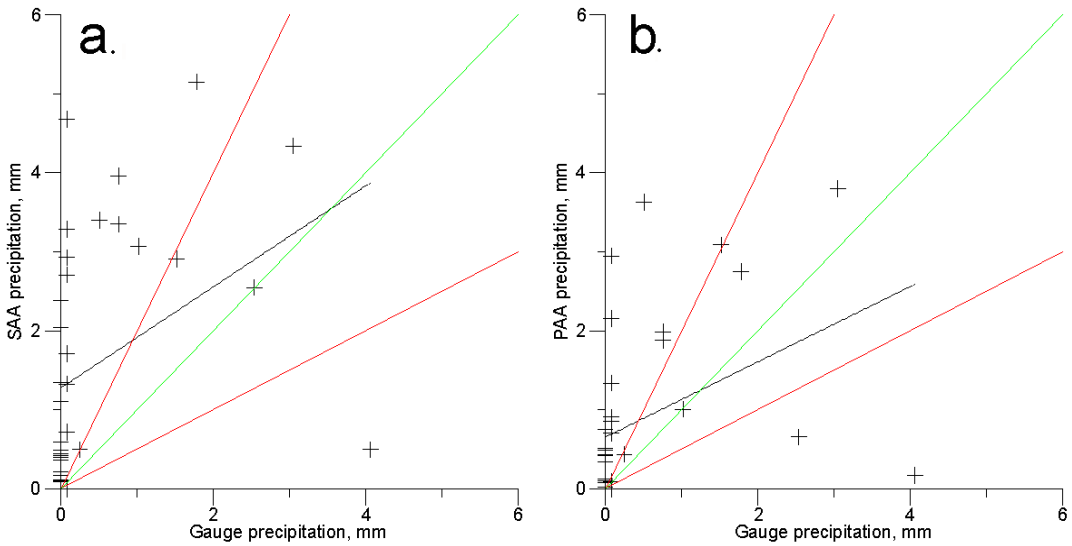

Figure 27.—Scatter plot of algorithm-estimated precipitation R versus gauge precipitation G for SAA (panel a.) and PAA (panel b.). As in figure 19, green line is 1:1 ratio and red lines are a factor of two either side of the green line. Black line is least squares fit line.

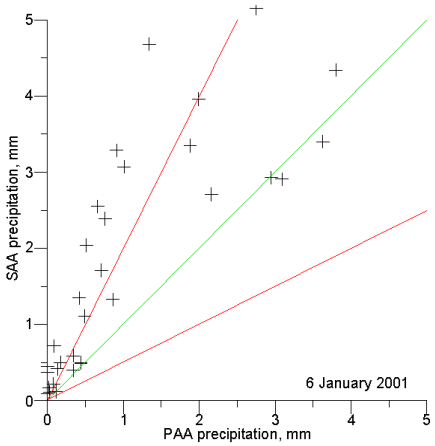

Figure 28.—Scatter plot of SAA-estimated R versus PAA-estimated R, with green and red lines analogous to figure 27.

6.6.5 30 January 2001 - Bright Band Parameter Determination

The SAA mosaic for 30 January 2001 (figure 29) indicates heavy precipitation in the southeastern part of the domain. The KMPX, Minneapolis, temperature time-height graph (bottom panel, figure 30) depicts a deep layer of above-freezing air aloft as the storm approached, with the melting band suddenly dropping to the surface in the later periods. A deep column of moist air (middle panel) coincides with the most intense echo core. The bright band also drops suddenly during the same period (top panel). The α of 300 for melting snow/bright band was selected based on this case study, with subsequent case studies confirming the accuracy of this value.

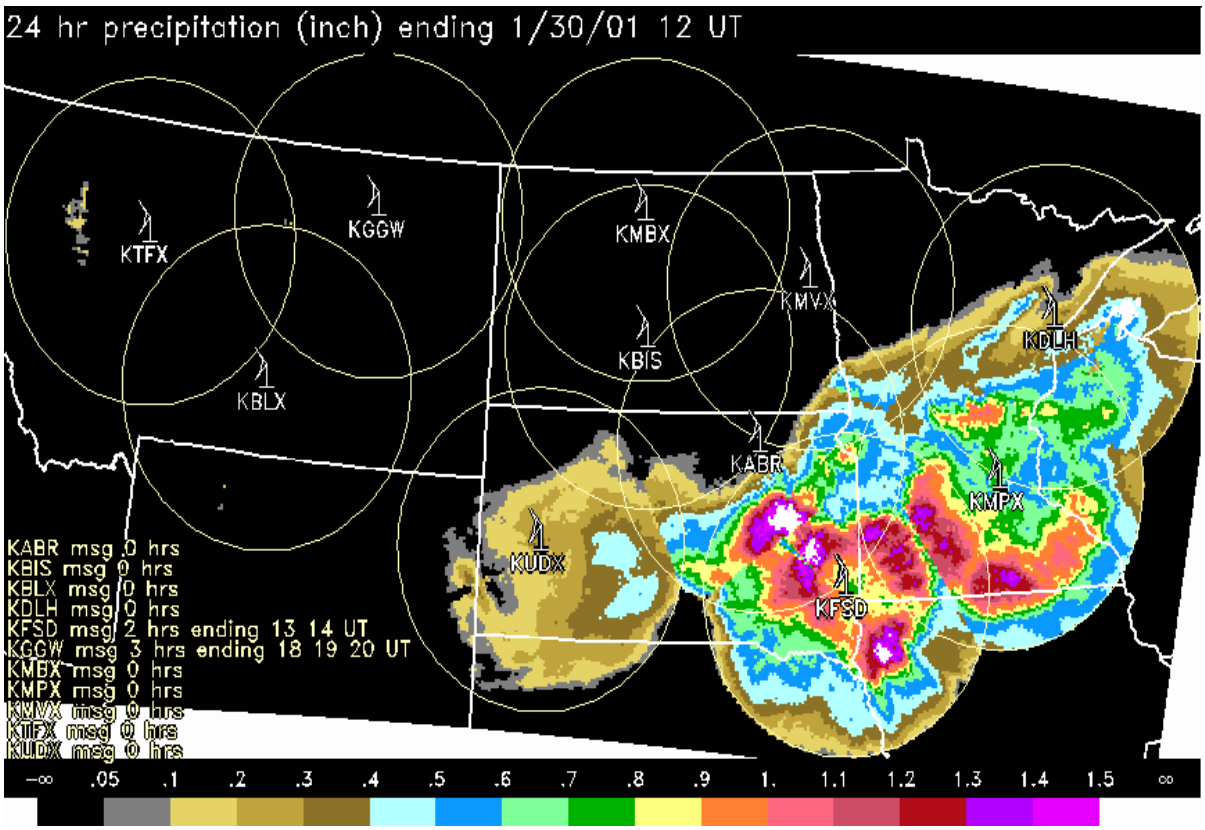

Figure 29.—SAA mosaic for ending time 1200 UTC 30 January 2001.

The R/G precipitation ratio graphs for the SAA and PAA are shown in figure 31. The PAA demonstrated significantly less overestimation from 75-150 km (panel a. versus c.), indicating that the bright band parameters caused improvement. As in section 6.6.1, the α for rain was set in the PAA at a preliminary value of 130 rather than the final 100. In this case, there was some slight PAA underestimation at near-range locations. Four gauge stations were omitted because they seem to have greatly under-reported precipitation compared to their neighbors. As for the case of section 6.6.3, there was some PAA underestimation beyond about 150 km (panel c.). Once again, the PAA reduced but did not eliminate SAA overestimation of light gauge amounts ($G < 10$ mm, panels b. and d.).

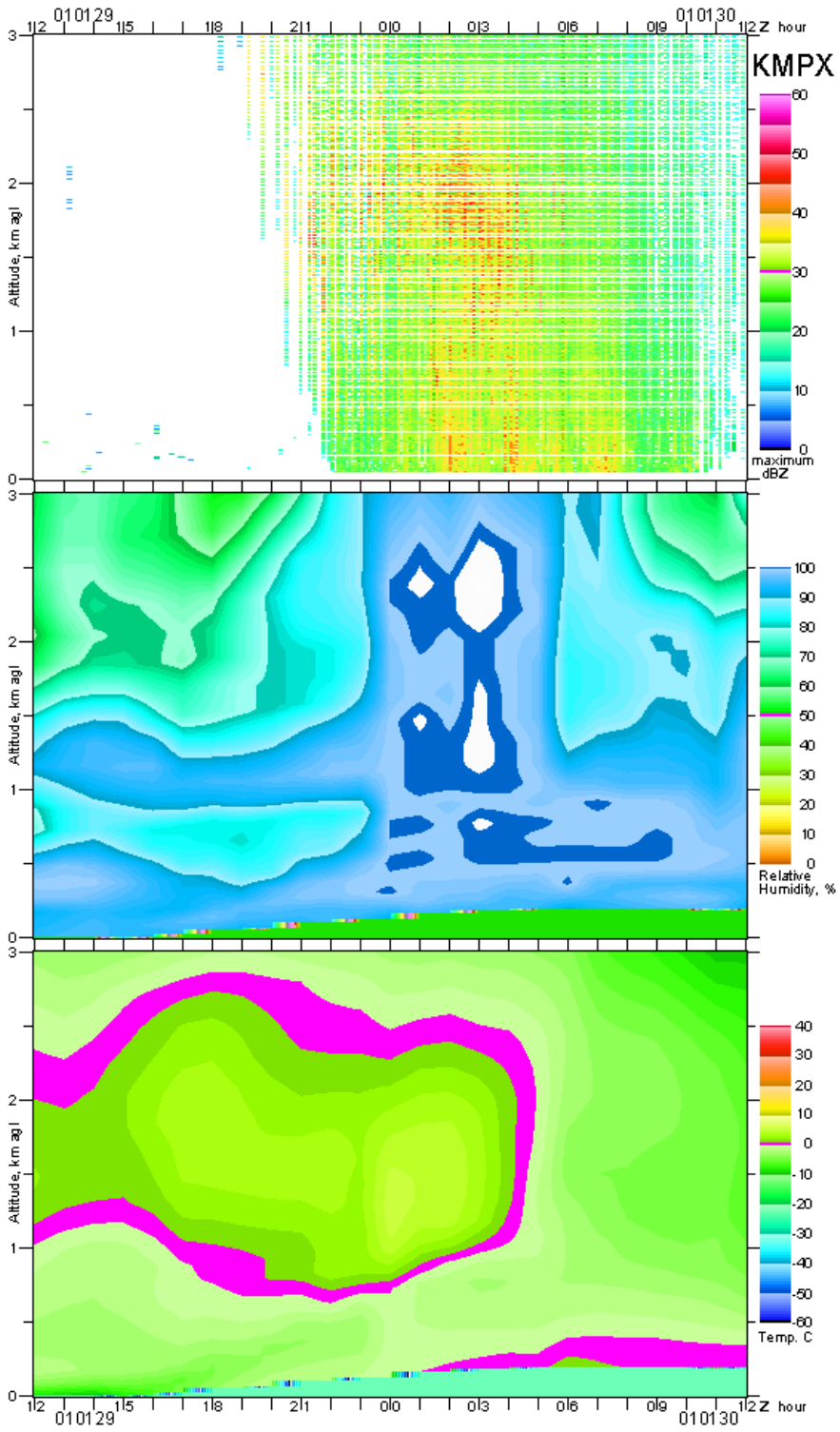

Figure 30.—Time-height diagrams of reflectivity, RH, and temperature from top to bottom. Values and units given by color bars to right of each panel. Data for lower two panels are from initialized Eta model surroundings, updated every hour. Further explanation is provided in section 6.5. All data are for radar site KMPX (Minneapolis), 29-30 January 2001.

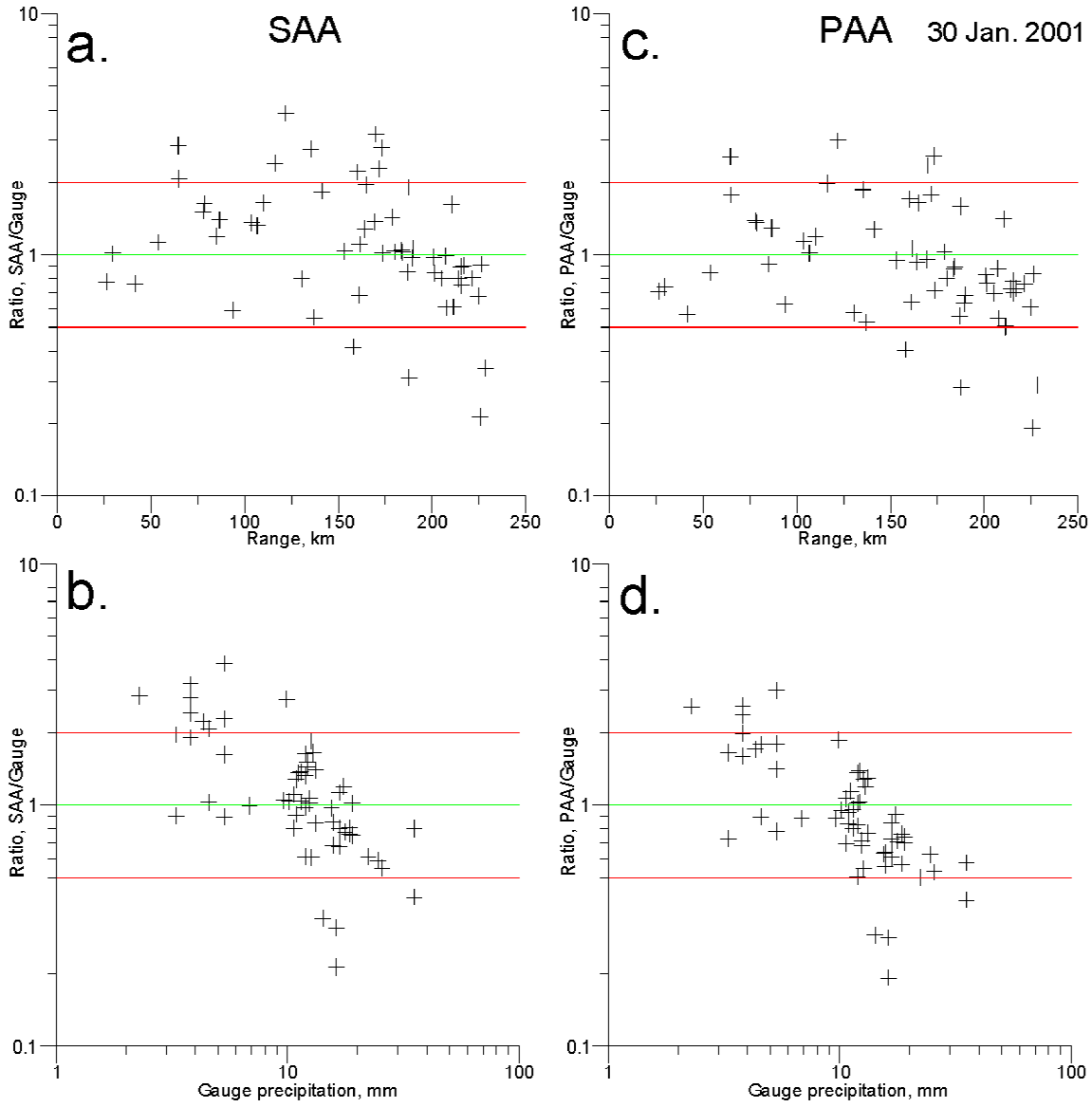

Figure 31.—Relationships of SAA (left panels) and PAA (right panels) radar estimates divided by gauge readings (R/G) to range (a. and c.) and gauge readings G (b. and d.) for 24 hours ending 1200 UTC 30 January 2001, radars KFSD (Sioux Falls), KMPX (Minneapolis), and KDLH (Duluth).

6.6.6 7-8 February 2001 - Shallow Wind-driven Snowfall

This case study had shallow snowfall confined to a narrow west-east band (figure 32). The KABR (Aberdeen, South Dakota) time-height graph is in figure 33. There was a strong vertical reflectivity gradient, with the most intense snow near the surface (top panel of figure 33). This led to discontinuities in SAA output from KABR because of the use of higher tilts at near ranges by the hybrid scan. In the lowest 1 km, where most of the precipitation was found, temperatures (bottom panel) were nearly isothermal and moisture (middle panel) was highly stratified. The humidity maximized in a layer about 1 km above the surface.

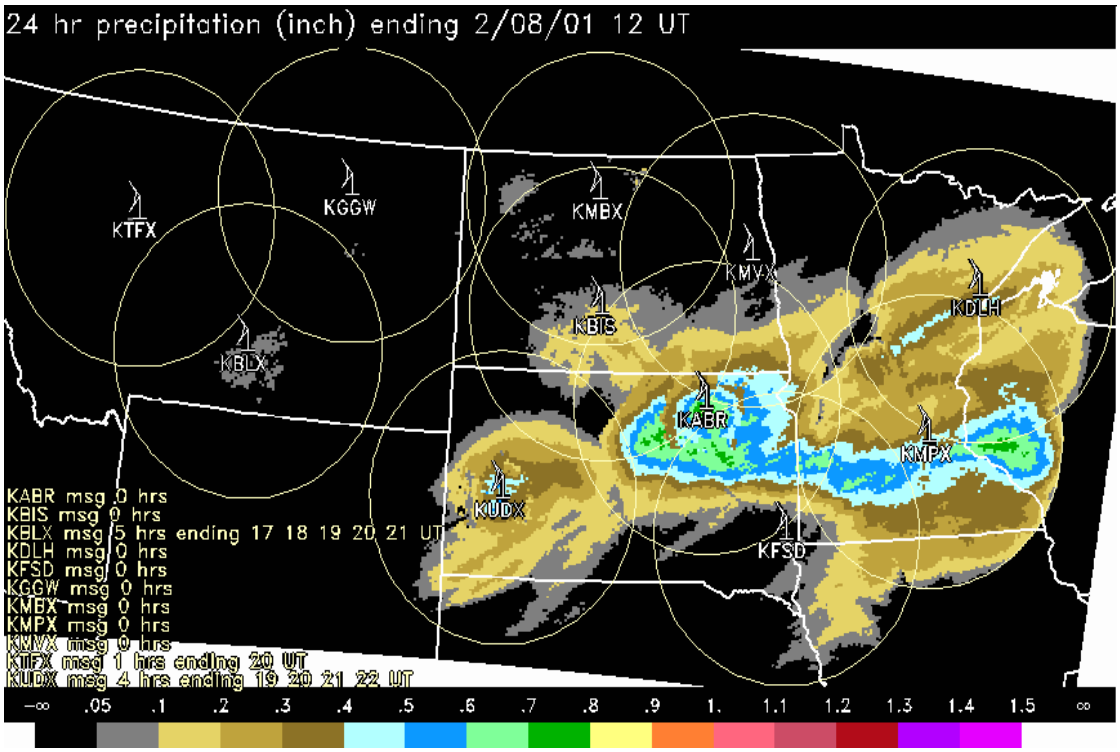

Figure 32.—SAA mosaic for ending time 1200 UTC 8 February 2001.

The R/G precipitation ratios versus range for the SAA and PAA are shown in figure 34 (panels a. and c.). There appears to be little difference between the performance of the two algorithms in this case study, except for slightly more underestimation by the PAA at far ranges. Both PAA and SAA overestimated gauge precipitation at ranges < 150 km. This type of case study will severely test any algorithm, however, because strong winds cause the *gauges* to underestimate precipitation. There were hourly mean winds of nearly 6 meters per second (m/s) in the snowfall region. As cited in section 6.6, Rasmussen et al. (2001) showed that gauge undercatch of about 40% may be expected with surface winds of these magnitudes. This situation is borne out by the PAA's R estimates, which had the poorest correlation with gauge estimates, G, of any case. The R versus G plots (panels b. and d.) again show little discernable difference between the SAA and PAA.

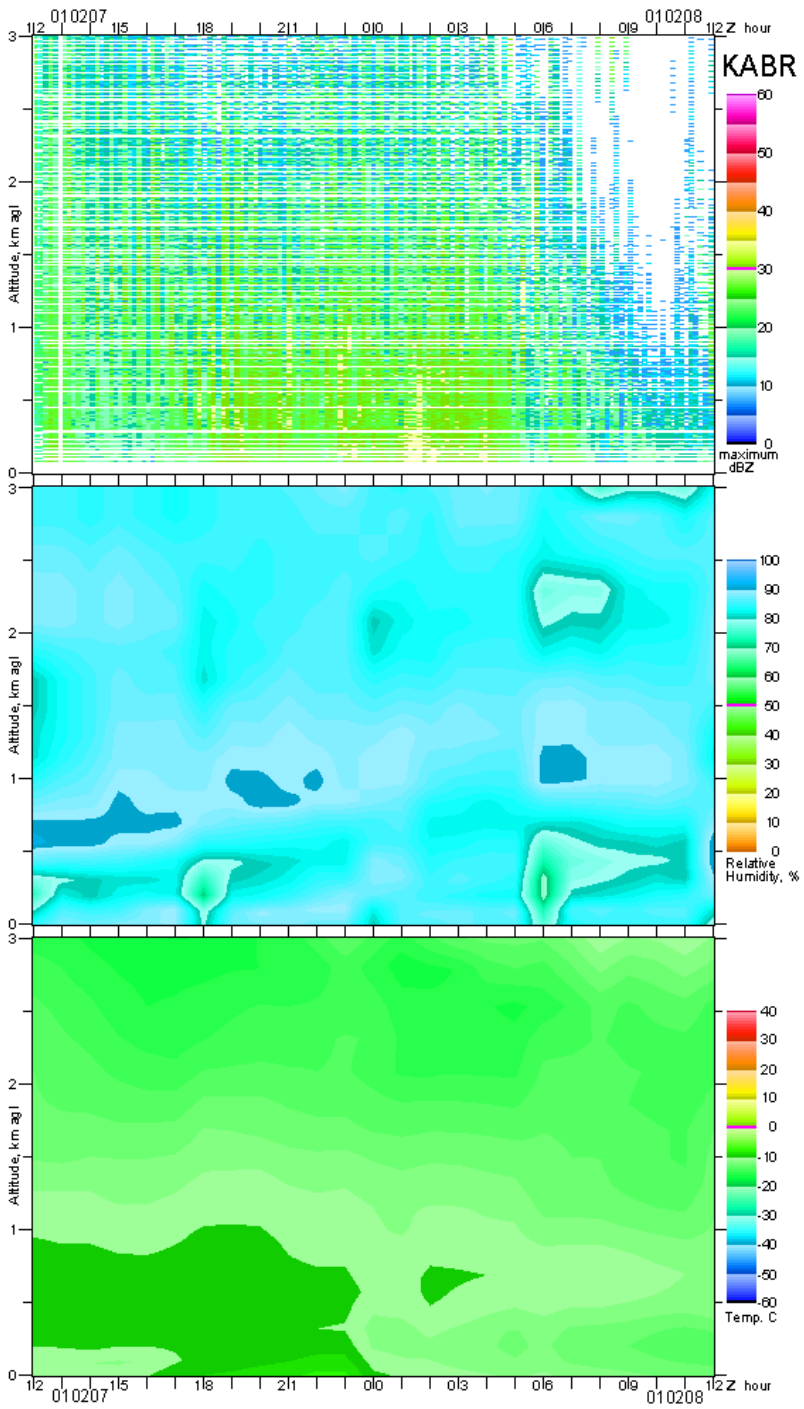

Figure 33.—Time-height diagrams of reflectivity, RH, and temperature from top to bottom. Values and units given by color bars to right of each panel. Data for lower two panels are from initialized Eta model soundings, updated every hour. Further explanation is provided in section 6.5. All data are for radar site KABR (Aberdeen, North Dakota), 7-8 February 2001.

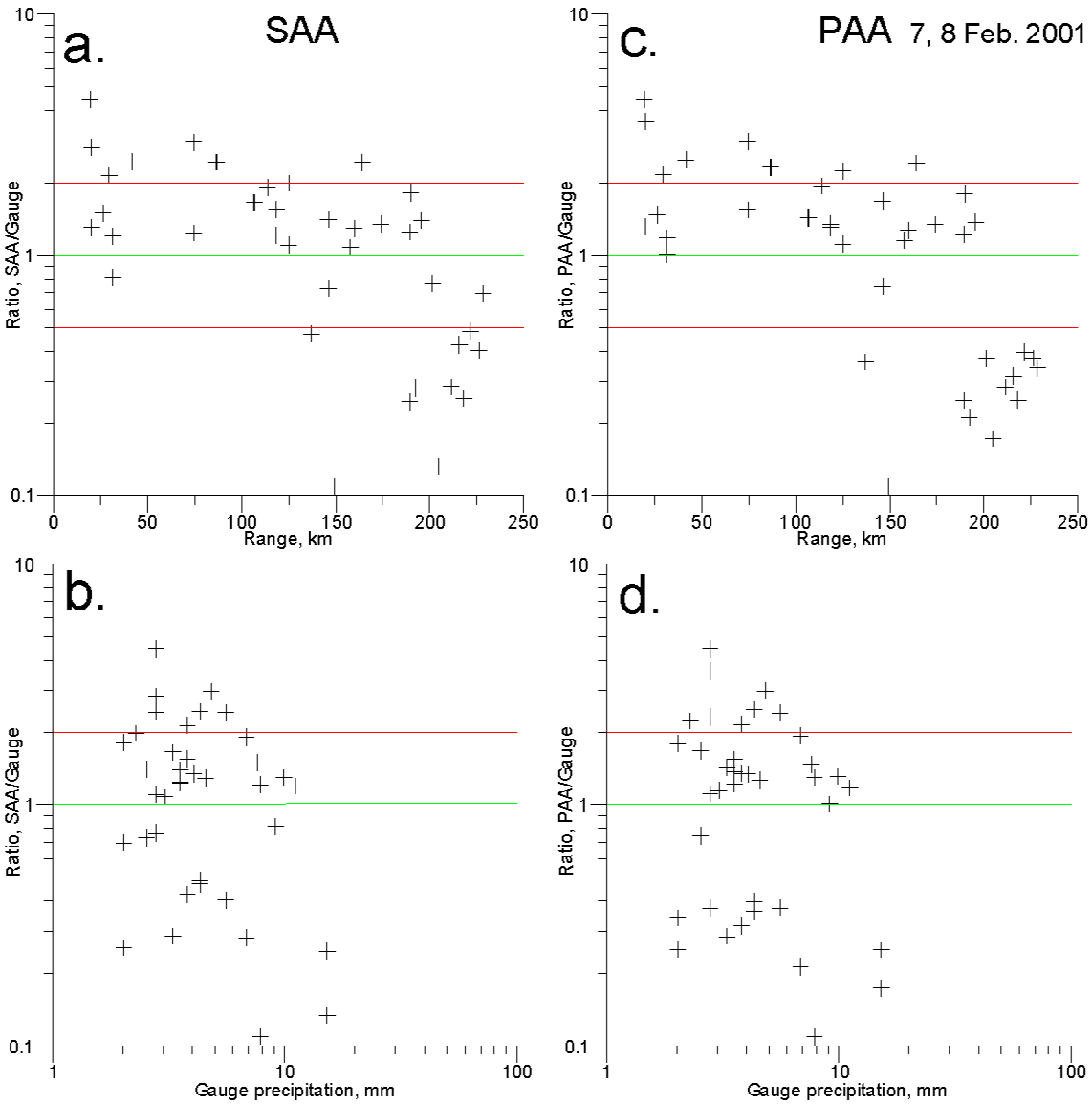

Figure 34.—Relationships of SAA (left panels) and PAA (right panels) radar estimates divided by gauge readings (R/G) to range (a. and c.) and gauge readings G (b. and d.) for 48 hours ending 1200 UTC 8 February 2001, for five radars (KUDX, KABR, KFSD, KMPX, KDLH).

6.7 Statistical Analyses of the Cases

Another way of presenting agreement between algorithm estimates, R, and gauge readings, G, is to do a linear least squares analysis of the two variables and calculate a square of the correlation coefficient r^2. This type of analysis is depicted graphically by the scatter plots of figures 27, 28, and 35. The value of r^2 quantifies the amount of variability, i.e., $r^2 = 0.15$ means that only 15% of the variance is explained. Such an analysis ignores range effects, however. This limitation is significant because, at long ranges, the radar beam overshoots precipitation and neither algorithm will be capable of producing good estimates. This is manifested by generally poor agreement (small r^2) that is evidenced in the sixth column of table 2, which lists r^2 for all points of each case, irrespective of range. This table also includes the number of points (n) used to calculate each r^2.

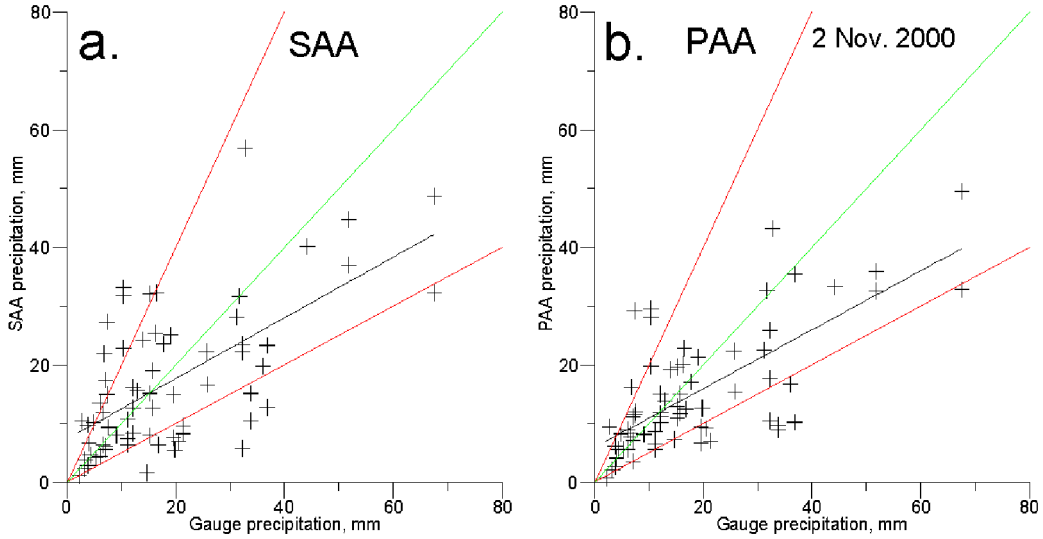

Figure 35.—Relationships of SAA (panel a.) and PAA (panel b.) radar estimates to gauge precipitation G for 24 hours ending 1200 UTC 2 November 2000, for seven radars (KGGW, KMBX, KMVX, KUDX, KBIS, KDLH, KMPX). Green and red lines denote the 1:1 ratio and a factor of two spread from that ratio, respectively. Black line is least squares fit to points.

When results are stratified according to range in the table, a clearer picture emerges. At short ranges (3-50 km), there are relatively few points (n); so statistical significance is weak. Nevertheless, for the cases with the most points in these ranges (2 November 2000 and 6-7 November 2000), there is reasonably good agreement for the PAA. At middle ranges (50-150 km) where there are many more points, there is moderate to good agreement with G for the PAA except for the shallow wind-driven snow case (7-8 February 2001). As expected, agreement decreases at the long ranges (150-230 km) for both algorithms, probably because of radar sampling limitations. Probably the main deduction from table 2 is that *the PAA showed better agreement with gauge amounts than the SAA in most instances.*

Table 2.—Square of the linear correlation coefficient r^2 between radar algorithm (SAA and PAA) R and gauge amount G for each case, stratified by range. Also included is the number of points (n) used to calculate r^2.

		Ranges (km)				
Cases	**Algorithm**	3-50 r^2 (n)	50-150 r^2 (n)	150-230 r^2 (n)	all r^2 (n)	Relevant Figure Number
14 October 2000 Rain	SAA	1.0 (2)	0.612 (4)	0.771 (7)	0.574 (13)	16 (a., c.)
	PAA	1.0 (2)	0.992 (4)	0.880 (7)	0.854 (13)	
2 November 2000 Rain showers	SAA	0.166 (11)	0.610 (16)	0.365 (42)	0.398 (69)	19 (a., c.)
	PAA	0.494 (11)	0.698 (16)	0.466 (42)	0.497 (69)	
6-7 November 2000 Stable bright band	SAA	0.844 (11)	0.584 (29)	0.186 (69)	0.270 (109)	24 (a., c.)
	PAA	0.805 (11)	0.486 (29)	0.199 (69)	0.281 (109)	
6 January 2001 Virga	SAA	1.0 (2)	0.313 (9)	0.142 (36)	0.154 (37)	27
	PAA	1.0 (2)	0.387 (9)	0.253 (36)	0.164 (37)	
30 January 2001 Bright band	SAA	0.697 (3)	0.226 (17)	0.189 (38)	0.198 (58)	31 (a., c.)
	PAA	0.094 (3)	0.369 (17)	0.292 (38)	0.277 (58)	
7-8 February 2001 Shallow snow	SAA	0.170 (8)	0.127 (13)	0.002 (17)	0.050 (38)	34 (a., c.)
	PAA	0.197 (8)	0.131 (13)	0.010 (17)	0.057 (38)	

A second method of assessing algorithm performance pertains to the numerous R/G *ratio* versus G figures from the case studies. Precipitation tends toward a normal distribution on a logarithmic scale. That is why these figures have logarithmic scales. It was seen from these figures that the PAA usually gave reasonable results (within a factor of two, as enveloped by the red lines) out to some range, beyond which the aforementioned radar sampling problems became severe, i.e., the beam was overshooting cloud tops and consequently not obtaining acceptable reflectivity values from which to calculate QPEs at the ground. The range in question was usually near 150 km.

We used the points presented in the PAA R/G versus G figures (panel d.) in five case studies; the virga case of 6 January 2001 was omitted because the precipitation ratio is meaningless for zero precipitation at the ground. The results are summarized in table 3. The data were partitioned into two range groups, separated at 150 km, because of the logic presented in the previous paragraph. The number of data points for each partition is shown in the column labeled "n." To properly describe the approximate log-normal distributions, the logarithms (base 10) of the R/G ratios were summarized to produce a mean and standard deviation. The results were transformed from logarithms to linear space by raising 10 to the power of each mean and standard deviation and entering them in table 3 as "offset" and "variability," respectively. The transformation allows interpretation of the table's results as multiplication factors (linear) rather than summations (logarithms).

Table 3.—Offset and variability for the PAA R/G versus G ratios for five case studies, expressed as factors relative to the gauge readings. Virga case of 6 January 2001 not included.

Dates	Range (km)	n	Offset	Variability	Relevant Figure Number
14 October 2000	< 150 > 150	6 7	0.96 1.11	1.20 1.53	16
2 November 2000	< 150 > 150	27 42	0.88 0.85	1.67 1.92	19
6-7 November 2000	< 150 > 150	40 69	1.06 0.58	1.62 2.08	24
30 January 2001	< 150 > 150	20 38	1.12 0.80	1.66 1.72	31
7-8 February 2001	< 150 > 150	21 17	1.41 0.56	2.23 2.37	34

For the first four case studies, the offset (error) of the ratio is less than 12% from the gauge values for the shorter (< 150 km) ranges. The variability is much less than the factor of two indicated by the red lines in the figures. Again, results degrade at far (> 150 km) ranges.

The last case (7-8 February 2001) was for shallow wind-driven snow. Apparently, the standard VPR overestimated precipitation at ranges < 150 km by about 41% and underestimated precipitation at the overshooting far ranges (> 185 km) by about 44% (see figure 34c.). There may have been greater concentrations of snow in the shallow cloud tops, with little reaching the ground (a negative gradient).

Like their corresponding case study figures, the second statistical method (using R/G ratios) depicts the PAA as producing much more accurate QPEs than the first (r^2) method. Furthermore, the PAA is likely to be shown more accurate if better shielded and sited gauges and snow boards are used in place of ASOS gauges, as was done during development of the SAA. A few recent case studies indicate that National Weather Service Cooperative Observer snow measurements show better agreement with the SAA than do ASOS gauges. We will pursue the Cooperative Observer data more vigorously for future case studies.

6.8 Other Refinements

Before the cool season of 2000-2001, five WSR-88D radars were added to the PAA domain: KFSD, Sioux Falls, South Dakota; KRTX, Portland, Oregon; KMAX, Medford, Oregon; KOTX, Spokane, Washington; and KPDT, Pendleton, Oregon. The latter four radars are the first outside the GCIP domain in the north-central U.S. These Oregon and Washington sites were added in response to Reclamation water resource projects in those States (Hartzell and Super, 2000). This brought the total of WSR-88Ds with near-real-time PAA output to 15. Early in 2001, we added KMSX, Missoula, Montana, to meet end-user needs for upper Missouri Basin water operations.

In December 2000, we began receiving some base reflectivity data from NWS's central radar server. These data are pulled via file transfer protocol (FTP) over the Internet, with checks for new data every 5 minutes. The central radar server became operational in January 2001. We terminated our NIDS connection and relied solely on the NWS server in February 2001, realizing significant monthly cost savings. Occasionally, there are delays in receiving these data when Internet traffic is heavy. These delays do not significantly slow production of our top-of-the-hour products.

As of the end of 2001, the *web site display* was still generated by the SAA (RADAR11.F). We plan to use output from the PAA (RADAR14.F) instead, beginning in early 2002. The new PAA output (SWE and SD products) for the north-central U.S. will be displayed on a finer (2 by 2 km) grid, matching the resolution of the data to be sent to SNODAS. At the top of each hour, last-1-hour, last-2-hour, and last-3-hour files will be posted. These files are overwritten each hour. At the top of each standard 6-hour period, a 6-hour integration will be posted. At 1200 UTC each day, 24-hour totals will be posted. The 6-hour and 24-hour products have date and time file names and are stored for reference.

Before the precipitation-typing enhancement of the PAA, research was conducted in Oregon that attempted to expand the algorithm into a PAA (Hartzell et al., 2001). The approach was different from the one reported here, however. Various Z-R (or Z-S) relationships, range correction factors, and minimum/maximum decibel (dBZ) thresholds were applied to data pairs of radar-estimated liquid water equivalents (from rain or snow) and gauge accumulations. Varying Z-R or Z-S and applying a range correction factor are akin to employing a VPR correction. The results showed that no single Z-R or Z-S is appropriate for all sectors, tilts, and ranges under the radar umbrella. As during the 1999-2000 winter in the north-central U.S., the bright band was frequently a problem in this region. In addition, blockage of the lowest beam by the terrain compounded the problem by causing higher tilts (usually 1.5°) to be used for precipitation estimates. This usually resulted in underestimation. We believe the new PAA using the precipitation-typing and VPR logic will mitigate, but not eliminate, such problems.

7. PAA OUTPUT INTO SNODAS

7.1 SNODAS Background

As mentioned in section 1.4, the Snow Data Assimilation System, or SNODAS, was recently implemented at the NOHRSC. The SNODAS supersedes SEUS, the system originally targeted for SAA data ingest. The following description is adapted from Carroll and Cline (2000). The SNODAS is based on a spatially distributed snow energy and mass balance model, which is forced by gridded solar radiation, air temperature, relative humidity, and wind speed, and is physically scaled to 1-km resolution using multiple atmospheric layers and a digital elevation model. The model is run every morning at 1200 UTC and can be updated with all available snow water equivalent, snow depth, and snow cover information at a present frequency of 6 hours. Output is routinely available by 1800 UTC. SNODAS was first run in a demonstration/ evaluation mode beginning in January 2001. It was run in a full-resolution mode for a few selected areas in the U.S. This evaluation mode was run through spring 2001. Based on the evaluation of the model

during this time, it will be decided when to run it operationally. In the meantime, experimental products may be viewed online at http://www.nohrsc.nws.noaa.gov/experimental_products/snow_model.

Figure 36 shows an early flowchart for SNODAS. Hourly data input to the model include temperature, relative humidity, wind speed, solar radiation, atmospheric radiation, amount and type of precipitation. Note that radar data are currently used only for precipitation *extent*. This would change with the inclusion of PAA output, which supplies quantitative liquid water content (SWE) from snowfall and rainfall.

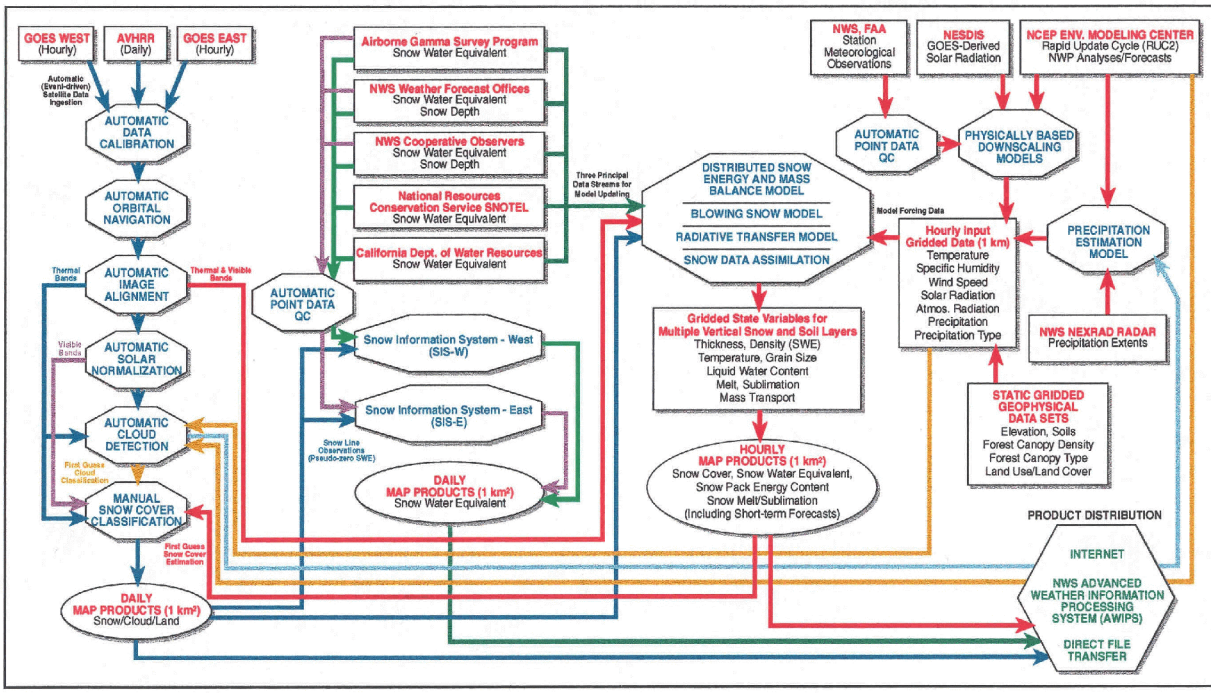

Figure 36.—Flowchart for SNODAS, including model components, data sources, flow, and output.

7.2 PAA Data Formatting for SNODAS

To take advantage of the 1° azimuthal and 1-km range resolution of the radar data and to provide SNODAS with the finest resolution possible, the spatial resolution of the PAA grid in the north-central U.S. was increased in early 2001 from the 4- by 4-km HRAP grid to a subset 2- by 2-km grid. The radar beam is approximately 2 km in diameter at 130-km range. Thus, at ranges < 130 km, the higher resolution grid is an improvement because it is taking advantage of even higher resolution radar data. Conversely, at ranges of 130-230 km, beam resolution is poorer than the PAA output grid size. At these longer ranges, the algorithm output grid uses nearest-neighbor radar bins to "fill in" missing grid boxes. We discontinued the last 1-hour and 3-hour files that were continuously updated every volume scan. Instead, at the top of every hour, integrations are restarted for the 1-hour product. During the hour itself, all integrations will be incomplete. The algorithm initially outputs three products for each time period: (1) liquid

equivalent precipitation (SWE), units mm*100; (2) snow depth, units mm*10; (3) precipitation classifications, byte codes. As with the old SAA, all these products will be converted to raster, net CDF format. The SWE and precipitation type products from all available integration periods will be furnished to SNODAS by FTP on an automated basis; these products are described in the following paragraphs.

The SWE file data consist of 16-bit unsigned integers, with units = mm*100. The data are on the quartered HRAP grid (about 2 by 2 km). The files will be hourly and their integration will be terminated close to the top of each hour. The products will be extrapolated (or interpolated) to a full hour, based on what was observed during that hour and the duration of the observations. In other words, data gaps will be filled.

The precipitation classification data are 8-bit (1 byte) unsigned integers. The byte is separated into 4-bit settings, each made from the Eta temperature profiles and thresholds described in section 6.3.2. The least significant four bits refer to the classes the *radar beam* detects, as follows: 0 = unclassified, 1 = snow in radar beam, 2 = rain in radar beam, 3 = 1 + 2 = melting snow (bright band) in radar beam, 4 = virga suspected in radar beam. The most significant four bits (only two are used) use the same codes but refer to *surface conditions* at each location. Therefore 4-bit totals of 16 = snow at the ground, 32 = rain at the ground, 48 = 16 + 32 = wet snow at the ground. These codes are all additive, so the program has to check the settings of the bits. For example, the final code could be a 7, indicating virga producing a bright band, or it could be a 33, indicating snow in the beam and rain at the ground.

During a long integration period, the class can change, as from rain to snow. The classification code will have the bits set for whatever happened during the period. So during a 24-hr period, virga changing to rain, then to snow will produce a 7 for what the beam samples. This classification style is experimental, but it should provide a way to discern what happened during the integration period in terms of what precipitation the radar sensed and what arrived at the ground. Variable weather over the integration period may complicate the final determination of precipitation type.

Precipitation amounts will be accumulated for snow, melting snow, and rain, but not virga. The snow *depth* file will accept dry fluffy snow and dense wet snow, but not rain. Initially, we will not change snow density during arctic snow conditions and the PAA will, therefore, continue to underestimate the depth of very cold and fluffy snowfalls. In a future revision, the algorithm will identify AP with code 8 (bit 4 “on”); in which case, precipitation will also not accumulate.

Until now, SEUS output has been available to MBRFC but was used only in qualitative ways. Once the NOHRSC is satisfied with test results, SNODAS output (including SWE) should be input to the operational NWSRFS at MBRFC. These data may differ in precipitation type from that specified by the PAA because they are subject to further quality control by that system’s Rapid Update Cycle NWP model and satellite data (figure 36). Nevertheless, SNODAS output should be improved by SWE input from Reclamation’s PAA, and the improvement should also be reflected in NWSRFS streamflow forecasts.

8. RELATED EFFORTS

Support for PAA development will continue from Reclamation's Science and Technology Program through at least fiscal year 2002. This development will focus on the Pacific Northwest and Montana, where testing of the new PAA in complex terrain will occur. We endeavor to verify algorithm output versus gauge data, thereby tailoring to those areas the PAA's VPR and bright band corrections, as well as α and β parameters. We are exploring the possibility of real-time VPR corrections that vary with the topography under the radar umbrella. Such corrections are being tested in the Reno, Nevada, area by the Desert Research Institute and NWS Reno (Huggins, personal communication), and hold the promise of more accurate estimation of shallow orographic snowfall over high mountain ranges.

Reclamation is currently engaged with the MBRFC in an experimental streamflow forecasting project in the upper Missouri Basin. MBRFC is generating and distributing products that demonstrate the NWS's new AHPS. The forecasts are for 40 sites in Montana and Wyoming. For each site, six graphical products are composed: (1) weekly chance of exceeding stage, (2) flow, (3) volume, and chance of exceedance for entire period for (4) stage, (5) flow, and (6) volume. The output is designed to yield probabilistic guidance to water operations managers. The forecasts have a period of 6 months (April 1 through September 30) and are produced from the Ensemble Streamflow Prediction (ESP) system. ESP uses conceptual rainfall/runoff models within the NWSRFS and historical meteorological data and current basin conditions (e.g., soil moisture, streamflow, and reservoir storage) to forecast future streamflow. Although this system is designed primarily for long-term forecasts, the sensitivity of these forecasts depends on initial basin conditions. The PAA has the potential to provide accurate input for the specification of such conditions.

Reclamation and the NSSL/WISH group have begun to collaborate (section 6.3.2) on a plan to involve that group's Quantitative Precipitation Estimation and Segregation Using Multiple Sensors (QPE-SUMS) system (Gourley et al., 2001). This system will use radar, satellite, and gauge data to yield the best QPE possible in the complex terrain of the Western U.S. QPE-SUMS will output data on a 1- by 1-km grid, initially for the State of Arizona. We anticipate incorporation of portions of the PAA into QPE-SUMS, or vice-versa. As mentioned previously, QPE-SUMS will incorporate a bright band algorithm that operates in real time using radar data. The temporal update frequency of this algorithm will be every volume scan (5-6 minutes), more frequent than the 3-hour Eta sounding updates to our precipitation-typing algorithm. The NSSL bright band algorithm may also afford real-time VPR corrections. The initial demonstration of the combined QPE-SUMS/PAA system is planned for the Lower Colorado River Basin. There, we plan to couple the system's QPE data to one or more distributed hydrologic models, producing streamflow estimates in near-real-time. This powerful capability may then be extended to other Reclamation project areas. In the process, we can refine the PAA and develop site-specific algorithm parameters.

9. RECOMMENDATIONS FOR FUTURE WORK

9.1 Precipitation-Typing Refinements

The current precipitation-typing logic within the PAA was explained in section 6.3.2. The logic depends on altitude thresholds of the 0 °C and 4 °C temperatures from the hourly Eta forecast soundings. These thresholds are based on bright band and precipitation type observations. It may be possible to improve the PAA's implementation of model forecast soundings by using two existing methods. The first is the operational scheme used by the Canadian Meteorological Centre since 1995. This method, outlined by Bourgouin (2000), calculates positive areas associated with layers warmer than 0 °C and negative areas associated with layers colder than 0 °C. Such areas are related to those on aerological diagrams. A statistical analysis was applied using data from the North American rawinsonde network. The methodology was shown to work well with model temperature soundings, and this is done operationally using the Canadian Global Environmental Multiscale (GEM) model. How the scheme might be integrated with the existing PAA precipitation-typing logic will require some thought.

The second precipitation typing method (Baldwin et al., 1994), like the Canadian routine, uses energy-area logic but applies it to Eta model soundings. The results are displayed in loops of 3-hour precipitation type maps online at http://www.hpc.ncep.noaa.gov/roz/ptype. A preliminary evaluation of the Bourgouin (2000) and Baldwin et al. (1994) techniques, along with evaluation of four other techniques, was presented by Cortinas and Baldwin (1999). This evaluation found small differences in output quality between the algorithms.

The aforementioned NSSL bright band algorithm (Calvert and Gourley, 2000) is another possibility for distinguishing the rain/snow transition layer. It has the advantage of being radar-based and, therefore, updated every volume scan. We should have access to this algorithm during our anticipated collaboration with the NSSL/WISH group.

It is also possible to incorporate surface observations of precipitation type directly into the PAA. We already collect and archive surface reports in METAR format. Given that surface observations in the U.S. are now mostly automated, however, this might pose problems. Most first-order stations use the ASOS. The ASOS precipitation identification sensor is described in the ASOS User's Guide (1998). The sensor is designed to discriminate rain from snow but, on many occasions, it is unable to do so, reporting instead "unknown precipitation." Moreover, in the complex terrain of the West, there are representative-ness issues with surface data. SNODAS already uses surface precipitation type reports. NWS plans to improve the ASOS precipitation gauge.

Finally, there are usually several Eta model sounding sites within a radar umbrella, and more sites could be requested from the National Centers for Environmental Prediction. This should give a better portrayal of precipitation type in those cases in which it has substantial spatial variability.

9.2 Other Refinements

First and foremost, more case studies are needed to arrive at site-specific, stable parameters for the Z-R and VPR relationships. As was found during SAA development, such parameters may vary significantly from place to place. The six case studies of section 6.6 employed far fewer and less reliable data than in the early SAA development. Moreover, the data were confined to the north-central U.S. We have extended the PAA to other regions, such as the mountainous areas of Arizona and the Northwest U.S. The shallow nature of widespread, orographically enhanced cool season storms and beam blocking in mountains poses strong challenges to radar QPE, as attempted by the PAA and PPS. The PAA in these regions would be greatly aided by verification studies using adequate surface snow-measuring networks. Existing surface networks, which are designed largely for rain, present obstacles to further research. Installation of additional snow boards or wind-shielded gauges, as in the SAA's development, would reduce these obstacles.

As pointed out in section 6.6.4, although the virga rejection algorithm is a substantial improvement over the old SAA's treatment of virga, it needs further work. This work might take the form of further case studies, which could lead to changes in the algorithm logic. The same need for further studies applies to the PAA bright band identification and precipitation adjustment. Compare figures 37 and 38, which display SAA and PAA output, respectively, for a strong bright band event (section 6.6.3) at KMPX, Minneapolis radar site. Note that while the PAA reduces precipitation estimates in the bright band annulus compared to the SAA estimates, the annulus pattern remains, and it still shows (lesser) radar overestimation versus gauge amounts at intermediate ranges.

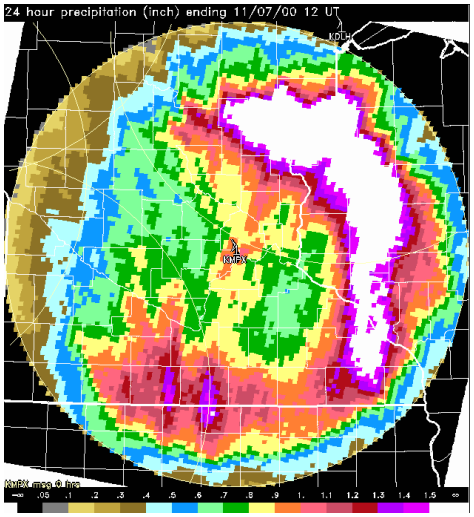

Figure 37.—SAA SWE accumulation for 24 hours ending 1200 UTC 7 November 2000, at KMPX. Grid size is 4 by 4 km.

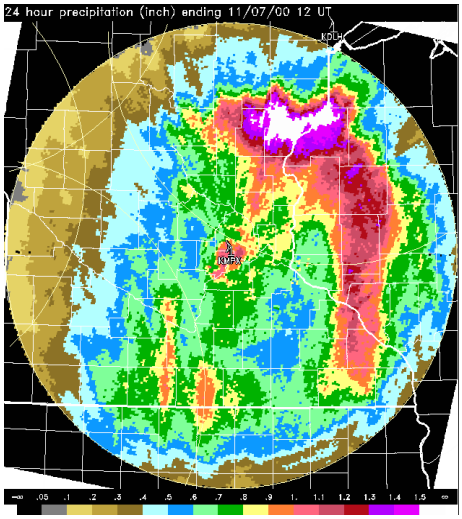

Figure 38.—Same as figure 37, except with PAA output on a grid size of 2 by 2 km.

Section 6.3.2 mentioned briefly that coding has been added to experimentally estimate the proportion of the beam contaminated by the bright band. This is desirable because of the current use of $\alpha = 300$ whenever *any part* of the sampling beam is within the bright band (0 ° to 4 °C layer). Whenever only a small part of the beam is actually within this layer (as could be common when the beam is broad at far ranges), radar underestimation might ensue. For example, see figure 7a. From about 80-110 km in range, the beam is still largely sampling rain, but the PAA dictates the bright band α value rather than the value for rain. The same argument applies when the beam starts to measure primarily snow, so that the snow $\alpha = 150$ should instead be applied. Knowing beam widths at various ranges, an intermediate α value or some factor could be used to reflect the proportion of the beam sampling each precipitation type.

We plan to convert the web site to display PAA rather than SAA products during 2002 for all regions. In the longer term, we wish to devise a scheme that delineates areas (polygons, perhaps) on the SWE gridded product for the precipitation types—rain, snow, bright band, and virga. The new time-height diagrams discussed in section 6.5 might be included on the web site.

Per the unfinished item 17 of section 2, it would be highly desirable to measure the effect of the new PAA SWEs on NWSRFS streamflow forecasts. The originally intended means for accomplishing this was to send the SWEs through SNODAS, which would subsequently feed snowpack and snowmelt data to the NWSRFS. This data channel does not exist. Its introduction is pending further SNODAS testing, so the value assessment must await completion of that testing. It may be possible to send the SWEs directly to NWSRFS, however, which was recently proposed by Reclamation (GC01-102) to the GEWEX Americas Prediction Project (GAPP, a follow-on to GCIP). This proposal was not funded. The NWSRFS is undergoing changes in preparation for implementation of AHPS (section 8).

As alluded in section 6.4, further analysis is necessary to present precipitation from storms receding from the radar site being classified as virga. Finally, we would like to pursue a means to identify AP echo and eliminate it from precipitation processing. The NWS is also investigating this task and has pursued a neural network approach (Grecu and Krajewski, 2000). We are pondering an approach that keys on the reduced coherence ("speckle") of AP echoes. The Eta model soundings might identify inversion and humidity profiles that promote AP.

10. SUMMARY AND RECOMMENDATIONS

Reclamation developed the Snow Accumulation Algorithm from 1995-98 under the auspices of the WSR-88D Operational Support Facility, Reclamation's Science and Technology Program, and the GEWEX Continental-Scale International Project. The algorithm responded to a need within the WSR-88D system for snow precipitation, because that system's operational Precipitation Processing Subsystem applies only to rain. The SAA was designed to work for dry (not melting) snow.

The SAA was developed with WSR-88D radar reflectivity (Z_e) data and meticulous surface snow measurements from several geographically diverse locations in the United States. Measurement sources included precipitation gauges and snow boards. Data were used as input to the standard

radar precipitation estimation equation $Z_e = \alpha S^{\beta}$, where S is snowfall rate in mm hr^{-1}. β was found to be stable near a value of 2.0, but α varied geographically and with radar range.

Reclamation transformed the SAA into a near-real-time algorithm whose output was posted to a web page on the Internet. This transformation necessitated the ability to ingest NEXRAD Information Dissemination System reflectivity data every volume scan. This was accomplished for five radars in the north-central U.S. during the 1998-99 cool season. The number of radars was expanded to 10 for the 1999-2000 cool season, and to 11 the following season. Output consisted of snow water equivalent and snow depth for a variety of periods up to 24 hours.

Reflectivity data from nine Minneapolis-area snowstorms were used to construct a climatological range correction for the SAA. This correction compensated for the usual decrease in reflectivity and SWE estimates with increasing range (and radar beam elevation). The correction was applied in real time for all north-central U.S. radars.

Examination of SWE products revealed that when the radar's hybrid scan or our empirical hybrid scan forced data collection from tilts higher than the lowest 0.5° tilt, a drastic reduction in Z_e and SWE resulted. This effect was caused by partial beam filling, since snowstorms are typically shallow and have a steep gradient of Z_e in the vertical. While not usually a problem in flat locations, the hybrid scan "jumps" are common in areas with mountainous terrain near the radar, such as Montana. To alleviate the elevated hybrid scan problem, Reclamation developed a true correction within the algorithm for the vertical profile of reflectivity. This correction borrowed from the logic of the range correction, but made an adjustment to α, based on the clearance C between the sampling beam center and the underlying surface, for each bin location. The VPR correction is also climatologically based but is formulated using data from four geographically diverse sites.

There were numerous cases, especially in the late and early periods of the cool season, in which storms produced mixed-phase precipitation (snow, melting snow, freezing rain, ice pellets, rain). Since the SAA was fashioned for dry snow only, such storms caused the algorithm to generate inaccurate SWE and SD estimates. A particularly frequent difficulty was presented by melting snow, which produces significant bright-band overestimation of precipitation.

In 2001, a precipitation-typing routine was incorporated into a more generic Precipitation Accumulation Algorithm to address the shortcomings with the mixed-phase events just described. This routine uses forecast vertical temperature from the operational Eta numerical model ("model soundings"). For the precipitation phase determination, levels of the 0 °C and 4 °C temperatures from these soundings are compared to sampling beam and ground elevations at each radar bin. This defines areas of rain; snow; and melting snow ("slush"), or bright band. A liquid equivalent precipitation is calculated for bins in each area according to different α values for each precipitation type. These α values were determined from several case studies of radar and gauge data from the 2000-2001 cool season. Preliminary α values from these case studies were 100 for rain, 150 for snow, and 300 for melting snow. No SD is accumulated in areas of rain.

The PAA was further enhanced by an ability to distinguish a fourth precipitation type, virga (precipitation not reaching the ground). The SAA has been hampered by false precipitation

accumulations caused by virga, especially with storms approaching or receding from the radar coverage area. The virga identification scheme consists of two tests, one model sounding-based and the other radar echo-based. The model sounding part uses forecast relative humidity profiles. Areas identified as having virga are not allowed to accumulate precipitation.

Results from a limited number of cases in the north-central United States suggest that the PAA is superior to the SAA in estimating precipitation from bright band and virga regions. PAA QPEs were within 12% of operational gauge precipitation values in non-shallow, non-virga cases at ranges less than 150 km. More testing is needed in other areas to refine the parameterizations for the bright band and virga algorithms. Use of carefully sited and sheltered snow gauges and boards, as were used in the SAA's development, would likely improve agreement between the PAA and gauge precipitation amounts. The PAA continues to underestimate precipitation at far ranges (> 150 km), but it's unclear if this is correctable with software adjustment because of radar sampling problems at these ranges. If further case studies support it, however, we may substitute the old range correction, F_R, for the new VPR correction, F_C, at these far ranges.

A time-height diagram was added as a PAA product. This diagram portrays Eta model temperature and RH, plus maximum radar reflectivities for each volume scan and height, over a 24-hour period.

We began acquiring Level III base reflectivity data from a NOAA/NWS server in real time via FTP at no cost to Reclamation.

Several potential refinements to the PAA have been identified that could be incorporated into the algorithm through future projects. These refinements include more case studies for VPR and Z-R parameter adjustment, site-specific adjustments to the algorithm for other regions, energy-area algorithms for better precipitation typing, improved bright band adjustment and virga exclusion routines, and a new AP rejection technique. Field studies similar to the study performed in the SAA development, with carefully sited snow gauges and boards, should be conducted in different geographic regions. Multi-sensor approaches to precipitation measurement, such as the approach of QPE-SUMS, should be incorporated to improve the PAA.

The PAA can output data to the Snow Data Assimilation System, a sophisticated mass and energy balance modeling system devised by the National Operational Hydrologic Remote Sensing Center. We hope that this data feed will become operational in the future. The PAA data should improve SNODAS output, which will eventually be input to the National Weather Service operational river forecast models. This eventuality should advance the accuracy of streamflow forecasts used by water operations managers within Reclamation and elsewhere.

11. REFERENCES

Andrieu, H., and J.D. Creutin, 1991: Effect of the vertical profile of reflectivity on the rain rate assessment at ground level. Preprints, *25th International Conference on Radar Meteorology*. American Meteorological Society, 832-835.

ASOS User's Guide, 1998: Available from National Weather Service Headquarters, Silver Spring, Maryland. [Also available on-line at http://www.nws.noaa.gov/asos/aum-toc.pdf]

Austin, P.M., 1987: Relation between measured radar reflectivity and surface rainfall. *Monthly Weather Review*, vol. 115, 1053-1071.

Baldwin, M., Treadon, R., and S. Contorno, 1994: Precipitation type prediction using a decision tree approach with NMC's mesoscale eta model. Preprints, *10th Conference on Numerical Weather Prediction*. American Meteorological Society, Portland, Oregon, 30-31.

Barker, T., 1994: Program Name: RDRHGT.EXE. *NWS Western Region Programming Note No. 109*, 19 pp.

Barker, T., P. Felsch, T. Mathewson, C. Sullivan, and M. Zenner, 2000: Test of the WSR-88D snow accumulation algorithm at WFO Missoula. National Weather Service Western Region Technical Attachment No. 00-13; also available at http://www.wrh.noaa.gov/wrhq/00TAs/0013/index.html

Benjamin, S.G., J.M. Brown, K.J. Brundage, B.E. Schwartz, T.G. Smirnova, and T.L. Smith, 1998: The operational RUC-2. Preprints, *16th Conference on Weather Analysis and Forecasting*. American Meteorological Society, Phoenix, Arizona, 249-252.

Bourgouin, P., 2000: A method to determine precipitation types. *Weather and Forecasting*, vol. 15, 583-592.

Burnash, R.J.C., 1995: The NWS River Forecast System - catchment modeling. In *Computer Models of Watershed Hydrology*, edited by V.P. Singh, 311-366.

Cairns, M., M. Fresch, L.E. Osterman, and S. Otteson, 1999: Assessment of a real-time snow accumulation algorithm at Reno, Nevada. Preprints, *16th International Conference on Radar Meteorology*. American Meteorological Society, Montreal, Quebec, Canada, 798-801.

Calvert, C., and J.J. Gourley, 2000: Bright Band Identification Algorithm. [Available on-line from http://www.nssl.noaa.gov/teams/western/qpe/bbid/index.htm]

Carroll, T., and D. Cline, 2000: Remote Sensing, Now and Future. Presentation at National Weather Service Cold Region Hydrology Workshop, Kansas City, Missouri. [Available on-line from http://ww2.wrh.noaa.gov/public/hydws/index.htm]

Cortinas, J.V., and M.E. Baldwin, 1999: Proceedings, 6th Workshop on Operational Meteorology, Halifax, Nova Scotia, Environment Canada, 207-211. [Also available on-line at http://www.nssl.noaa.gov/~cortinas/preprints/canada6.html]

Crum, Timothy D., and R.L. Alberty, 1993: The WSR-88D and the WSR-88D Operational Support Facility. *Bulletin of the American Meteorological Society,* vol. 74, 1669–1688.

Evans, M.S., and R.H. Grumm, 2000: An examination of Eta model forecast soundings during mixed-precipitation events. *National Weather Digest*, vol. 24, 14-36.

Fabry, F., and I. Zawadzki, 1995: Long-term radar observations of the melting layer of precipitation and their interpretation. *Journal of Atmospheric Science*, vol. 52, 838-851.

Fulton, R.A., J.P. Breidenbach, D.J. Seo, D.A. Miller, and T. O'Bannon, 1998: The WSR-88D rainfall algorithm. *Weather and Forecasting*, vol. 13, 377-395.

Galli, G., and J. Joss, 1991: Using and adjusting conventional radar reflectivity data for estimation of precipitation: past, present and future studies in Switzerland. In *Hydrological Applications of Weather Radar*. Edited by I.E. Cluckie and C.G. Collier. Ellis Horwood, Chichester, England, 65-73.

Gourley, J.J., J. Zhang, R.A. Maddox, C.M. Calvert, and K.W. Howard, 2001: A real-time monitoring algorithm - Quantitative Precipitation Estimation and Segregation Using Multiple Sensors (QPE-SUMS). Preprints, *Symposium on Precipitation Extremes: Prediction, Impacts, and Responses*. American Meteorological Society, Albuquerque, New Mexico, 57-60.

Grecu, M., and W.F. Krajewski, 2000: An Efficient Methodology for Detection of Anomalous Propagation Echoes in Radar Reflectivity Data Using Neural Networks. *Journal of Atmospheric and Oceanic Technology*, vol. 17, 121-129.

Hartzell, C.L., and A.B. Super, 2000: Development of a WSR-88D Based Snow Accumulation Algorithm for Quantitative Precipitation Estimates Over Southwestern Oregon. Preprints, *16th International Conference on Interactive Information and Processing Systems (IIPS) for Meteorology, Oceanography and Hydrology*. American Meteorological Society, Long Beach, California, 373-376.

Hartzell, C.L., S.M. Hunter, and E.W. Holroyd, 2001: Development of a WSR-88D based precipitation algorithm for quantitative precipitation estimates over northwest Oregon. Preprints, *17th International Conference on Interactive Information and Processing Systems (IIPS) for Meteorology, Oceanography and Hydrology*. American Meteorological Society, Albuquerque, New Mexico, 146-150.

Holroyd, E.W., 1999: Snow accumulation algorithm for the WSR-88D radar: supplemental report. Bureau of Reclamation Report R-99-11, Denver, Colorado, June, 30 pp.

Hunter, S.M., 1996: WSR-88D radar rainfall estimation: Capabilities, limitations and potential improvements. *National Weather Digest*, vol. 20, 26-38.

Hunter, S.M., E.W. Holroyd, III, and C.L. Hartzell, 2001: Improvements to the WSR-88D Snow Accumulation Algorithm. Preprints, *30th International Conference on Radar Meteorology*. American Meteorological Society, Munich, Germany, 716-718.

Johnson, E.R., T.E. Adler, J.W. Schiesl, R. Dombrowsky, L. Larson, G. Goodge, and J. Bradley, 1994: Frozen precipitation technical working group recommendations for the automated surface observing system precipitation gauge. NOAA issue paper, 17 pp.

Joss, J., and A. Waldvogel, 1989: Precipitation estimates and vertical reflectivity profile corrections. Preprints, *24th Conference on Radar Meteorology*. American Meteorological Society, 682-688.

_____,1990: Precipitation measurements and hydrology. In *Radar in Meteorology*. Edited by D. Atlas. American Meteorological Society, Boston, Massachusetts, 577-606.

Joss, J., and R. Lee, 1995: The application of radar-gauge comparisons to operational precipitation profile corrections. *Journal of Applied Meteorology,* vol. 34, 2612-2630.

Kain, J.S., S.M. Goss, and M.E. Baldwin, 2000: The melting effect as a factor in precipitation-type forecasting. *Weather and Forecasting*, vol. 15, 700-714.

Koistinen, 1991: Operational correction of radar rainfall errors due to the vertical reflectivity profile. Preprints, *25th International Conference on Radar Meteorology*, American Meteorological Society, Boston, Massachusetts, 91-94.

Matthews, D., A. Super, C. Hartzell, and E. Holroyd, 2000: Demonstration of Improved Operational Water Resources Management Through Utilization of Better Snow Water Equivalent Information. Second Annual Report to GCIP, OGP, NOAA April 11, 2000. Available from the Bureau of Reclamation.

Matrosov, S.Y., 1992: Radar reflectivity in snowfall. *IEEE Transactions on Geoscience and Remote Sensing*, vol. 30, 454-461.

O'Bannon, T., 1997: Using a 'terrain-based' hybrid scan to improve WSR-88D precipitation estimates. Preprints, *28th Conference on Radar Meteorology*. American Meteorological Society, Austin, Texas, 506-507.

Quinlan, J.S., and E.J. Sinsabaugh, 1999: An evaluation of the performance of the snow accumulation algorithm at NWFO Albany, New York, during the 1997-1998 winter season. Preprints, *29th Conference on Radar Meteorology*. American Meteorological Society Montreal, Quebec, Canada, 794-797.

Rasmussen, R., M. Dixon, F. Hage, J. Cole, C. Wade, J. Tuttle, S. McGettigan, T. Carty, L. Steenson, W. Fellner, S. Knight, E. Karplus, and N. Rehak, 2001: Weather support to deicing decisionmaking (WSDDM): A winter weather nowcasting system. *Bulletin of the American Meteorological Society*, vol. 82, 579-596.

Sekhon, R.S., and R.C. Srivastava, 1970: Snow size and radar reflectivity. *Journal of Atmospheric Science*, vol. 27, 299-307.

Seo, D.J., J.P. Breidenbach, R.A. Fulton, D.A. Miller, and T. O'Bannon, 2000: Real-time adjustment of range-dependent biases in WSR-88D rainfall estimates due to nonuniform vertical profile of reflectivity. *Journal of Hydrometeorology*, vol. 1, 222-240.

Smith, P.L., 1984: Equivalent radar reflectivity factors for snow and ice particles. *Journal of Climate and Applied Meteorology*, vol. 23, 1258-1260.

_____, 1990: Precipitation measurement and hydrology: Panel report. In *Radar in Meteorology*. Edited by D. Atlas. American Meteorological Society, Boston, Massachusetts, 607-618.

Smith, P.L., D.E. Cain, and A.S. Dennis, 1975: Derivation of an R-Z relationship by computer optimization and its use in measuring daily areal rainfall. Preprints, *16th Radar Meteorology Conference*. American Meteorological Society, Houston, Texas, 461-466.

Steigerwaldt, H., 1998: The role of dynamic cooling in the snowstorm on the eastern highland rim and Cumberland plateau of Tennessee. National Weather Service Southern Region Headquarters Technical Attachment SR/SSD 98-10. [Available on-line at http://www.srh.noaa.gov/ftproot/topics/attach/html/ssd98-10.htm]

Steiner, M., and J.A. Smith, 2000: Reflectivity, rain rate, and kinetic energy flux relationships based on raindrop spectra. *Journal of Applied Meteorology*, vol. 39, 1923-1940.

Super, A.B., 1998: Use of NEXRAD WSR-88D radar snow accumulation algorithm in the GCIP LSA-NC. First Annual Report for NOAA/OGP/GCIP Research, Bureau of Reclamation Report R-98-01, January, 24 pp.

_____, 1999: Demonstration of improved operational water resources management through utilization of better snow water equivalent information. First annual report to NOAA/OGP/GCIP. February 26, 1999, 6 pp.

Super, A.B., and E.W. Holroyd, 1996: Snow Accumulation Algorithm for the WSR-88D Radar, Version 1. Bureau of Reclamation Report R-96-04, Denver Colorado, June, 133 pp.

_____, 1997a: Snow Accumulation Algorithm for the WSR-88D Radar: Second Annual Report. Bureau of Reclamation Report R-97-06, Denver, Colorado, June, 79 pp.

_____, 1997b: Snow Accumulation Algorithm Development for the WSR-88D Radar. Preprints, *28th Conference on Radar Meteorology*. American Meteorological Society, 324-325.

_____, 1998: Snow Accumulation Algorithm for the WSR-88D Radar: Final Report. Bureau of Reclamation Report R-98-05, Denver, Colorado, June, 75 pp.

Vasiloff, S., 2002 (in progress): Investigation of a WSR-88D Z-R relation for snowfall in northern Utah. Submitted to *Weather Analysis and Forecasting*.

Vignal, B., G. Galli, J. Joss, and U. Germann, 2000: Three methods to determine profiles of reflectivity from volumetric radar data to correct precipitation estimates. *Journal of Applied Meteorology*, vol. 39, 1715-1726.

Appendix A

RADAR14.F — PROGRAM UNITS AND DESCRIPTIONS

The program units are in RADAR14.FOR. The ENTRY points are listed below the subroutine name in which they are located:

```
PROGRAM UNITS                (called by)
PROGRAM RADAR14
SUBROUTINE STARTUP           (by RADAR14)
  ENTRY NEWGRAF              (by RESET624)
  ENTRY UPDATE               (by RADAR14)
SUBROUTINE FILLTABL          (by STARTUP)
SUBROUTINE FINDFILE          (by RADAR14)
SUBROUTINE INITALL           (by RADAR14)
SUBROUTINE CLEARANC          (by RADAR14)
  ENTRY NEWMELT              (by RADAR14)
SUBROUTINE GETNIDS           (by RADAR14)
  ENTRY READ1ST              (by RADAR14)
SUBROUTINE OCCULT            (by RADAR14)
SUBROUTINE NOSPIKES          (by RADAR14)
SUBROUTINE PRECIP            (by RADAR14)
SUBROUTINE INCRMENT          (by RADAR14)
SUBROUTINE TOPHOUR           (by RADAR14)
  ENTRY HALFHOUR             (by RADAR14)
SUBROUTINE RESET             (by TOPHOUR)
  ENTRY RESET624             (by TOPHOUR)
  ENTRY SOUNDOUT             (by SOUNDING)
SUBROUTINE SOUNDING          (by RADAR14)
SUBROUTINE ADDDAY(JDATE,JD)  (by SOUNDING)
SUBROUTINE HHMMSS(IT,IH,IM,IS) (by NOSPIKES, ADDDAY)
SUBROUTINE GETMED(MEDIAN)    (by PRECIP)
SUBROUTINE TIMESPAN(ITIME,IDATE,JTIME,JDATE,DH) (by INCRMENT)
SUBROUTINE JTOG(JD,IY,MO,ID) (by DATEJ)
  ENTRY GTOG(JD,IY,MO,ID)    (by TIMESPAN)
SUBROUTINE DATEJ(NDA,IYMD)   (by GETNIDS)
```

Unit Descriptions

PROGRAM RADAR14

The main program, RADAR14, describes the structure of line 361 in the output files, some historic modifications, the operations of the C functions, the names of all variables included in named commons (local variables are described in each subroutine), and the expected file names and logical unit assignments. The program structure is very simple. It calls appropriate subroutines at the proper times while operating in an infinite loop until a stop time is encountered.

SUBROUTINE STARTUP

STARTUP opens, reads, and closes several files to acquire initialization data. These data include instructions about live versus postprocessing runs, adaptable parameters, snow density, the occultation file, the hybrid scan file, and the terrain file. It tests for the existence of former files in

case a power outage interrupted the program. It calls for the filling of a look-up table with precipitation rates. It names the sounding file and calls for its reading. If gauge comparisons are desired, a list of gauge locations is read.

ENTRY NEWGRAF

NEWGRAF reads in an annotated background image on which to draw the time-height diagram. Annotations for dates and radar identification are not supplied nor is a color look-up table; these must be added by an image processing program after the output file is created.

ENTRY UPDATE

UPDATE gets the latest value of the inverse snow density for dry snow and slush (melting snow). These can be changed at any time by the operator.

SUBROUTINE FILLTABL

FILLTABL has the same basic structure as equivalent routines in the Precipitation Processing Station (PPS) and older Snow Accumulation Algorithm (SAA). However, it deals with three precipitation types: dry snow, slush, and rain. Using the nominated minimum and maximum decibel (dB) thresholds for each type, and the nominated alpha and beta for each type, the routine calculates the precipitation rate for all reflectivity levels at 0.5-dB resolution. The results are saved in arrays indexed by the numerical value of the biased dB [biased dB = NINT(2.*(DBZ+32.))+2]. The arrays are used as look-up tables in the PRECIP routine.

SUBROUTINE FINDFILE

FINDFILE searches a list of file names that were actually received. The file names have date and time notation. Nominated start and stop dates and times in postprocessing mode confine the analyses to those files with the desired times. The rest of the files are ignored. In real-time mode, the program runs forever but routinely enters a sleep mode until new files are available.

SUBROUTINE INITALL

INITALL creates clean (zeroed) files for classifications, snow depths, and precipitation. The later RESET routine will rezero the files at appropriate times.

SUBROUTINE CLEARANC

CLEARANC calculates, if any tilts have changed, the top, center, and bottom of each range bin with respect to sea level. It then uses the terrain file to measure the distance (clearance) between the beam center and the surface for only those range bins specified by the hybrid scan file. Only these bins will be used for the precipitation output. The clearance number will be used to extrapolate precipitation intensities to the surface according to the typical vertical gradient of reflectivity. The routine exits directly into NEWMELT for an update of precipitation classifications.

ENTRY NEWMELT

NEWMELT is called at the top of each hour after the lastest sounding information is read. The altitudes of the highest 0 degree Centigrade (°C) (melting, "MELTHIGH") level and the lowest +4 °C (transition from slush to rain, "MELT4C") level are compared with the altitudes of the top and bottom of the beam, all with respect to sea level. If the bottom of the beam is higher than MELTHIGH, the radar is seeing dry snow, and the classification code is set to 1. If the top of the beam is lower than MELT4C, the radar is seeing rain, and the classification code is set to 2. For intermediate conditions, the radar beam might be contaminated with bright band echoes. The classification code is set to 3, which is the setting of the binary bits for both 1 (snow) and 2 (rain). These codes are set even if no echo is present; it is the potential precipitation classification that is being set.

The terrain file is then examined. The clearance between the surface and the radar beam center is calculated. The surface elevation is then compared to the altitudes of the same two temperature thresholds for an estimate of the precipitation type classification at the surface. The surface classification is encoded into the four most significant bits of the classification number. If snow is expected, the bit for 16 is set. If rain is expected at the surface, the bit for 32 is set. If wet snow (slush) is expected at the surface, both bits are set. The classifications of the precipitation type aloft and at the surface are both constant for at least an hour, being based on the latest sounding estimates.

The relative humidity is examined from the bottom of the sounding up to 1.5 kilometers (km) above the highest terrain within view of the radar. If it is everywhere drier than a user-defined threshold ("DRYAIR," such as 70%), the flag, ISDRY, is set to 1. If it is everywhere wetter than that threshold, then the flag ISWET is set to 1. Otherwise the relative humidity is integrated from the surface below each range bin to 1.5 km above that location and then averaged. If ISDRY is set to 1 or the average relative humidity is less than DRYAIR, then four is added to the classification code for the precipitation to indicate a potential for virga. A later routine will examine echoes close to the radar to see if they come close to the ground, thereby directly checking on virga. However, this initial virga classification is needed in case all echoes are remote.

SUBROUTINE GETNIDS

GETNIDS reads the Level III (NEXRAD Information Dissemination Service [NIDS] format) data, identifying all of the important variables (listed and identified in the comments) and loading an array with all four lowest tilts of biased dB reflectivities. Such data arrive as truncated into 4- or 5-dB steps. Adjustments are made to estimate the actual reflectivities based upon typical reflectivity distributions. An incoming reflectivity of 25 dB might be adjusted to 27 dB within the 25.0- to 29.8-dB range that the Level II data might exhibit. In the unlikely case that more than 370 radials are available at a particular tilt, the extra radials are ignored; 367 radials is a typical number encountered, ensuring a full 360° coverage for each tilt.

ENTRY READ1ST

READ1ST operates on only the first volume scan, reading into it far enough to identify the date and time. It then rewinds the file for a normal start.

SUBROUTINE OCCULT

OCCULT identifies the azimuth of each radial for each tilt and looks up the correction indices for the nearest azimuth at 0.2 degree resolution. The indices indicate the ranges beyond which 1, 2, 3, or 4 dB are to be added to the reflectivity because of beam blockages. In the PPS, if blockages are greater than 60%, nothing is added, and the hybrid scan file instructs the algorithm to go to the next tilt for ranges beyond the blockage. However, at far ranges, such a step upward may cause the beam to overshoot all echoes, eliminating their detection. Therefore, the occultation files in use for our studies have been altered to add 4 dB if the blockage is greater than 60%. The next tilt is used if, by experience during widespread storms, the signal from the next tilt is better than from that incompletely adjusted lower tilt. Occultation corrections are rarely needed for the higher tilts.

SUBROUTINE NOSPIKES

Much of NOSPIKES operates in an equivalent manner to a set of four subroutines in the NEXRAD PPS algorithm. If a range bin has at least the minimum reflectivity ("DBZMIN," such as 0 dB), the eight neighbors are checked to see how many of them also have at least that minimum value. If there is no more than one such neighbor, the biased reflectivity value is set to 0 (-33 dB), and the bin is considered as "isolated." If a range bin has more than a maximum reflectivity ("DBZMAX," such as 53 dB for rain), the eight neighbors are checked to see how many of them also exceed the maximum value. If there are any such neighbors, the reflectivity is truncated to the maximum value. The range bin is considered to be "replaced." If there are no such neighbors, a replacement reflectivity is calculated from the average precipitation rate of the eight neighbors. The range bin is considered to be "interpolated."

Meanwhile, NOSPIKES also examines the volume scan for possible indications of virga. The routine totals the number of range bins within a range limit ("INSIDE," such as 100 km) that are at or higher than the tilt specified by the hybrid scan file, yet within an specified altitude range above the radar (from "BOTIN," about 0.2 km, to "TOPIN," about 1.5 km). It also totals the number of those acceptable range bins having reflectivities of at least the minimum value specified ("DBZMIN," such as 0 dB) for snow. At the end of the routine, a ratio is made of the number of bins with at least minimal echoes to the total number of acceptable bins. If this ratio is at least as great as a setable "FRACTION" (such as 0.05), then a flag ("INFLAG") is set indicating that adequate precipitation was found within the search volume and that virga restrictions need not be applied at ranges greater than "INSIDE."

The subroutine adds the observations of the present volume scan to the time-height diagram. At 10-meter vertical resolution for the lowest 3 km above the radar, the maximum reflectivity (for any azimuth and any tilt allowed by the hybrid scan file) at each vertical position is determined. Those maximum values are added to the graph at a time resolution of 1/20 hour for the duration of the volume scan.

SUBROUTINE PRECIP

PRECIP converts the data from the present volume scan into values for incrementing the precipitation and snow depth files. The duration of the volume scan, SUMT, is normally the time difference between the stop time of the present volume scan and the stop time of the previous volume scan. If it appears that a significant gap has occurred, SUMT (in fractional hours) is set to a value typical for the VCP (volume coverage pattern) mode: 290 seconds for VCP = 11 (severe weather), 345 seconds for VCP = 21 (precipitation), and 585 seconds for VCP = 31 or 32 (clear air).

There are typically 367 radials for the 360 1-degree azimuths in the summation files. The routine searches all four lowest tilts for the radials whose azimuths are closest to each desired azimuth, rejecting the contribution if the nearest available radial is more than 2 degrees away.

The routine then consults the hybrid scan file to identify the appropriate tilt to use for each range bin from 4 to 230 km. (Echoes from a range of 1 to 3 km are considered to be unreliable.) The classification of the precipitation type in the radar beam and at the surface is recovered from the classification file for each range bin. The biased dB value for each range bin is used as an index to look up, in the rate table for the appropriate precipitation type (1 = snow, 2 = rain, 3 = slush), the precipitation rate for that particular reflectivity. Using the clearance value, the value is extrapolated to the estimated surface value according to the standard vertical gradient parameters for the precipitation type. (The vertical gradient parameters are not yet determined for rain or slush in the study areas.)

If a flag has been set indicating possible virga conditions (mostly dry air near the surface), the vertical gradient extrapolation is not applied. A second flag is checked to see if enough echoes are present within a specified volume close to the radar and too close to the ground. If there are

insufficient echoes in the special volume under possible virga conditions, echoes beyond the assigned range threshold (like 100 km) are ignored by zeroing their contributions.

The precipitation rate is then multiplied by the time duration of the volume scan and saved in a temporary array in units of millimeters (mm)*100. Snow depth contributions are calculated from the precipitation amount by dividing by the snow density assigned for dry snow (about 1/14) or for slush (about 1/8), according to the FORTRAN variable, KSFC, (according to what is arriving at the surface). If rain is indicated for the surface conditions, the snow depth contribution is set to zero.

If gauge comparisons are desired, the biased dB values and precipitation classifications are written to a special file for each gauge location. A separate postprocessing program can then vary the adaptable parameters to seek refinements for those parameters.

If an option has been selected to reduce noise in the data, a 3 by 3 median filter is used on the precipitation file. If a precipitation value departs from the median (if the value is greater or smaller than the median) by more than an indicated amount, that value is replaced by the median of the eight neighboring range bins. (This median filter is not currently applied to the snow depth file.)

The three arrays (precipitation, snow depth, and classification) are then ready for combining with the summation files.

SUBROUTINE INCRMENT

INCREMENT combines the results of the present volume scan with the sums for the 1-, 2-, 3-, 6-, and 24-hour intervals. The duration of the present volume scan is added to the SUMT value in line 361 of all files. The timespan of the summation is recomputed for SPANT in line 361. The ratio of these times is eventually used to extrapolate to full time periods. The inclusive OR (IOR) relation is used to update the classifications by setting particular bits to show that a class of precipitation occurred at some time during the summation period. The precipitation and snow depth increments are simple sums with the previous integrations.

SUBROUTINE TOPHOUR

TOPHOUR works at the top of each hour. Output files for the latest 1-, 2-, and 3-hour totals are created from the summation files by extrapolating to the full time period. When the appropriate 6-, 24-, or special 24-hour ending time is reached, the desired output files are produced by extrapolation of the sums to full time periods.

ENTRY HALFHOUR

HALFHOUR works at the bottom of the hour, producing files for the first half of the hour only, if such outputs are desired. It copies the classification summation file to the appropriate output file. Snow depth and precipitation sums are extrapolated to a full half hour. To get the second half hour files, the files from the first half hour need to be subtracted from those of the full hour. (The logic of the classification file manipulation for the second half hour has not yet been examined.)

SUBROUTINE RESET

RESET moves the 1- and 2-hour summation files by 1 hour to the files of the next time period for a continuation of the sums. The 1-hour files are zeroed for a fresh start.

ENTRY RESET624

RESET624 zeroes the 6-, 24-, or special 24-hour summation files.

ENTRY SOUNDOUT

SOUNDOUT writes the time-height diagram to a file. It then calls NEWGRAF for a clean background on which to write the next diagram and calls GRAFSTRT to initialize it.

SUBROUTINE SOUNDING

SOUNDING analyzes Eta forecast soundings, localized to the radar center, searching for parameters useful in the radar analysis. It is called at startup and then at the top of each hour for an update. It searches through a list of hourly forecast soundings for a date and time that matches the latest radar date and time. If the run is in real time, a sounding file name of ETASOUND.KKK (where KKK is the last three letters in the radar station name, like MPX) is always examined, with the expectation that it will be updated every 6 hours with new estimates for the soundings. If the run is for postprocessing, the file name is in the form ETAyymmddhh.KKK, where yymmddhh is the year, month, day, and hour of the sounding initialization. The date and previous 6-hour time in the file name are updated at startup and hourly thereafter so that the best archived soundings are used. Altitudes are computed from the pressure as pressure-altitude above mean sea level; they, therefore, contain some slight error, but that is small compared to the radar beam height, even in severe arctic airmass conditions.

When SOUNDING identifies the sounding for the appropriate hour of the radar data, it searches downward until it finds the highest melting level (0 °C) and interpolates its altitude. If no such layer is found, the temperature of the bottom layer of the sounding is extrapolated downward according to the dry adiabatic lapse rate in order to estimate a melting level. This will be used if and where the terrain elevations are lower than the radar or sounding site or both.

SOUNDING then tests the temperature of the bottom sounding layer. If it is at +4.0 °C, the special altitude for the rain threshold is automatically identified. If it is colder, the bottom temperature is extrapolated downward to +4 °C according to the dry adiabatic lapse rate. If the sounding temperature at the bottom is warmer, the subroutine searches upward from the bottom of the sounding to find the lowest +4 °C level.

SOUNDING has access, in addition, to dewpoint depression, relative humidity, and winds aloft. The relative humidity profile is examined in NEWMELT for virga tests. A routine for guidance about anomalous propagation has not yet been designed.

ENTRY GRAFSTRT

SOUNDING flows into GRAFSTRT, which adds the next hour of sounding temperatures and relative humidities to the time-height graph, interpolating first with altitude and then with time to fill in the graph.

SUBROUTINE ADDDAY(JDATE,JD)

ADDDAY adds JD days to the date (JDATE) even if JD is negative.

SUBROUTINE HHMMSS (IT,IH,IM,IS)

HHMMSS converts time or date (IT in hhmmss or yymmdd format) into hour or year (IH), minute or month (IM), and second or day (IS).

SUBROUTINE GETMED (MEDIAN)

GETMED determines the median (MEDIAN) of a three by three array of nine numbers.

SUBROUTINE TIMESPAN (ITIME,IDATE,JTIME,JDATE,DH)

TIMESPAN calculates the fractional hours (DH) between a set of times (ITIME, JTIME in hhmmss format) and dates (IDATE, JDATE in yymmdd format).

SUBROUTINE JTOG (JD,IY,MO,ID)

JTOG converts the (Julian) day of the year (JD) to the (Gregorian) date of year (IY), month (MO), and day (ID).

ENTRY GTOG (JD,IY,MO,ID)

GTOG converts the (Gregorian) date of year (IY), month (MO), and day (ID) to (Julian) day of the year (JD).

SUBROUTINE DATEJ (NDA,IYMD)

DATEJ converts the number of (Julian) days, NDA, since the start of the year 1970 into year, month, day in yymmdd format, IYMD.